Extrasynaptic signalling and plasticity mediated by *N*-Methyl-D-aspartate receptors

by

Yu-Wei Wu

31st July 2012

Department of Clinical and Experimental Epilepsy

Institute of Neurology

University College London

Table of Contents

Table of Figures

Chapter 1

Chapter 2

Chapter 3

Chapter 4

Chapter 5

Chapter 6

Chapter 7

Declaration

I, Yu-Wei Wu, confirm that the work presented in this thesis is my own. Where information has been derived from other sources, I confirm that this has been indicated in the thesis.

Abstract

Synaptic *N*-Methyl-D-aspartate receptors (NMDARs) are crucial for neural coding and plasticity. However, little is known about the adaptive function of extrasynaptic NMDARs located on the dendritic shaft. Here we find that in CA1 pyramidal neurons backpropagating action potentials (bAPs) recruit shaft NMDARs exposed to ambient glutamate of non-vesicular origin. In contrast, spine NMDARs are "protected" under baseline conditions from such glutamate by perisynaptic transporters: bAP-evoked Ca^{2+} entry through these receptors can be detected upon synaptic glutamate release or local glutamate uncaging. During theta-burst firing, NMDAR-dependent Ca^{2+} entry either upregulates or downregulates an *h*-channel conductance (G_h) of the cell depending on whether synaptic glutamate release is intact or blocked. G_h plasticity in turn regulates dendritic input probed by local glutamate uncaging. Thus, the balance between activation of synaptic and extrasynaptic NMDARs can determine the sign of G_h-dependent plasticity. These results uncover a novel meta-plasticity mechanism potentially important for neural coding and memory formation.

Abbreviations

Aβ	Amyloid-β peptide
ABD	Agonist binding domain
AMPA	α–amino-3-hydroxy-5-methyl-4-isoxazolepropionic acid
ATP	Adenosine 5'-triphosphate
bAP	Backpropagating action potential
BDNF	Brain-derived neurotrophic factor
CA1	Cornu Ammonis 1
CA3	Cornu Ammonis 3
CaMKII	Calcium/calmodulin-dependent protein kinase II
ClQ	(3-chlorophenyl)(6,7-dimethoxy-1-((4-methoxyphenoxy) methyl)-3,4-dihydroisoquinolin-2(1H)-yl)methanone
CNS	Central nervous system
CREB	cAMP response element binding protein
DAS	Directly activated spines
Dox	Doxycycline
EAAT	Excitatory amino-acid transporter
EC_{50}	Effective concentration required to induce a 50% effect
EOS	Glutamate optical sensor
EPSC	Excitatory postsynaptic current
EPSP	Excitatory postsynaptic potential
ERK	Extracellular signal-regulated kinases
FWHM	Full-width-at-half-maximum
GABA	γ -aminobutyric acid
GAIP	Gαi3-interacting protein
G_h	*h*-channel conductance
GIPC	GAIP-interacting protein, C terminus
GSH	Glutathione
Halothane	2-Bromo-2-chloro-1,1,1-trifluroethane
HCN channel	Hyperpolarization-activated cyclic nucleotide-gated channel
MAGUK	Membrane-associated guanylate kinase
mAChR	Muscarinic cholinergic receptor
mGluR	Metabotropic glutamate receptor
NMDA	*N*-Methyl-D-aspartate
NMDAR	NMDA receptor
NPPB	5-Nitro-2-(3-phenylpropylamino) benzoic acid
NTD	Amino-terminal domain

$P2X_7R$	$P2X_7$ purinergic receptor
p38 MAPK	p38 mitogen-activated protein kinase
PI3K	Phosphoinositide 3-kinase (PI3K)
PPDA	[±]-Cis-1-[phenanthren-2yl-carbonyl]piperazine-2,3-dicarboxylic acid
PSD	Post-synaptic densities
REM	rapid-eye-movement
ROI	Region of interest
SAS	Spillover-activated spine
SD	Sprague–Dawley
SE	Status epilepticus
SIC	Slow inward current
SK channel	small conductance Ca^{2+}-activated potassium channel
SNAP	Synaptosomal-associated protein
SNARE	SNAP receptor protein
TBF	Theta-burst firing
TBOA	DL-threo-β-Benzyloxyaspartic acid
TeTX	Tetanus toxin
UPB141	(2R*,3S*)-1-(phenanthrene-3-carbonyl)piperazine-2,3-dicarboxylic acid
VAMP	Vesicle-associated membrane protein
VDCC	Voltage-dependent Ca^{2+} channel
VGLUT	Vesicular glutamate transporter
VRAC	Volume-regulated anion channel
VSOR	Volume-sensitive outward rectifying chloride channel

Publication arising from this thesis

Wu YW, Grebenyuk S, McHugh TJ, Rusakov DA, Semyanov A. (2012) Backpropagating action potentials enable detection of extrasynaptic glutamate by NMDA receptors. *Cell Reports.* 1: 495-505.

Published Abstracts

Wu YW, Grebenyuk S, McHugh TJ, Rusakov DA, Semyanov A. (2010) Extrasynaptic NMDA receptors regulate neuronal excitability through activity-dependent detection of ambient glutamate. Poster no. 548.17, Annual Meeting for Society for Neuroscience, San Diego, California, USA

Wu YW, Grebenyuk S, Rusakov DA, Semyanov A. (2010) Activity-dependent mechanism of ambient glutamate detection by extrasynaptic NMDA receptors in hippocampal pyramidal neurons. Poster no. 103.70, 7^{th} FENS Forum, Amsterdam, Netherlands

Acknowledgements

It is a pleasure to thank all the people who have helped me in various ways to finish this thesis.

First and foremost, I would like to thank my supervisors, Dr. Alexey Semyanov and Prof. Matthew Walker. I am incredibly lucky to have both of them as my supervisors. Alexey has always been very supportive, generous and helped me in every possible way. He creates a very stimulating research environment for my graduate study and gives me many opportunities to attend international conferences, give presentations, and meet great scientists all around the world. Matthew has been always kind and patient and helped me pass through all the difficult processes in my graduate study. Without their encouragement, guidance and support, this thesis would not have been possible. I would also like to thank my former supervisor, Prof. Ming-Yuan Min, for being my life mentor even after I left his lab for many years. I am indebted to our collaborators, Prof. Dmitri Rusakov and Dr. Thomas McHugh. A big thanks goes to Dmitri for his insightful and practical comments throughout the processes of project developing, paper writing, and publishing. Another warm thank goes to Tom for kindly providing the NR1 knockout and CA3-TeTX mice. Without their active involvement, I could not have completed this project. I would also like to send my deepest gratitude to my two thesis examiners, Dr. Andrew Constanti and Dr. Karri Lamsa, for making this thesis toward a real completion with their patient guidance and incredible vision.

I would like to express my sincere gratitude to all my former and current colleagues for their various forms of support and for providing an inspiring and fun environment in which I have learned and grown. A thank goes to Ms Pei-Yu Shih for many-year-friendship and support. Many thanks go to Dr. Sergei Grebenyuk, Dr. Sylvain Rama, Dr. Vetrivel Lakshmanan, and Mr Alexander Lebedinskiy for teaching and sharing with me all the experiences on imaging and programing techniques. Thanks to Dr. Inseon Song, Dr. Alexey Pimashikin, Dr. Jaeyon Koo, Dr. Tanja Brenner, Dr. Xiaofang Tang, Dr. Ivan Pavlov, and Dr. Pi-Shan Change for helping me in different stages of my study. Special thanks go to Dr. Tanja Brenner, Mr Sheng-Hsia Hsu, and Mr Alistair Jennings for reading and correcting my dissertation. I would also like to thank the staffs in BSI-Olympus Collaboration Center (BOCC), especially Mr Tetsuya Tajima and Ms Satomi Katahira, for helping me use the two-photon uncaging system. Many thanks go to Ms Akiko Ashikari for assisting me in all kinds of paperwork, ordering and delivering etc. She is just like the lab mom, who takes care of everyone and everything.

Finally, I would like to express my deepest gratitude to my wife, Wei-Shan, and my family, for always being so supportive throughout my life. This thesis is dedicated to them.

Chapter 1: Introduction

Brain functions, such as learning, memory and consciousness, are based on information processing at cellular and molecular levels. The computational units for such processing have been suggested to be synapses. Synapses are specialized structures where two neurons communicate. Presynaptic neurons can release signal molecules into synaptic clefts from axonal terminals, and these molecules then bind with their receptors on adjacent postsynaptic membrane (Fig. 1.1a). There are more than 100 trillion (10^{14}) connections of this type in the human neocortex (Pakkenberg et al., 2003). They link neurons into complex circuits and networks which make it possible for the human brain to compute and deal with diverse tasks. The communication between neurons, however, is not limited to point-to-point synaptic wiring. Diffusive chemical signals also allow communication between neurons that are not connected by synapses between them.

The diffusive chemicals were thought to be only include neuromodulators, such as dopamine, serotonin, and norepinephrine etc (Vizi, 2000; Vizi et al., 2004). These, unlike fast neurotransmitters, e.g. glutamate and γ-aminobutyric acid (GABA), are released from axonal boutons without an associated specialized synaptic structure. After being released, they can diffuse a considerable distance, and act on their receptors before being removed by uptake. Therefore, they can serve as signalling molecules that mediate the communication between cells without any synaptic connections (Fig. 1.1b). This type of signal transmission is called “volume transmission” because communication takes place within a large volume. On the

other hand, fast neurotransmitters were considered only to mediate point-to-point synaptic communication. They are released into the narrow synaptic cleft and then cleared within a confined space and time. Thus they are unlikely to play a role in "volume transmission". However, when fast neurotransmitters are released during high synaptic activity, they can escape the synaptic cleft (this is termed "spillout") and spill into the extrasynaptic space (Kullmann et al., 2005). When the concentration in the extrasynaptic space reaches a certain threshold, they can activate extrasynaptic receptors (Fig. 1.1c). Therefore, fast neurotransmitters may also work as signalling molecules in volume transmission-like extrasynaptic communication (Okubo and Iino, 2011).

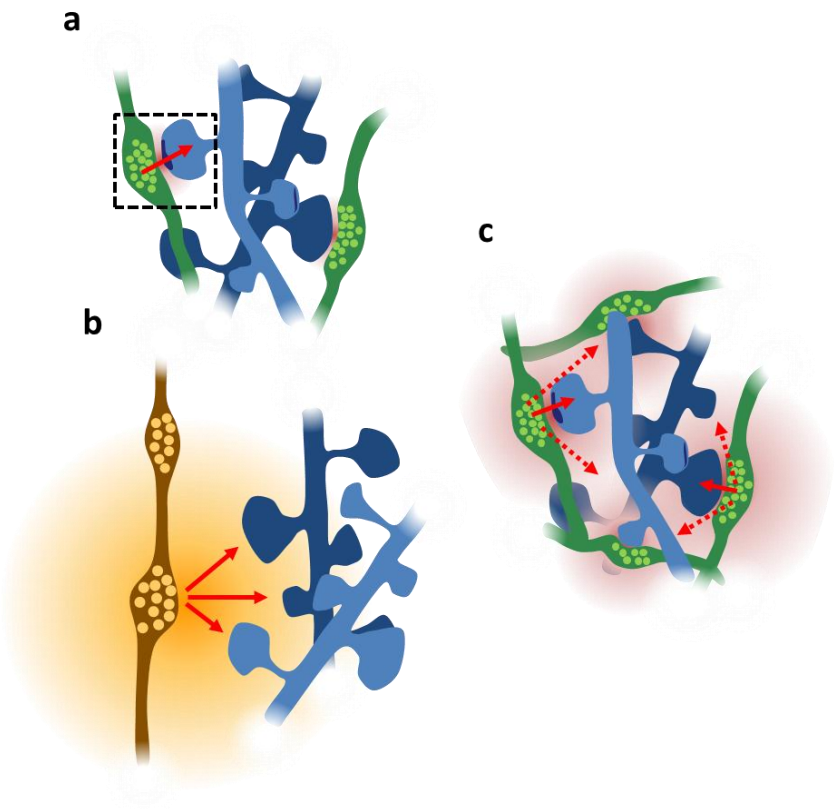

Figure 1.1 Neuronal communications via diffusive chemical signals

a, A typical view of neuronal communications via point-to-point synaptic connections. The boxed region indicates a typical glutamatergic synapse. Neurotransmitters (pink) are released by presynaptic boutons (green) and act on the immediate postsynaptic membrane (blue). The red arrow indicates the direction of information flow. **b,** A scheme for "volume transmission". Neuromodulators (orange) are released via a bouton (brown) without specialized postsynaptic targets and act on several dendrites (blue). The information can flow from one source to multiple targets. **c,** A scheme for a "volume transmission-like" neuronal communication mediated by spillout of fast neurotransmitters from the synaptic clefts during higher synaptic activities. The information flow extends from one-to-one to one-to-multiple manner. Red arrows with dash-lines indicate the information flow mediated by "spillout".

Besides synaptic spillout, the sources of extrasynaptic signalling molecules also include non-synaptic neuronal and astrocytic release (Malarkey and Parpura, 2008). The diverse agonist sources and the spatially distributed receptors make extrasynaptic communication more complicated than initially thought. Only in recent years, have researchers started to investigate this type of communication in detail, finding that extrasynaptic signalling indeed plays crucial roles in neuronal functions and dysfunctions. Extrasynaptic signals can potentially interact with synaptic networks. In addition to modulation, this interaction may also guide the information flows of the synaptic networks (Semyanov, 2008). Thus, they can be as important as synaptic communication for network activity.

This study focuses on glutamatergic extrasynaptic communication carried out by *N*-Methyl-D-aspartate receptors (NMDARs) in *Cornu Ammonis* 1 (CA1) pyramidal neurons of the rodent hippocampus. The main purpose of the study is to understand when and how extrasynaptic NMDARs are activated under physiological conditions, and the consequences of such activation. I will first discuss the properties of the NMDAR and how it is activated, before outlining the mechanisms that underlie subunit- and location-dependent downstream signalling of NMDARs. Basic knowledge of NMDARs and sources of extrasynaptic glutamate will be also discussed. Finally, I will explain how NMDARs detect the dynamics of extrasynaptic glutamate release from a variety of sources, providing a potential non-synaptic wiring between neurons and astrocytes.

1.1. The properties of the *N*-methyl-D-aspartate receptor (NMDAR)

Glutamate is the main excitatory neurotransmitter that mediates fast synaptic transmission in the mammalian brain. When glutamate is released from presynaptic terminals, mainly two types of glutamate receptors are activated: α–amino-3-hydroxy-5-methyl-4-isoxazolepropionic acid (AMPA) receptors (AMPARs) and NMDARs. Both AMPARs and NMDARs are ionotropic glutamate receptors. Upon AMPAR activation sodium (Na^+) and potassium (K^+) ions can pass through the channels and produce excitatory postsynaptic potentials (EPSPs). Unlike AMPARs, which are typically calcium impermeable, NMDARs are highly calcium (Ca^{2+}) permeable. Besides, NMDARs display several other special properties. They are voltage-dependently blocked by extracellular magnesium (Mg^{2+}), and have unique slow channel activation and deactivation kinetics. Activation of NMDARs also requires binding of co-agonists, such as glycine and D-serine. These peculiar features make NMDARs ideal for a variety of functions, such as brain development, cognition, learning and memory (Cull-Candy et al., 2001). Because of their high Ca^{2+} permeability, dysfunction and excessive activation of NMDARs also result in neurotoxicity and lead to neuronal death in many diseases including epilepsy, Huntington's, Parkinson's, and Alzheimer's diseases (Lau and Zukin, 2007).

1.1.1. Subunit composition and structure of NMDARs

There are three main subunit families for NMDARs, designated GluN1, GluN2, and GluN3. Among them, GluN1 has eight isoforms encoded by the same gene with variant alternative splicing; GluN2 subunits have four subtypes: GluN2A, -2B, -2C, and -2D, whereas GluN3 subunits have two (GluN3A and GluN3B) (Cull-Candy and Leszkiewicz, 2004). The ligand for GluN1 and GluN3 subunits is glycine, whereas GluN2 subunits bind glutamate. A functional NMDAR is most frequently a diheteromeric receptor of two identical GluN1 and two identical GluN2 subunits (dimer of dimers). Triheteromeric receptors composed of two GluN1 with two different GluN2, or with GluN3 subunits are also observed in native brain tissue(Cull-Candy and Leszkiewicz, 2004; Low and Wee, 2010) (fig 1.2a). Each NMDAR subunit includes four main parts: (1) an extracellular amino-terminal domain (NTD) which serves as the allosteric modulation site for Zn^{2+} and ifenprodil in the GluN2 subunits; (2) a transmembrane domain consisting of three membrane-spanning regions (M1,M3, and M4) and a channel pore forming re-entry loop (M2); (3) an agonist binding domain (ABD) formed by the remaining part of extracellular NTD (named S1) and the loop between M3 and M4 (named S2); (4) a cytoplasmic carboxyl-terminal domain (CTD) which interacts with scaffold proteins, cytoskeletons, and various downstream signalling pathways (Fig. 1.2b) (Cull-Candy and Leszkiewicz, 2004; Low and Wee, 2010).

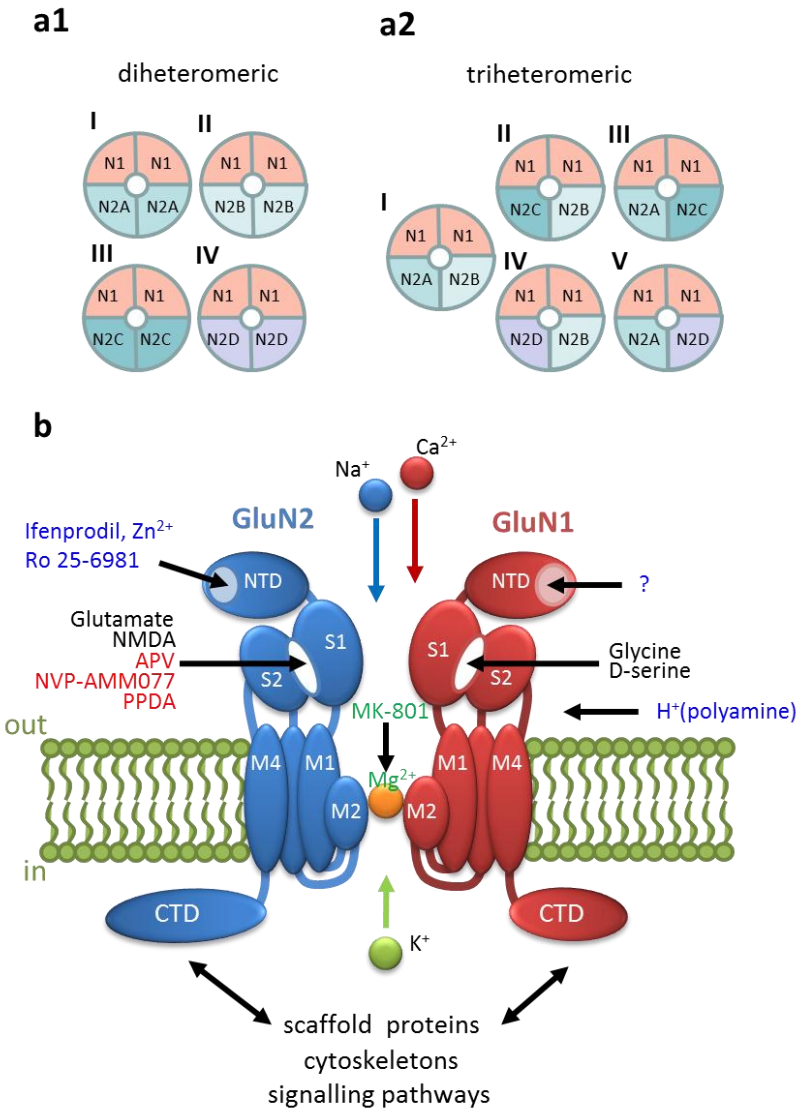

Figure 1.2 Subunit assemblies and topology of GluN1-GluN2 NMDAR

a, The scheme of subunit assemblies of NMDARs. Both diheteromeric (a1) and triheteromeric (a2) receptors are formed in native neurons. **b,** The topology scheme of GluN1 and GluN2 subunits. NMDAR is a cation channel and is permeable to K^+, Na^+ and Ca^{2+}. The binding sites for agonists (glutamate, NMDA), co-agonists (glycine, D-serine)(black), antagonist (APV, NVP-AMM007, and PPDA)(red), pore blockers (Mg^{2+} and MK-801)(green) and modulators (H^+, ifenprodil, Ro 25-6981, and Zn^{2+})(blue) are indicated. NTD denotes amino-terminal domain; CTD denotes carboxyl terminal domain.

1.1.2. NMDAR properties depend on subunit composition

The majority of NMDARs are diheteromeric receptors, which are composed of GluN1 and GluN2 subunits. The subtype of the GluN2 subunit largely determines the single channel properties of NMDARs. First, it was shown in a recombinant system that GluN2A and GluN2B-containing NMDARs exhibit high single channel conductance (40-50 pS), while GluN2C and GluN2D-containing NMDARs have lower conductance (16-35 pS) (Cull-Candy and Leszkiewicz, 2004). Secondly, GluN2A- and GluN2B-containing receptors display a higher sensitivity to Mg^{2+} block than GluN2C- and GluN2D-containing NMDARs (Farrant et al., 1994; Momiyama et al., 1996; Wyllie et al., 1998). The time required for Mg^{2+} to leave the channel pore (unblocking rate) during membrane depolarization is also different within GluN2 subtypes (Clarke and Johnson, 2006). GluN2A- and GluN2B-containing receptor show a slow and delayed Mg^{2+} unblocking rate compared to GluN2C- and GluN2D-containing receptors, which show almost instantaneous Mg^{2+} unblock upon membrane depolarization (Clarke and Johnson, 2006; Vargas-Caballero and Robinson, 2003). Such differences might result in subunit-dependent sensing of depolarization events: GluN2C- and GluN2D-containing NMDARs might sense fast events like bAPs, while GluN2A- and GluN2B-containing ones sense slower event like EPSPs more efficiently (Kampa et al., 2004).

Thirdly, the deactivation and inactivation time constants also vary in different subtypes. The GluN1/GluN2A-containing receptor shows deactivation and inactivation time constants within a range of several milliseconds, whereas the GluN1/GluN2D-containing receptor shows exceptionally slow deactivation time

constant (4 to 5 seconds) (Cull-Candy and Leszkiewicz, 2004; Wyllie et al., 1998) and almost no inactivation when it binds to a low concentration of glutamate (Wyllie et al., 1998). Therefore, the timing for synaptic NMDAR currents in the central nervous system (CNS) can be decisively determined by the GluN2 subunit composition in different synapses.

Fourthly, GluN2 subtypes display distinct pharmacological properties. A number of pharmacological tools were developed to distinguish the physiological functions between GluN2 subtypes. Ifenprodil, and its analogue, Ro 25-6981, bind to the NTD of GluN2B subunit, and allosterically modulate the GluN2B-containing NMDARs in an activity-dependent manner (Fig. 1.2b) (Fischer et al., 1997; Williams, 1993). NVP-AAM007 is a GluN2A-containing receptor antagonist (Liu et al., 2004). [±]-cis-1-[phenanthren-2yl-carbonyl]piperazine-2,3-dicarboxylic acid (PPDA) and the recently developed (2R*,3S*)-1-(phenanthrene-3-carbonyl)piperazine-2,3-dicarboxylic acid (UBP141) selectively block GluN2C- and GluN2D-containing receptors, though the selectivity is still not good enough (selectivity 10-fold over GluN2A and GluN2B) (Costa et al., 2009; Feng et al., 2004; Lozovaya et al., 2004b; Paoletti and Neyton, 2007). Notably, a recently developed GluN2C and GluN2D-selective potentiator, 3-chlorophenyl)(6,7-dimethoxy-1-((4-methoxyphenoxy)methyl)-3,4-dihydroisoquinolin-2(1H)-yl)methanone (CIQ), and non-competitive antagonists, quinazolin-4-one derivatives, show great improvement in selectivity over PPDA and UBP141 (Mosley et al., 2010; Mullasseril et al., 2010). Many important discoveries of NMDAR subunit-dependent properties and functions are actually based on using

these pharmacological tools. For example, GluN2A activation causes LTP while GluN2B activation triggers LTD (Liu et al., 2004). The subcellular locations of NMDARs are also functionally distinguished by using these antagonists/blockers. In adult cortical neurons, GluN1/GluN2A-containing receptors are predominantly localized in postsynaptic densities (Tovar and Westbrook, 1999), whereas GluN1/GluN2B-containing receptors are shown to be present in both synaptic and extrasynaptic regions (Li et al., 1998). Recent evidence further indicates the restricted expression of GluN2D-containing receptors in the extrasynaptic membrane in hippocampal CA1 and dentate gyrus areas (Harney et al., 2008; Lozovaya et al., 2004b).

Besides assemblies of two GluN1s with two identical GluN2s, triheteromeric NMDARs also exist. GluN1/GluN2A/GluN2B-, GluN1/GluN2A/GluN2D-, and GluN1/GluN2B/GluN2D-containing NMDARs have been shown to be expressed in different cell types (Brickley et al., 2003; Dingledine et al., 1999) (Fig. 1.2a). Triheteromeric NMDARs composed of GluN1/GluN2B/GluN2C and GluN1/GluN2A/GluN2C have also been identified (Cull-Candy and Leszkiewicz, 2004). They display different biophysical properties compared to those diheteromeric NMDARs described above. The different assemblies further increase the diversity of functional NMDARs, which control a broad spectrum of physiological events by their activation.

1.1.3. Mechanisms of NMDAR activation: agonist, co-agonist, and depolarization

Although NMDA receptors are considered glutamate receptors, activation of NMDARs requires other critical criteria besides binding of glutamate:

First, activation of NMDA receptors requires the binding of co-agonists glycine (Johnson and Ascher, 1987; Kleckner and Dingledine, 1988) or D-serine (Schell et al., 1995; Shleper et al., 2005) to its glycine-binding site on the GluN1 subunit (Fig. 1.3a). Glycine was previously thought to be the endogenous ligand for NMDARs (Johnson and Ascher, 1987). However, its concentration in hippocampal synapses is maintained by glycine transporters at a level that is too low to bind to many NMDARs (Xu and Gong, 2010). Instead, D-serine is considered as the endogenous ligand for the glycine-binding site (Mothet et al., 2000). It can be locally released into the synapse from astrocytes and modulate synaptic NMDAR activity (Henneberger et al., 2010; Yang et al., 2003). Therefore, the glycine-binding site of NMDARs can serve as a detector for the integrated activity of neuron and glia.

Secondly, the voltage-sensitive block of NMDARs by extracellular Mg^{2+} is a fundamental property (Cull-Candy and Leszkiewicz, 2004; Nowak et al., 1984). At resting membrane potential, even if the agonist and co-agonist are bound to NMDARs, there is only a small current flux. However, with the aid of depolarizing events like EPSPs and action potentials, NMDARs can produce remarkable Ca^{2+} influx when bound with agonists. When glutamate is released in large quantities, depolarization caused by the NMDAR itself can also relieve the Mg^{2+} block and

further trigger NMDAR-dependent regenerative spikes in the dendrites of cortical pyramidal cells (Schiller et al., 2000). Therefore, the voltage dependence enables NMDARs to serve as coincidence detectors of agonist binding and membrane depolarization (Fig. 1.3b).

In conclusion, glutamate, co-agonist (glycine or D-serine), and depolarization are the essential three components for NMDAR activation (Fig. 1.3). The different temporal and spatial interactions between release of glutamate and D-serine and membrane depolarizing events can thus provide a variety of combinations of paradigms for the activation of NMDARs, which differentially trigger Ca^{2+} influx and activate diverse downstream signalling cascades. For example, NMDAR activation induced by high frequency synaptic stimulation can trigger long-term potentiation (LTP) of synaptic currents, while low frequency stimulation results in long-term depression (LTD) (Helmchen, 2002; Zucker, 1999). The classical spike-timing dependent plasticity (STDP) is also caused by differential activation of NMDARs under different temporal interactions between presynaptic release of glutamate and postsynaptic action potentials (Dan and Poo, 2006; Kampa et al., 2007).

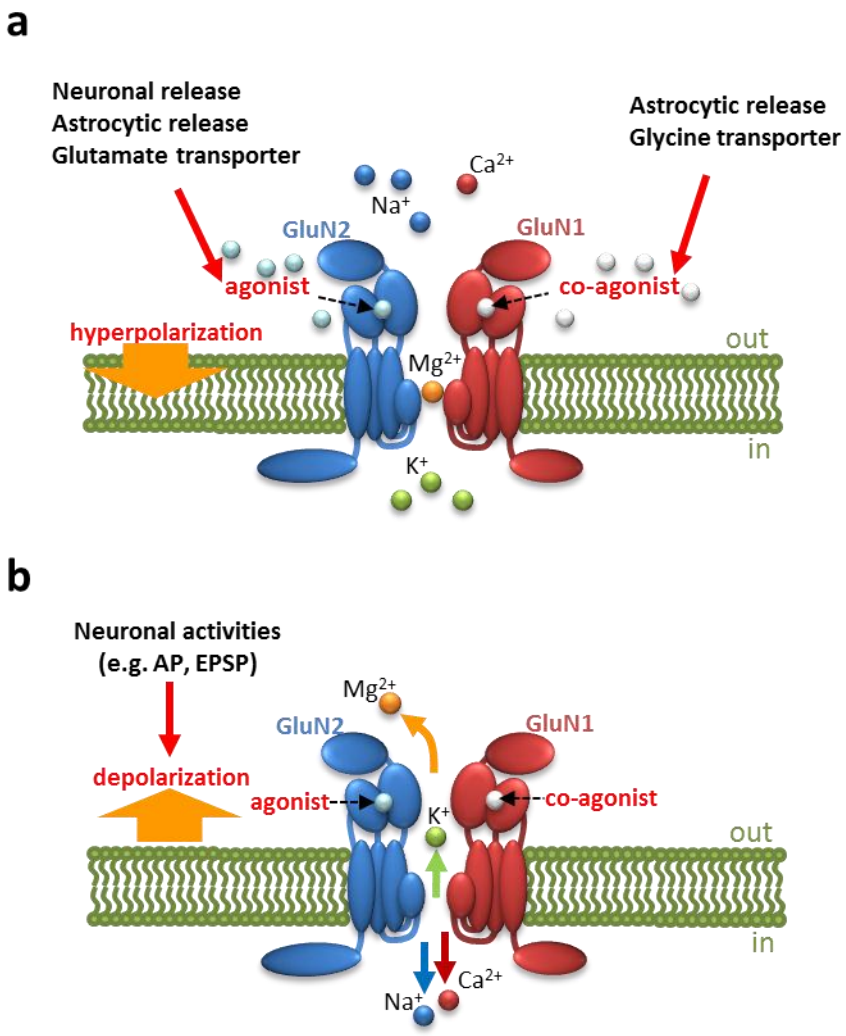

Figure 1.3 NMDAR activation depends on the presence of agonist, co-agonist and depolarization

a, Activation of NMDA receptors requires the binding of agonist (glutamate) and co-agonists (glycine or D-serine), which is controlled by neuronal and astrocytic release mechanisms, as well as transporter systems. However, without depolarization to relieve voltage-dependent Mg^{2+} block of NMDAR, ions cannot pass through. **b,** When binding with agonist and co-agonist, neuronal activities (e.g. action potentials (APs), and EPSPs) which depolarize the membrane can relieve the Mg^{2+} block and allow influx and efflux of ions. Red arrows in both **a** and **b** indicate the possible ways (black texts) for modulating the three key components of NMDAR activation.

1.1.4. Subcellular localization: Synaptic and extrasynaptic NMDARs

Most of our understanding about the role of NMDARs concentrates on those located in synapses, where they are confined to the area of post-synaptic densities (PSD). Here, they are structurally organized in a protein complex containing scaffold proteins, adaptors, and downstream signalling molecules (Husi et al., 2000; Newpher and Ehlers, 2008; Newpher and Ehlers, 2009; Rebola et al., 2010). However, evidence from electron microscopy (EM) and single molecule tracking demonstrated that NMDARs can be found not only in synapses but also in extrasynaptic areas, i.e. beyond the region of PSD (Groc et al., 2009; Newpher and Ehlers, 2008; Petralia et al., 2010). Because excitatory synapses are exclusively located on dendritic spines in adult cortical and hippocampal pyramidal neurons (Sheng and Hoogenraad, 2007), NMDARs which were observed on dendritic shafts are considered as extrasynaptic receptors (Petralia et al., 2010). Electrophysiological approaches also showed the existence of extrasynaptic NMDARs in different cell types by functionally defining extrasynaptic NMDARs as receptors not activated by glutamate released during low-frequency synaptic events (Brickley et al., 2003; Fellin et al., 2004; Harney et al., 2008; Lozovaya et al., 2004b; Tovar and Westbrook, 1999). Although the density of NMDARs in extrasynaptic regions is much less than in synapses, they represent two thirds of the total NMDAR population during early development, and still make up one third in adult rodents (Groc et al., 2009). Considering the existence of such a high number of extrasynaptic NMDARs, disproportionately little is known about their physiological functions.

1.1.5. Downstream signalling of extrasynaptic NMDARs

The downstream signalling pathways of extrasynaptic NMDARs are different from those of synaptic ones. Synaptic NMDAR activation induces cAMP response element binding protein (CREB) activity and brain-derived neurotrophic factor (BDNF) gene expression, whereas extrasynaptic NMDAR activation triggers CREB shut-off pathway and blocks BDNF expression (Hardingham et al., 2002). Also, synaptic and extrasynaptic NMDARs have opposite roles on the regulation of extracellular signal-regulated kinases (ERKs) (Ivanov et al., 2006; Kim et al., 2005). Recent studies also show that the balance between synaptic versus extrasynaptic NMDA receptor activity plays a crucial role in modulating mutant huntingtin protein and the production of amyloid-β peptide (Aβ) in Huntington's and Alzheimer's diseases, respectively (Bordji et al., 2010; Milnerwood et al., 2010; Milnerwood and Raymond, 2010; Okamoto et al., 2009).

Selective activation of synaptic and extrasynaptic NMDARs can also bi-directionally regulate neuronal excitability. Activation of extrasynaptic but not synaptic NMDARs triggers unclustering and dephosphorylation of the delayed-rectifier voltage-gated potassium channel, Kv2.1, which changes intrinsic neuronal excitability (Mulholland et al., 2008). Moreover, selective activation of extrasynaptic NMDARs also triggers dephosphorylation of the A-type potassium channel, Kv4.2, and decreases synaptic strength in hippocampal neurons. In contrast, driving synaptic activity increases phosphorylation and internalization of Kv4.2 which results

in increasing cell excitability and synaptic strength (Hammond et al., 2008; Kim et al., 2007; Kim et al., 2008; Lei et al., 2009; Mulholland and Chandler, 2009).

The underlying mechanisms for such different downstream signalling are still not well understood. Two possible mechanisms, or a combination of them, were proposed. First, the subunit composition of the receptors is different from synaptic to extrasynaptic NMDARs. For example, in adult cortical neurons, GluN2A-containing NMDARs are predominantly localized in PSDs (Tovar and Westbrook, 1999), whereas GluN2B-containing NMDARs are shown to be present in both synaptic and extrasynaptic regions (Li et al., 1998). A restricted expression pattern of GluN2D-containing receptors in the extrasynaptic membrane was also demonstrated (Harney et al., 2008; Lozovaya et al., 2004b). Because the GluN2 subunits have different molecular identities and structural differences on their CTDs, they bind with different scaffold proteins and adaptors, and hence activate specific downstream signalling machineries.

Secondly, the NMDARs with the same subunit composition can link to different scaffold proteins. The major group of NMDAR-associated scaffold proteins, membrane-associated guanylate kinases (MAGUKs) were shown to locate differently in synapses and extrasynaptic areas. For example, PSD-95 is mainly and stably located in synapses, while SAP102 shows a broader distribution with peak localization further away from PSDs (Zheng et al., 2010). EM studies also showed that SAP102 labelling density and frequency were higher in dendrites and lower in spines compared to PSD-93/95 (Petralia et al., 2010). GIPC (GAIP-interacting protein,

C terminus), a novel NMDAR interacting protein, was shown to be excluded from synapses and preferentially associated with extrasynaptic NMDARs (Yi et al., 2007). These scaffold proteins then further link NMDARs to different downstream signalling protein complexes. The mechanisms determining the location of NMDARs with the same subunit composition are still unclear. Different phosphorylation of tyrosine residues of CTDs is one of the possibilities (Goebel-Goody et al., 2009).

In conclusion, these observations suggest that the specific responses of NMDAR activation can be determined not only by their molecular identities, but also by their localizations.

1.1.6. Functions of extrasynaptic NMDAR activation

It was hypothesized that extrasynaptic NMDARs are non-functioning, and form a reserve pool for synaptic NMDARs. However, since the diverse extrasynaptic NMDAR-mediated downstream signalling pathways were observed, more functions are being proposed (Groc et al., 2009). Most of the studies consider activation of extrasynaptic NMDARs as a pathological process. It is thought to trigger excitotoxicity and neuronal death as the consequence of pathological neuronal activity and excessive glutamate release. These processes were shown to contribute to neuronal death in neurological disorders, such as Huntington's disease and stroke (Hardingham and Bading, 2010). However, it is not difficult to infer that triggering neuronal death should not be the major function of extrasynaptic NMDARs. Indeed,

in the rat/mouse brain during early postnatal development, extrasynaptic NMDARs play the major role in generating slow network oscillations (Ben-Ari, 2001). In adults, the balance between activation of extrasynaptic NMDARs and $GABA_A$Rs on interneurons controls the frequency of hippocampal gamma oscillations (Mann and Mody, 2010). GluN2B-containg NMDARs, which are localized to mainly extrasynaptic areas, can detect glutamate arising from multiple synaptic releases (Chalifoux and Carter, 2011; Scimemi et al., 2004). They can also detect glutamate released from astrocytes and promote synchronized neuronal activity in hippocampal CA1 pyramidal neurons (Fellin et al., 2004).

Together, the evidence leads us to hypothesize that the major function of extrasynaptic NMDARs is to sense global glutamate signals generated from population activity of neurons and astrocytes. Nevertheless, the detailed mechanisms as well as the potential sources of extrasynaptic glutamate are still not well studied. In the next paragraph, I discuss the possible sources of glutamate that contribute to the activation of extrasynaptic NMDARs.

1.2. Sources of extrasynaptic glutamate

Glutamate is the most common and important excitatory neurotransmitter that mediates synaptic signalling in the synaptic clefts of the mammalian brain. Nevertheless, it is also present in extrasynaptic regions. Glutamate reaching

extrasynaptic regions mainly comes from two sources, i.e. neuronal and astrocytic release.

1.2.1. Neuronal origin of extrasynaptic glutamate

1.2.1.1. Glutamate spillover

Extrasynaptic glutamate mainly originates from synaptic vesicular release and then spill out from the synaptic cleft. Glutamate usually is released into the synaptic cleft and rapidly cleared from the cleft by diffusion and uptake (Diamond and Jahr, 1997; Tong and Jahr, 1994). Its concentration profile in the synapse is tightly controlled by neuronal and astrocytic glutamate transporters. (Asztely et al., 1997; Diamond and Jahr, 2000; Rusakov and Kullmann, 1998). Therefore, glutamate released by a single action potential from boutons of a same neuron cannot diffuse out of the synaptic cleft (Arnth-Jensen et al., 2002). However, under several circumstances, glutamate can spill out of synapses and increase its concentration in extrasynaptic regions or even activate receptors at neighbouring synapses. This phenomenon is generally referred to as “glutamate spillover” (Asztely et al., 1997). First, when glutamate is released synchronously from multiple axons, even under low frequency it can cooperatively activate NMDARs of neighbouring synapses through the confluence of released glutamate (Arnth-Jensen et al., 2002; Scimemi et al., 2004). Secondly, when glutamate is released during high frequency synaptic activity, it can also break through the glutamate uptake system and activate extrasynaptic receptors (Semyanov and Kullmann, 2000; Semyanov and Kullmann,

2001). This implies that the concentration of extrasynaptic glutamate can be spatially and temporally determined by glutamate spillover reflecting neuronal activity.

Glutamate spillover mediates several types of synaptic modulation in many brain regions. In cerebellum, glutamate spillover from mossy fibre-granule cell synapses inhibits GABA release from GABAergic terminals of Golgi cells through activation of metabotropic glutamate receptors (mGluRs) (Mitchell and Silver, 2000). Similar heterosynaptic inhibition is also observed between hippocampal CA3-CA1 synapses and local GABAergic inputs (Min et al., 1999; Semyanov and Kullmann, 2000). Such heterosynaptic modulation is likely to boost the efficacy of active excitatory inputs by local disinhibition. Homosynaptic modulation mediated by glutamate spillover is also present at hippocampal mossy fiber-CA3 synapses (Min et al., 1998; Scanziani et al., 1997). Glutamate spill out from the synaptic cleft can activate extrasynaptic mGluRs on its immediate presynaptic bouton and inhibit subsequent glutamate release which provides a negative feedback mechanism for controlling synaptic transmission (Scanziani et al., 1997). A recent report showed that recruitment of extrasynaptic NMDARs via glutamate spillover contributes to the initiation of NMDA spikes in hippocampal CA1 pyramidal neurons (Chalifoux and Carter, 2011). These results suggest computational roles in neural circuits for extrasynaptic glutamate that originates from synaptic spillover.

1.2.1.2. Ectopic glutamate release

Ectopic glutamate release is another neuronal origin of extrasynaptic glutamate. Aside from the conventional synaptic exocytosis mechanism, vesicles can also fuse with the plasma membrane outside synaptic zones (ectopic sites) and release glutamate directly into extrasynaptic regions (Matsui and Jahr, 2003). This phenomenon has been shown in dendrites of neocortical pyramidal cells (Zilberter, 2000), cerebellar Purkinje cells (Shin et al., 2008a) , and mitral cells of the olfactory bulb (Castro and Urban, 2009; Christie and Westbrook, 2006). Ectopically released glutamate from the dendrite triggered by membrane depolarization can work as an autocrine agent that provides feedback regulation (Shin et al., 2008a), as well as activate neighbouring dendrites without direct synaptic connections (Castro and Urban, 2009; Christie and Westbrook, 2006). Ectopic glutamate release is also observed in cerebellar climbing fibres, olfactory receptor axons, and unmyelinated axons in white matter (Kukley et al., 2007; Matsui and Jahr, 2003; Thyssen et al., 2010; Ziskin et al., 2007). Glutamate released from ectopic sites of the axon activates astrocytic receptors rather than neuronal receptors at extrasynaptic regions and triggers both electrical and calcium activity. Thus it is an important mechanism for neural-glial communication.

1.2.1.3. Summary for neuronal origins of extrasynaptic glutamate

So far all the known neuronal sources of extrasynaptic glutamate are from vesicular release, synaptically and ectopically. The possible sources of extrasynaptic glutamate of neuronal origin are outlined in figure 1.4 b-d. Glutamate that originates from synaptic release reaches extrasynaptic areas only when spillover occurs. Spillover occurs when glutamate passes between nearby synapses during synchronous release (Fig. 1.4b) and when glutamate temporarily accumulates in extrasynaptic areas during high frequency release (Fig. 1.4c). Aside from synaptic spillover, direct release of glutamate into extrasynaptic regions via ectopic release from dendrites (Fig. 1.4d) and axons (Fig. 1.4e) is another source for extrasynaptic glutamate.

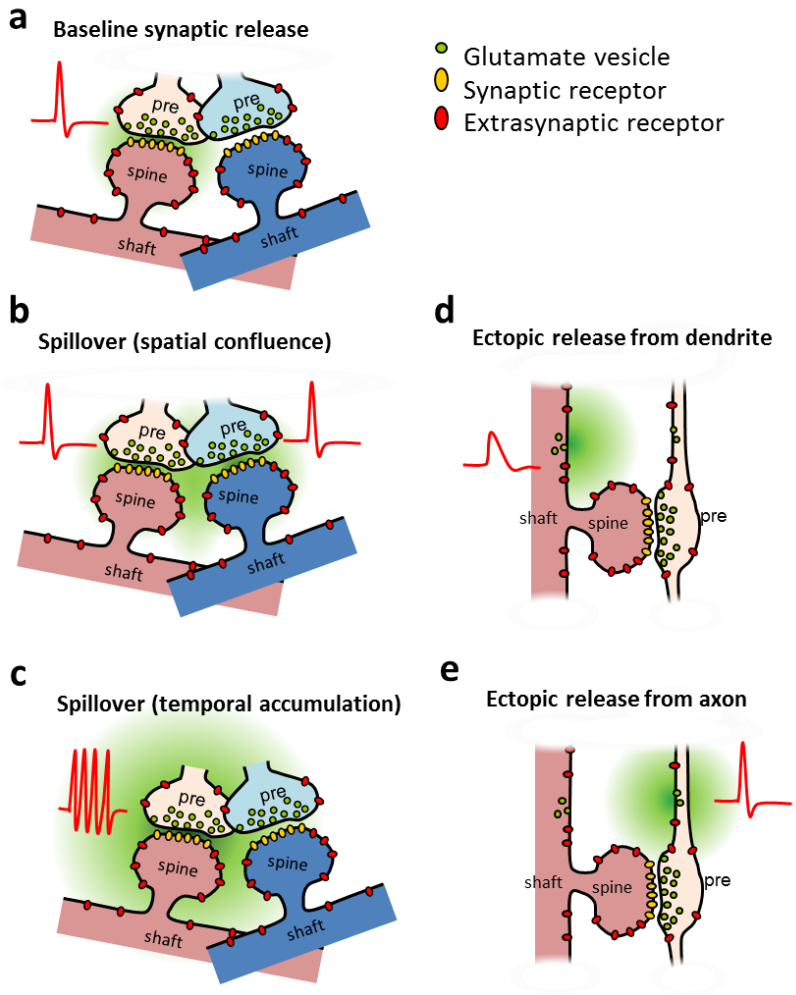

Figure 1.4 Neuronal origins of extrasynaptic glutamate

a, Glutamate released from baseline synaptic activity only activates synaptic receptors. Red trace indicates the action potential that triggers glutamate release from one of the presynaptic cells. **b and c,** Spillover of glutamate can be induced by two ways: during synchronous release, glutamate interflows between spatially close synapses and activates extrasynaptic receptors (**b**); during high frequency release, glutamate can be temporally accumulated in the extrasynaptic region (**c**). **d and e,** Ectopic release triggered by membrane depolarization*, e.g.* EPSP (the red trace in **d**), or action potential (the red trace in **e**) can directly release of glutamate into extrasynaptic region from dendrite (**d**) and axon(**e**).

1.2.2. Astrocytic origin of extrasynaptic glutamate

It has been shown in the early 1990s that, besides neurons, astrocytes can release glutamate and other amino acids under several pathological conditions such as anoxia and ischemia (Kimelberg et al., 1990; Nicholls and Attwell, 1990). Astrocytic glutamate release was later shown to be regulated by intracellular Ca^{2+} signalling which can be triggered by neuronal activity (Nedergaard, 1994; Parpura et al., 1994). Because there is no synaptic structure on the astrocytic membrane, glutamate released from astrocytes is considered extrasynaptic. Although the mechanisms underlying astrocytic glutamate release are still controversial (Hamilton and Attwell, 2010), they can be categorized in three major ways: 1) vesicular-mediated exocytotic release; 2) carrier(transporter)-mediated release; and 3) channel-mediated release.

1.2.2.1. Vesicular-mediated exocytotic release of glutamate

Although it is still under debate, evidence has shown that an astrocyte contains small vesicles (~30 nm in diameter) which have characteristics resembling synaptic vesicles in neurons (Bezzi et al., 2004). These vesicles express vesicular glutamate transporter 1 (VGLUT1)/VGLUT2, vesicle-associated membrane protein 2 (VAMP2)/VAMP3, and synaptotagmin 4/5/11 (Bezzi et al., 2004; Bowser and Khakh, 2007). VGLUTs are essential for loading glutamate into the vesicles, whereas VAMPs and synaptotagmins mediate Ca^{2+}-dependent exocytosis (Araque et al., 2000; Marchaland et al., 2008). Furthermore, the essential elements for forming the

SNARE complex, synaptosomal-associated protein 25 (SNAP25)/SNAP23 and syntaxin, are also expressed in astrocytes, implying that astrocytes are capable of sensing intracellular Ca^{2+} triggering glutamate exocytosis. Astrocytic glutamate released into extrasynaptic areas in such a manner targets presynaptic mGluRs (Perea and Araque, 2007) and NMDARs (Jourdain et al., 2007) or postsynaptic NMDARs (particularly GluN2B-containing NMDARs) (Angulo et al., 2004; Bezzi et al., 2004; D'Ascenzo et al., 2007; Fellin et al., 2004; Parri et al., 2001). The activation of presynaptic mGluRs and NMDARs modulates the synaptic release probability (Jourdain et al., 2007; Perea and Araque, 2007), whereas activation of post/extrasynaptic NMDARs on neurons (particularly GluN2B-containing NMDARs) generates slow inward currents (SICs) inducing synchronous firing of neurons (Angulo et al., 2004; D'Ascenzo et al., 2007; Fellin et al., 2004; Parri et al., 2001). SICs were shown to be exclusively mediated by NMDARs but not AMPARs confirming that glutamate which mediates SICs originates from the extrasynaptic area. However, the detailed mechanisms underlying the SIC-triggering release, such as the number of released vesicles and the membrane location at which release occurs etc., are still unclear and need to be further investigated.

1.2.2.2. Carrier (transporter)-mediated glutamate release

Under physiological conditions, extracellular glutamate is taken up by astrocytes via astrocytic glutamate transporters, excitatory amino-acid transporter 1 (EAAT1)

and EAAT2 (Tzingounis and Wadiche, 2007). Normally the uptake is powered by the cross membrane electrochemical gradient of Na^+ and K^+. Uptake of one glutamate molecule is accompanied by co-transport of 3 Na^+ and 1 H^+, and counter-transport of 1 K^+ (Tzingounis and Wadiche, 2007). In pathological conditions like ischemia or metabolic collapse, the electrochemical gradient of Na^+ and K^+ that maintain glutamate uptake can bedissipate and result in reversal of glutamate transport and the release of glutamate (Rossi et al., 2000; Szatkowski et al., 1990). However, since this only happens during severe brain ischemia, this type of mechanism is unlikely to contribute significantly to physiological astrocytic glutamate release.

The cystine-glutamate exchanger, or system x_c^-, is an antiporter that imports one extracellular cystine in exchange for one glutamate (McBean, 2002). This exchanger is mainly expressed in astrocytes (Pow, 2001) and was shown to contribute to major extrasynaptic glutamate (around 60 %) in physiological conditions in brain areas such as nucleus accumbens (Baker et al., 2002; Moran et al., 2005), striatum (Massie et al., 2011), and hippocampus (De Bundel et al., 2011). The uptake of extracellular cystine supports intracellular glutathione (GSH) synthesis and the reduction of oxidative stress which were believed to be the main functions of system x_c^- (Bannai, 1986). However, a recent study showed that genetic deletion of the system x_c^- gene in mice does not lower GSH content or increase oxidative stress in the hippocampus *in vivo* (De Bundel et al., 2011). Instead, the mice have deficits in spatial working memory which might be caused by a lower concentration of extrasynaptic glutamate in the hippocampus (De Bundel et al., 2011), suggesting

another major role for system x_c^- in controlling the extrasynaptic glutamate level (Warr et al., 1999). Astrocytic glutamate released from system x_c^- has been shown to activate mGluRs and modulate presynaptic release (Moran et al., 2005). Although work performed in acute brain slices showed that system x_c^- does not contribute to extrasynaptic glutamate unless an unphysiologically high concentration of cystine was present (Cavelier and Attwell, 2005), the same study showed that system x_c^--mediated glutamate release can also tonically activate NMDARs. Together, these studies indicate that the astrocytic system x_c^- plays a key role in modulating extrasynaptic glutamate concentration which can affect learning and memory.

1.2.2.3. Channel-mediated glutamate release

There are several types of channels in astrocytes that directly release glutamate through the pore of the channel. These channels have a common feature that their open channel pores are large and permeable to some organic molecules such as glutamate and adenosine 5'-triphosphate (ATP).

First, the $P2X_7$ purinergic receptor ($P2X_7R$) is a ligand-gated channel which opens in response to the binding of extracellular ATP (Burnstock, 2008). $P2X_7R$ is shown to generate efflux of glutamate and ATP from its open channel pore in cultured astrocytes (Duan et al., 2003). Later it was demonstrated in hippocampal slices that activation of $P2X_7R$ indeed triggers a sustained glutamate efflux and activates an NMDAR-dependent tonic current (Fellin et al., 2006). Furthermore, $P2X_7R$ is sensitive

to extracellular Ca^{2+} (Duan et al., 2003). Lowering extracellular Ca^{2+} concentration potentiates the sustained tonic glutamate efflux from $P2X_7R$ (Fellin et al., 2006). This suggests that $P2X_7R$ on astrocytes can serve as a sensor integrating extracellular ATP and Ca^{2+} signals, and translating them to a glutamate signal. Further study on the physiological relevance of such sustained glutamate efflux is needed.

Hemichannels are large pore ion channels that were also shown to mediate glutamate release in cultured astrocytes (Ye et al., 2003). They are defined as halves of gap junction channels that do not form intercellular junctions but open to the extracellular space (Thompson and Macvicar, 2008). Both connexin 43 and pannexin 1 have been proposed to form functional hemichannels and account for glial release of glutamate and ATP (Iglesias et al., 2009; Ye et al., 2003). The open probability of hemichannels is highly sensitive to extracellular calcium (Spray et al., 2006; Thimm et al., 2005). Recently it was shown in hippocampal astrocytes that hemichannels detect extracellular Ca^{2+} depletion due to neuronal activity and release ATP to trigger Ca^{2+} waves in the astrocytic network (Rusakov, 2012; Torres et al., 2012). Although whether glutamate, accompanied by ATP, is released was not investigated in this work, it is likely that glutamate efflux from hemichannels might also play a role in response to changes in extracellular Ca^{2+} concentrations. Indeed, in a slice model of Alzheimer's disease, pathogenic Aβ can trigger hemichannel-mediated glial release of glutamate and ATP that induce neuronal death (Orellana et al., 2011). Although the direct regulation mechanisms are still largely unknown, these results suggest

that hemichannel-mediated glutamate release can play important roles both in physiological and pathological conditions.

Volume-regulated anion channels (VRACs) on astrocytes were also shown to release glutamate, as well as aspartate and taurine, during cell swelling in ischemia conditions *in vivo* (Kimelberg et al., 1990; O'Connor and Kimelberg, 1993). Such release was shown to be Ca^{2+}-independent (O'Connor and Kimelberg, 1993). However, it can be also triggered by ATP-induced cell swelling in a Ca^{2+} dependent manner (Takano et al., 2005). Among many types of anion channels in VRACs families, volume-sensitive outward rectifying chloride channels (VSORs) and maxi-anion channels were shown to contribute to the swelling-induced glutamate release in cultured astrocytes (Liu et al., 2006). VSORs also mediate cell swelling-independent glutamate release in response to an inflammatory peptide, bradykinin (Liu et al., 2009), suggesting that the VSORs-mediated release does not happen solely in pathological conditions with cell swelling. Optogenetic activation of solely photoactivatable Ca^{2+}-permeable ion channels in cultured astrocytes induces glutamate release from anion-channels without other external agonists (Li et al., 2012). This again suggests that anion channel-mediated glutamate release (Ca^{2+}-dependent or -independent) from astrocytes has a physiological role *per se* in glia-to-neuron as well as glia-to-glia communication. In most studies, these anion channels were identified based on their electrophysiological and pharmacological properties. However, the molecular identities of these anion channels are still largely unknown. Bestrophin-1, a Ca^{2+}-activated anion channel that is expressed in cortical astrocytes

could be a possible substrate for anion-mediated glutamate release (Park et al., 2009).

Apart from the induced glutamate release, there is a continuous and non-vesicular release of glutamate from hippocampal astrocytes that contributes to the basal ambient glutamate concentration (Cavelier and Attwell, 2005; Jabaudon et al., 1999; Le Meur et al., 2007). This tonic release of glutamate is not sensitive to NPPB (5-nitro-2-(3-phenylpropylamino) benzoic acid) and tamoxifen, which were found to block VRACs. However, another anion channel blocker, DIDS (4,4'-diisothiocyanostilbene-2,2'-disulphonic acid) reduces the tonic glutamate release, suggesting anion channels other than VRACs might be involved in this tonic release (Cavelier and Attwell, 2005).

1.2.2.4. Summary for astrocytic origins of extrasynaptic glutamate

As discussed above, astrocytes are able to release glutamate via a variety of mechanisms. All the possible sources and ways to induce glutamate release are summarized in figure 1.5. However, there are still many controversies concerning these reported possible mechanisms (Hamilton and Attwell, 2010). This may be due to the limitations of the available pharmacological tools, as many anion channel inhibitors are not sufficiently specific and were also shown to block hemichannels (Eskandari et al., 2002; Ye et al., 2009). Besides, the methods to stimulate glutamate release are also quite diverse and sometimes not physiologically relevant (Hamilton

and Attwell, 2010). It will be important to know whether the specific release mechanisms only operate in response to particular stimulation paradigms. Furthermore, many of the seminal studies addressing astrocytic glutamate release were performed in cell culture systems (Nedergaard, 1994; Parpura et al., 1994). It will be necessary to know whether contradictory findings were due to different culture conditions and whether these mechanisms also apply to *ex-vivo* brain slice preparations and *in vivo*.

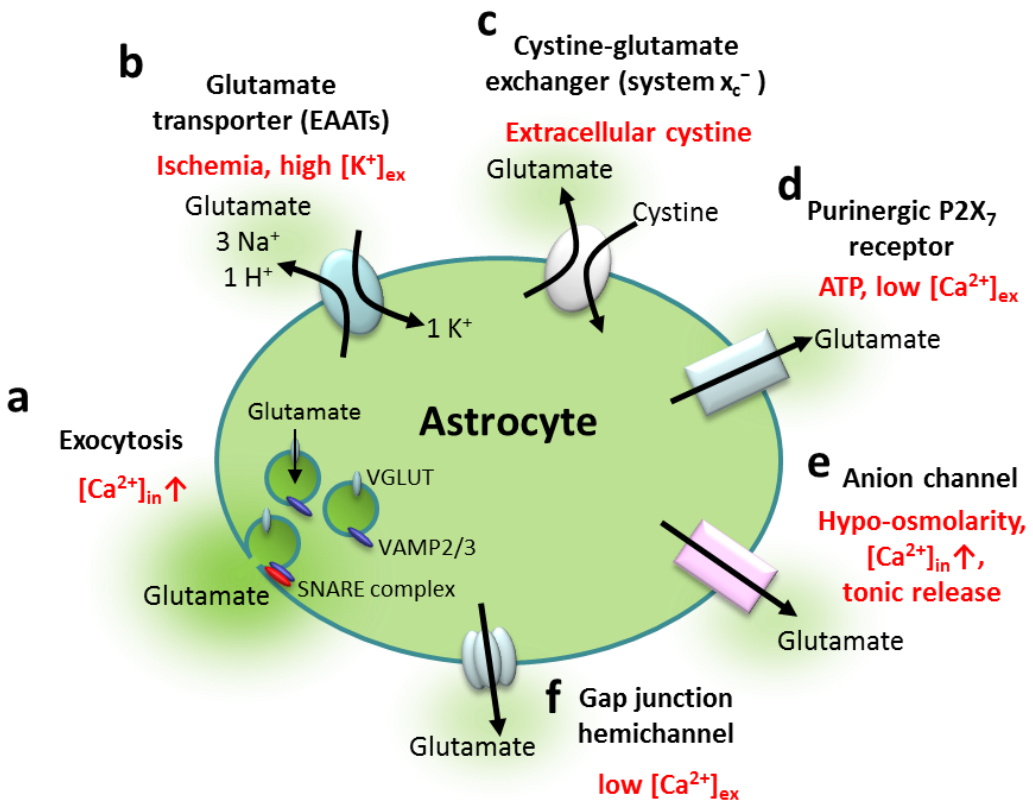

Figure 1.5 Astrocytic origins of glutamate release

a, Ca^{2+}-mediated vesicular exocytosis. Glutamate uptake in the vesicles though VGLUT1/2. Astrocytes also express essential elements for forming SNARE complex that mediates exocytosis in response to intracellular Ca^{2+} rise ($[Ca^{2+}]_{in}$ ↑) **b,** Reversal of glutamate transporter (EAATs) only happens under severe ischemia condition that induces built up in extracellular K^+ ($[K^+]_{ex}$). **c,** Cystine-glutamate exchanger (system x_c^-) takes up an extracellular cystine in exchange for release a glutamate molecule. **d,** Purinergic P2X7 receptor is activated by extracellular ATP and is enhanced when lowering extracellular Ca^{2+} (low $[Ca^{2+}]_{ex}$). **e,** Volume-regulated anion channel is activated by cell-swelling induced by hypo-osmolarity, as well as activated by intracellular Ca^{2+} signalling. **f,** Gap junction hemichannel is opened in response to low $[Ca^{2+}]_{ex}$. Mechanisms to induce astrocytic glutamate release are outlined in red.

1.3. Extrasynaptic glutamate signalling via NMDARs

It was long believed that neuronal computation is conducted exclusively through synaptic transmission between neurons. Whether extrasynaptic neurotransmitters carry any meaningful information remains elusive. In this chapter, I will introduce the dynamics of extrasynaptic glutamate and show potential mechanisms of how neuronal NMDARs detect and convert such dynamics into meaningful signalling.

1.3.1. Ambient extrasynaptic glutamate concentration

Unlike glutamate released in the synaptic cleft, which can reach millimolar (mM) or sub-millimolar concentrations, the concentration of baseline ambient extrasynaptic glutamate is relatively low. In typical *in viv*o microdialysis experiments, the concentration of extracellular, presumably extrasynaptic, glutamate was shown to range from 0.2 to 7 µM (Cavelier et al., 2005). Studies using enzyme-based electrochemical sensors *in vivo* even report steady-state glutamate concentrations as high as 45 µM (range from 2 to 45 µM) (Dash et al., 2009; Hascup et al., 2011; Rutherford et al., 2007). On the other hand, Herman and Jahr (2007) used patch-clamp recording of neuronal NMDAR currents as a sensor for glutamate in brain slices and reported only 25 – 50 nM of ambient extracellular glutamate (Herman and Jahr, 2007; Herman et al., 2011). Theoretical calculations also suggested 30 – 50 nM as the baseline ambient glutamate concentration (Cavelier and Attwell, 2005; Zheng et al., 2008). Such discrepancies between reported values might be due to the

methods used. Since every method has its own drawbacks the concentration of ambient glutamate is still not conclusive.

Theoretically, the baseline ambient extrasynaptic glutamate concentration is determined by the balance between tonic release and uptake of glutamate (Cavelier and Attwell, 2005; Diamond and Jahr, 1997; Tong and Jahr, 1994). The cystine-glutamate exchanger, system x_c^-, was shown to contribute most of the ambient glutamate *in vivo* in many brain areas including hippocampus (Baker et al., 2002; De Bundel et al., 2011; Massie et al., 2011). However, in hippocampal slices, glutamate uptake is so efficient that it is not overwhelmed during high-frequency synaptic release (Diamond and Jahr, 2000). Only when glutamate transporters are blocked was the enhanced tonic release from system x_c^- unmasked (Cavelier and Attwell, 2005; Jabaudon et al., 1999), suggesting that the ambient glutamate concentration is set by the efficiency of uptake rather than the rate of tonic release. Conversely, in a recent study, knocking down the functional system x_c^- in mice decreased the amount of extrasynaptic glutamate in hippocampus, even though the expression of glutamate transporters was not affected, suggesting that the ambient glutamate concentration in wild type animals is maintained by tonic glutamate release from system x_c^- (De Bundel et al., 2011). Whether the release or the uptake system of glutamate was predominates in regulating ambient glutamate concentration remains an important question to be answered.

1.3.2. Dynamics of extrasynaptic glutamate

Instead of a constant level of ambient glutamate, the concentration of extracellular glutamate changes dynamically. By using *in vivo* microdialysis and amperometric approaches, it was shown that extracellular glutamate is able to reflect the real-time neuronal network activities and the behavioural state of the animals (Baker et al., 2002; Dash et al., 2009; Del Arco et al., 2003; Mattinson et al., 2011; Rutherford et al., 2007). For example, it was shown in freely moving rats that the extracellular glutamate concentration increased during the waking state whereas it decreased during non- rapid eye movement sleep (Dash et al., 2009). The change in the extracellular concentration is suggested to be an index of overall extrasynaptic glutamate released from neurons and astrocytes (Del Arco et al., 2003). However, it was also argued that these invasive methods might damage the cells and blood vessels, affecting the real extracellular glutamate concentration. These approaches also have limitations in spatiotemporal resolution, because the sensors have sizes of tens to hundreds of μm, and need seconds to minutes to read out the concentration (Mattinson et al., 2011).

To overcome these limitations, several fluorescent sensors have been developed to directly monitor the dynamics of extracellular glutamate in culture system (Hires et al., 2008; Namiki et al., 2007; Okumoto et al., 2005). Among these sensors, glutamate (E) optical sensors (EOS) were the first used to evaluate extrasynaptic glutamate dynamics *in vivo*, and showed that cortical extrasynaptic glutamate concentrations increased due to glutamate spillover in response to a tactile

stimulation of the hind paw (Okubo et al., 2010). These results, consistent with the findings using the microdialysis approach, indicate that extrasynaptic glutamate dynamics can reflect neuronal activity under physiological conditions. Besides, other origins of glutamate release introduced in the previous section can also bring extra dynamics to extrasynaptic glutamate concentrations.

1.3.3. Detection of extrasynaptic glutamate by NMDARs

The glutamate EC_{50} (effective concentration required to induce a 50% effect) is about 2 μM for NMDARs and 10 μM for most of the mGluRs. The EC_{50}s for NMDARs and mGluRs are almost 50 to 500 times more potent than AMPARs (EC_{50} = ~ 100 - 1000 μM) (Featherstone and Shippy, 2008), explaining the reason why extrasynaptic glutamate is detected mostly by NMDARs and mGluRs (Featherstone and Shippy, 2008). Potentially all the extrasynaptic glutamate originating from different sources can be detected by neuronal extrasynaptic NMDARs. NMDAR-mediated currents activated by glutamate spillover and astrocytic tonic and phasic glutamate release have been recorded by the whole-cell patch-clamp technique.

A tonic current mediated by NMDARs has been observed upon prolonged depolarization in hippocampal pyramidal cells, suggesting that neurons are able to detect low levels of baseline ambient glutamate through NMDARs (Cavelier and Attwell, 2005; Dalby and Mody, 2003; Herman and Jahr, 2007; Jabaudon et al., 1999; Le Meur et al., 2007; Sah et al., 1989). It was later found that extrasynaptic but not

synaptic NMDARs are activated by ambient glutamate and the tonic current is sensitive to GluN2A- and GluN2C/D-containing NMDAR selective blockers (Le Meur et al., 2007). Although Sah and colleagues showed that tonic activation of NMDARs by ambient glutamate enhances neuronal excitability in hippocampal slices (Sah et al., 1989), this strong effect of ambient glutamate was not seen in the following reports (Cavelier and Attwell, 2005; Jabaudon et al., 1999; Le Meur et al., 2007). Therefore whether this tonic NMDAR-mediated current has any physiological impact remains unanswered (Featherstone and Shippy, 2008).

Slow inward current (SIC) induced by transient astrocytic glutamate release has also been recorded in hippocampal pyramidal neurons (Angulo et al., 2004; Fellin et al., 2004). Specifically, SIC has a slow rise time around 100 ms, which is much slower than excitatory postsynaptic current (EPSC) (rise time < 10 ms), suggesting that it is mediated by extrasynaptic release which takes more time to diffuse before binding with its receptors. Indeed, SIC is sensitive to ifenprodil and APV but not non-NMDAR blockers, indicating that it is mediated by extrasynaptic GluN2B-containing NMDARs (Fellin et al., 2004; Pirttimaki et al., 2011). Besides, SIC also has common voltage-dependent block by extracellular Mg^{2+} like synaptic NMDAR currents (Angulo et al., 2004; Fellin et al., 2004). SIC was shown to induce synchronous neuronal activity and promote burst firing (Fellin et al., 2004; Pirttimaki et al., 2011). Furthermore, the frequency of SIC exhibits plasticity resulting in the enhancement of neuronal burst activity (Pirttimaki et al., 2011), which suggests that the extrasynaptic NMDAR is an active player in neuro-gial communication.

Altogether the evidence suggests that extrasynaptic NMDARs are able to detect the extracellular glutamate dynamics reflecting neuronal and astrocytic network activity. However, extrasynaptic NMDARs have a similar voltage-dependent block by Mg^{2+}, but in order to recruit more NMDARs, in most of the studies experiments were performed in non-physiological conditions, i.e. in Mg^{2+}-free solution or under artificially prolonged depolarizing membrane potential (Arnth-Jensen et al., 2002; Cavelier and Attwell, 2005; Le Meur et al., 2007; Scimemi et al., 2004). Under physiological conditions, binding with glutamate alone does not produce current through NMDARs, indicating that apart from the presence of extrasynaptic glutamate, a depolarizing event is needed to activate neuronal NMDARs and generate Ca^{2+} influx.

1.3.4. Depolarization is required for 'readout' of extrasynaptic NMDAR activation

As mentioned above (Chapter 1.1.3), the activation of NMDARs requires not only agonists and co-agonists, but also membrane depolarization to relieve Mg^{2+} block. Depolarizing events in neurons are usually initiated by activation of synaptic AMPARs which are able to induce a Na^{+} inward current generating an EPSP under resting membrane potential. Therefore during glutamatergic synaptic events, the EPSP contributed by AMPARs can relieve Mg^{2+} block of NMDARs generating Ca^{2+} influx (Fig. 1.6a) (Bloodgood and Sabatini, 2007a; Nevian and Sakmann, 2006). However, unlike usual synaptically-released glutamate which reaches millimolar

concentrations in the synaptic clefts and thus activating low-affinity AMPARs, extrasynaptic glutamate concentration between sub-micromolar to tens of micromolar range is not high enough to involve AMPARs, providing depolarization (Rusakov and Kullmann, 1998). Without depolarization events, extrasynaptic signalling mediated by NMDARs stays silent.

In addition to EPSPs, action potentials (AP) are another major depolarizing event in neurons. A classical view of the AP is that it is generated in the axon initial segment when the EPSP reaches the AP-generating threshold. The AP then propagates forward to the axon terminal to trigger neurotransmitter release. However, APs also propagate backward into dendrites (called backpropagating APs, bAPs). bAPs contribute to functional changes associated with synaptic plasticity (Magee and Johnston, 1997; Markram et al., 1997; Stuart and Hausser, 2001a) and homeostatic changes in dendritic excitability (Campanac et al., 2008; Losonczy et al., 2008). In dendrites, bAPs not only trigger Ca^{2+} entry mainly by activating voltage-dependent Ca^{2+} channels (VDCCs) (Sabatini and Svoboda, 2000), but also enhance synaptic NMDAR mediated Ca^{2+} influx by removal of the voltage-dependent Mg^{2+} block (Nevian and Sakmann, 2004; Schiller et al., 1998; Yuste and Denk, 1995). Therefore, potentially, the bAP could also be a good candidate to provide the depolarization that recruits extrasynaptic NMDARs.

Simple illustrations are made in figure 1.6 to explain the hypothetical impact of the depolarizing event on reading out the extrasynaptic glutamate signalling. For example, glutamate from spillover is able to bind to extrasynaptic NMDARs on the

immediate postsynaptic neuron as well as on the neighboring neuron (Fig. 1.6b and c). The extrasynaptic NMDARs on the immediate postsynaptic neuron gain the depolarization from activation of synaptic AMPARs, and hence generate Ca^{2+} influx. AMPARs on the neighbouring neuron are not activated by the low concentration of spillover glutamate and do not provide depolarization, so the extrasynaptic NMDARs stay silent. However, when depolarizing events (here a bAP) occur on the neighbouring neuron coinciding with the glutamate spillover, the Mg^{2+} block can be relieved from extrasynaptic NMDARs generating Ca^{2+} influx (Fig. 1.6e). Such depolarizing events possibly provide 'readout' for extrasynaptic signalling mediated by NMDARs. Moreover, in addition to glutamate spillover, glutamate from tonic and transient astrocytic release that binds with extrasynaptic NMDARs potentially also requires depolarization for readout (Fig. 1.7). The readout mechanisms for extrasynaptic glutamate signalling mediated by NMDARs, however, remain elusive. Therefore, the main object of this study is to investigate whether and how the physiological depolarizing event, here bAP, provides 'readout' for the dynamics of extrasynaptic glutamate.

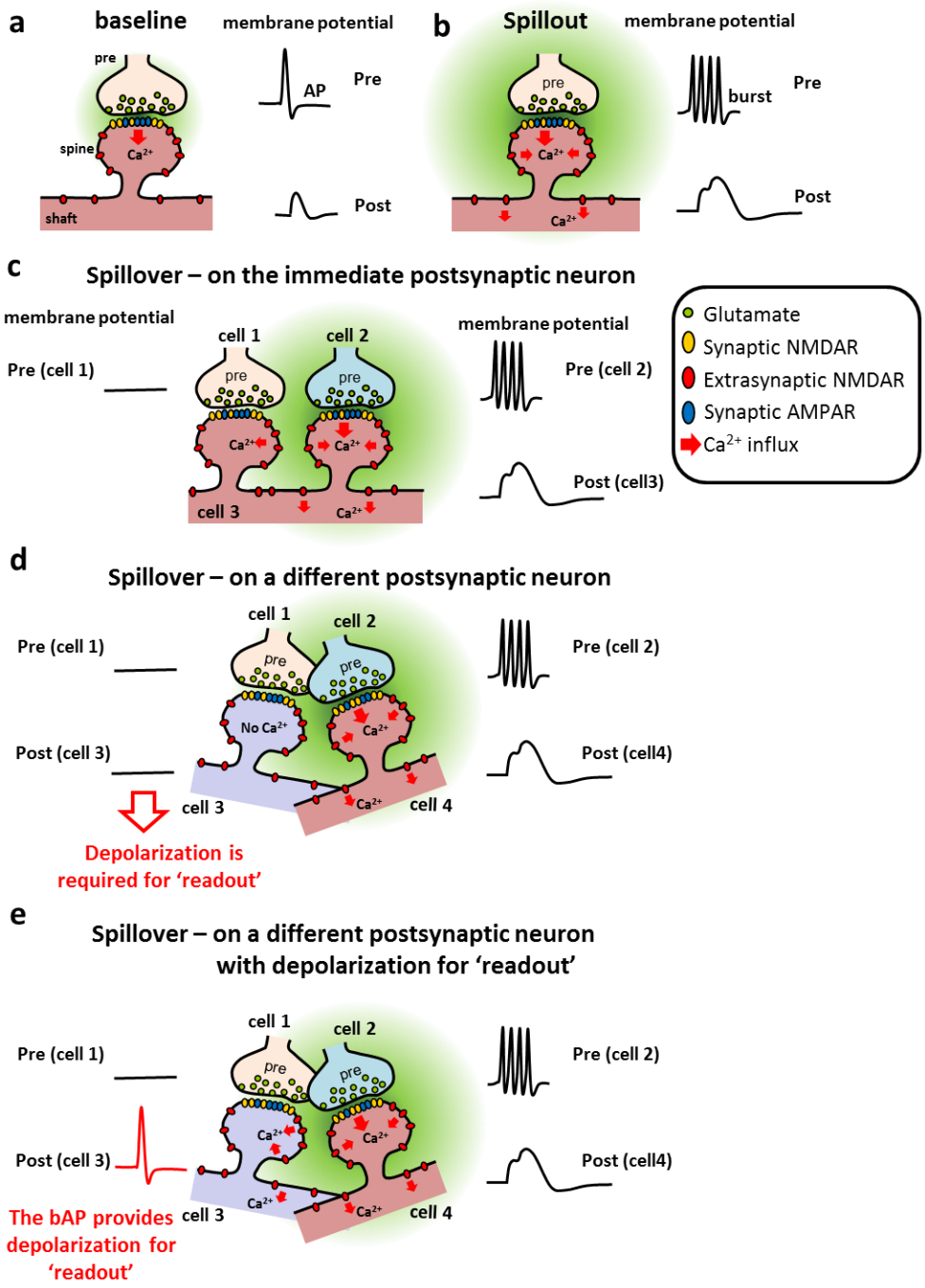

Figure 1.6 Depolarization is required for 'readout' of glutamate spillover

a to c, Schemes for glutamatergic signalling targets to one postsynaptic cell. Glutamate released from presynaptic (pre) bouton binds with synaptic AMPARs and synaptic NMDARs on the immediate postsynaptic cell under baseline condition (**a**), and further binds with extrasynaptic NMDARs when glutamate spillout (**b**) and spillover (**c**). Activation of AMPARs generates EPSP (black trace) which relieves the Mg^{2+} block of NMDARs producing Ca^{2+} influx

(red arrows). **d and e,** Hypothetical schemes for glutamate spillover to the neighboring neuron without (**d**) and with (**e**) a depolarizing event for 'readout'. Glutamate released from cell2 can bind with NMDARs on spines of cell3 but cannot generate Ca^{2+} influx due to lacking membrane depolarization for 'readout' (**d**). When a depolarizing event (ex: a bAP) coincidently occurs in cell3, extrasynaptic NMDARs can be relieved from the Mg^{2+} block and generates Ca^{2+} influx (**e**).

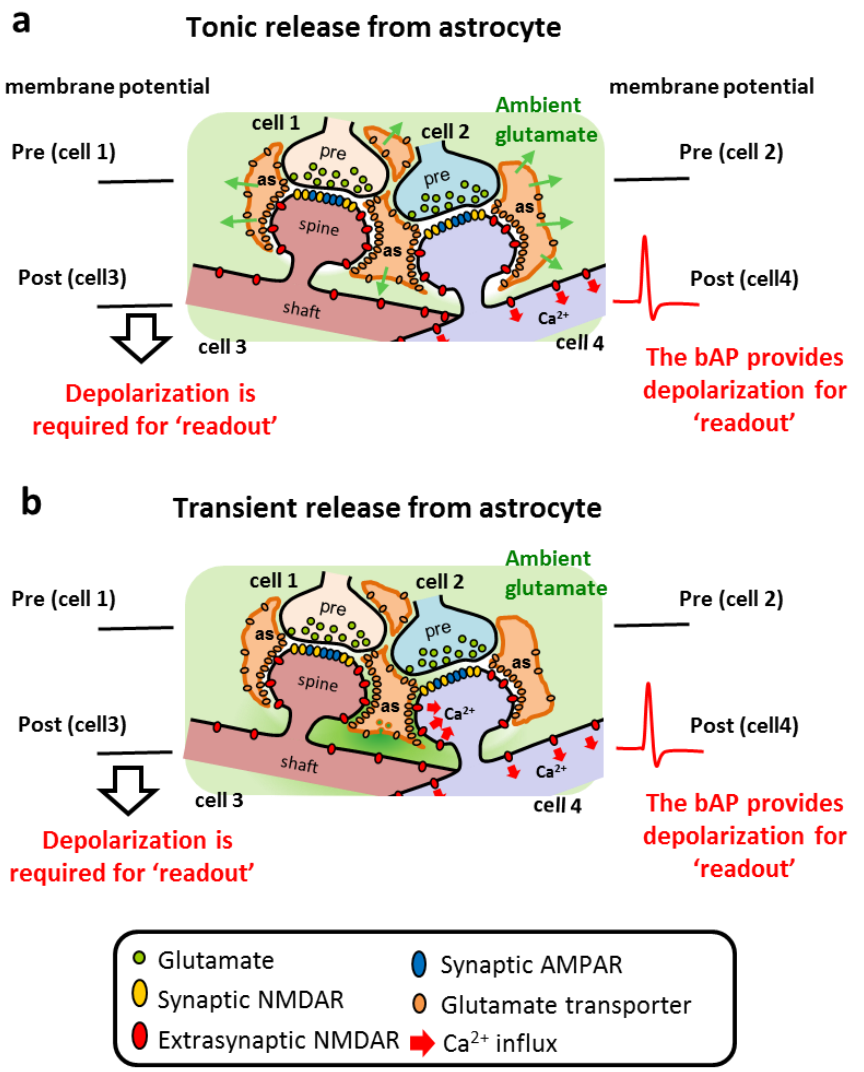

Figure 1.7 Depolarization is required for 'readout' of tonic and transient glutamate release from astrocytes

a, A hypothetical scheme for NMDAR-mediated detection of ambient glutamate released from astrocyte (as). The ambient glutamate-bound extrasynaptic NMDARs generate Ca^{2+} influx in cell4 when 'readout' is triggered by depolarization (here, a bAP), whereas cell3 stays silent. The ambient glutamate is indicated by green background. Green arrows indicate tonic glutamate release. **b,** A hypothetical scheme for NMDAR-mediated detection of transient glutamate released from astrocyte. Transient glutamate release (the green gradient) from astrocytes also binds with extrasynaptic NMDARs. Only when 'readout' is triggered by depolarization NMDARs generate Ca^{2+} influx (cell4), otherwise the cell stays silent (cell3).

1.4. Aims of the current study

The overarching hypothesis of this thesis is that extrasynaptic NMDARs detect extracellular glutamate and provide a readout of this during depolarizing events. Within this the specific aims are:

1. To test whether a physiological depolarization event, here bAP, enables ambient glutamate-bound extrasynaptic NMDARs and generates Ca^{2+} entry.
2. To test whether depolarization provided by bAP triggers 'readout' for extrasynaptic NMDAR-mediated detection of local rises of extracellular glutamate.
3. To build a theoretical model of tonic activated NMDAR conductance and test whether the model is able to reproduce the experimental findings on bAP-evoked Ca^{2+} entry.
4. To test whether burst firing of bAPs triggers larger 'readout', generating more extrasynaptic NMDAR-mediated Ca^{2+} entry.
5. To test whether activation of extrasynaptic NMDARs during repeated burst firing of bAPs (theta-burst-firing) triggers neuronal plasticity and modulates synaptic inputs.

Chapter 2: Materials and Methods

2.1. Introduction

In this study, I address the question of how hippocampal CA1 pyramidal cells communicate via NMDARs and extrasynaptic glutamate. Experiments were done in acute hippocampal slices from mice and rats. There are several benefits of using acute hippocampal slices to study the questions posed above. First, the properties of synaptic transmission and connections onto CA1 pyramidal neurons are well studied. Secondly, it is easy to superfuse and rapidly exchange the solution containing different pharmacological tools (usually in 3-5 min), while the slice is supplied with nutrition and oxygen to maintain the health of the tissue. Thirdly, electrophysiology and two-photon imaging can be easily combined and recorded simultaneously.

To monitor NMDAR activities in apical oblique dendrites of CA1 pyramidal cells during bAPs, I combined whole-cell patch-clamp recording and two-photon calcium imaging. Therefore, I could control the cell membrane potential and acquire fluorescent signals from subcellular structures simultaneously. Two-photon calcium imaging was performed by using a two-photon scanning microscope equipped with an ultra-fast, pulsed (<140 fs at peak) tunable laser tuned to 810 or 830 nm. CA1 pyramidal cells were filled with Alexa Fluor 594 (20-50 μM) to reveal the morphology and Fluo-4 (250 μM) for calcium imaging. bAPs were triggered by somatic current injection. Intrinsic membrane properties were also monitored by whole-cell

recording. Extracellular electrical stimulation via microelectrode, two-photon and single-photon photolysis of 4-Methoxy-7-nitroindolinyl (MNI)-caged L-glutamate were performed in some sets of experiments to mimic glutamate released from different synaptic and extrasynaptic origins.

2.2. Animals

Male Sprague–Dawley (SD) rats, aged 21 to 35 days (p21 –p35), were used in most of the experiments. Rats were kept under controlled environmental conditions (24–25 °C; 50–60% humidity; 12 h light/dark cycle) with free access to food and filtered water.

Two types of genetically- modified mice were also used:

1) CA1-GluN1 (CA1-NR1) KO mice [GluN1 (NR1) *fl/fl; CaMKII-Cre*] and littermate controls [GluN1 *fl/fl*], age 42 to 49 days. In this mouse line, NMDARs were specifically knocked-out in CA1 pyramidal cells at this age (Tsien et al., 1996). The CA1 pyramidal cells of these mice still preserve place-related activity. However, the spatial specificity of individual place fields is significantly reduced. The coordinated firing of pairs of neurons at similar spatial locations was also shown to be defected (Tsien et al., 1996).

2) A triple transgenic line, CA3-TeTX mice [*KA1-Cre/+*; *TetO-TeTX/+*; *αCaMKII-loxP-STOP-loxP-tTA/+*], age 42 to 49 days. In this mouse line, tetanus toxin (TeTX) light

chain was expressed selectively in CA3 pyramidal cells and temporally controlled by doxycycline (Dox) diet. TeTX is an endopeptidase targeting to VAMP2, which is essential for neurotransmitter release from synaptic terminals. Therefore, synaptic transmission from CA3 to CA1 pyramidal cells is blocked in CA3-TeTX mice with Dox-off state for more than 3 weeks (Nakashiba et al., 2008). These mice have defects in the consolidation of contextual fear memory. The defect might result from the reduction of intrinsic frequency of sharp-wave ripples driven by CA3 pyramidal cells in CA1 area. Moreover, the coordinated reactivation of CA1 cell pairs associated with ripples is also reduced (Nakashiba et al., 2008).

All experiments were performed in accordance with the RIKEN regulations and the Home Office regulations under the Animal (Scientific Procedures) Act, 1986.

2.3. Hippocampal slice preparation

Transverse slices were prepared from the different animals mentioned above. Animals were anaesthetised with volatile anaesthetic 2-bromo-2-chloro-1,1,1-trifluroethane (halothane) and decapitated. The brain was removed, chilled with ice-cold solution (cutting solution) containing (mM): 75 Sucrose, 87 NaCl, 2.5 KCl, 0.5 $CaCl_2$, 1.25 NaH_2PO_4, 7 $MgCl_2$, 25 $NaHCO_3$, 1 Na-Ascorbate, and 11 D-glucose. Hippocampi from both hemispheres were isolated and placed in an agar (8%) block with anterior part of hippocampus facing upward (Fig. 2.1a). Transverse slices with thickness of 350 μm were cut with an angle of 30^o perpendicular to the long-axis

(septotemporal axis) with a vibroslicer (Fig. 2.1e) (Microm HM 650 V, Thermo Fisher Scientific Inc., USA). Only slices from the middle one-third part of hippocampus were collected (Fig. 2.1f). They were left to recover for 20 to 30 min at 34°C in a submerged chamber in cutting or storage solution containing (mM): 127 NaCl, 2.5 KCl, 1.25 NaH_2PO_4, 1 $MgCl_2$, 1 $CaCl_2$, 25 $NaHCO_3$, and 11 D-glucose. Then they were transferred and incubated on either an interface- or submerged-type chamber (mostly submerged-type) at room temperature for at least 1 hour for recovery with storage solution. After that, the slices were transferred to the recording chamber and were continuously superfused at 33-34^{o}C with ACSF containing (mM): 127 NaCl, 2.5 KCl, 1.25 NaH_2PO_4, 1 $MgCl_2$, 2 $CaCl_2$, 25 $NaHCO_3$, and 11 D-glucose. All solutions were saturated with 95% O_2 and 5% CO_2. Osmolarity was adjusted to 298 ± 3 mOsm. The slices were used up to 8 hours after slice preparation.

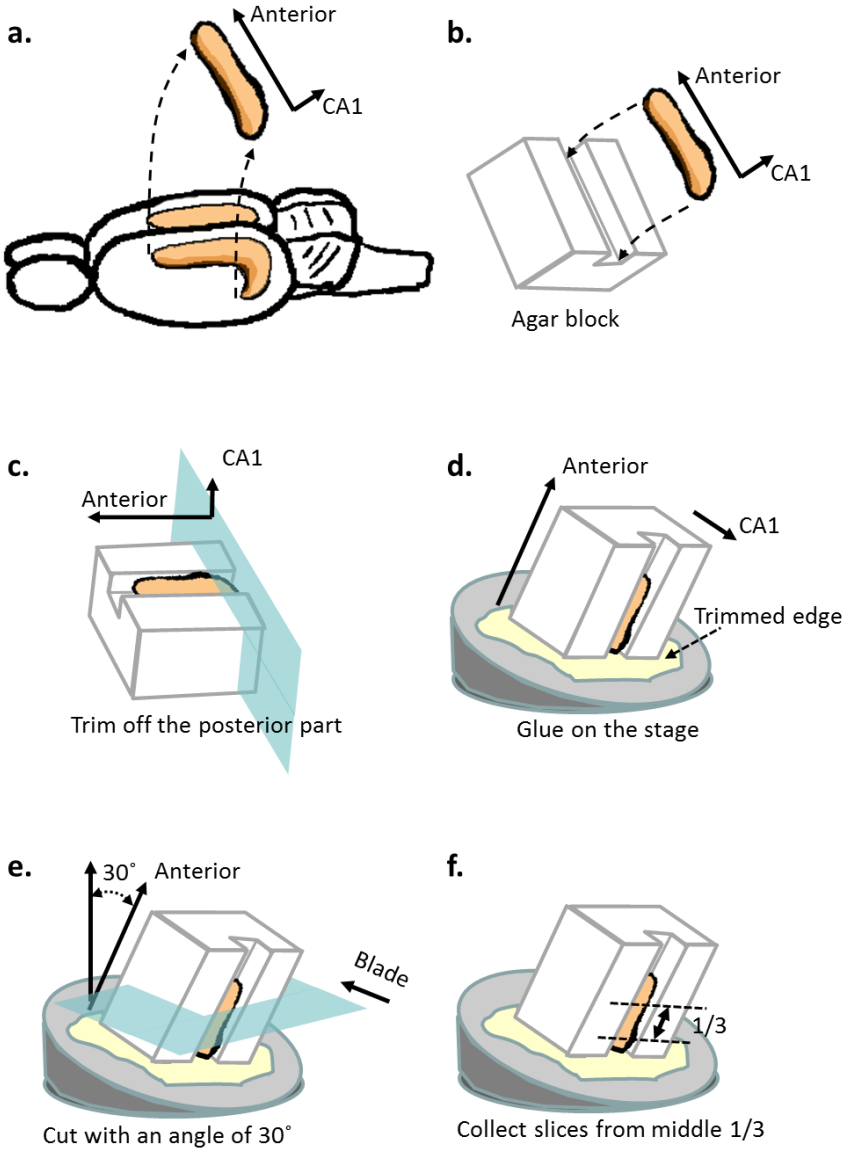

Figure 2.1 Procedures for transverse hippocampal slice preparation

a, The hippocampus was isolated from the inside of the cortical mantle. **b,** The isolated hippocampus was placed in the groove of an agar block with the anterior part facing upward and CA1 region facing outside. **c,** The 1/4 posterior part of hippocampus was trimmed off to create a flat interface. **e.** The trimmed age then was glued on a metal stage. **d,** The trimmed age then was glued on a metal stage. **e,** The slices were cut with an angle of 30˚ perpendicular to the long-axis of the hippocampus. **F,** Only slices cut from the middle 1/3 part of the hippocampus were collected.

2.4. Blockage of vesicular/synaptic release with bafilomycin A1

In order to block all the synaptic release of neurotransmitters, bafilomycin A1 was used to prevent packing of neurotransmitters into synaptic vesicles. Bafilomycin A1 is an antibiotic that inhibits vacuolar H^+-ATPase with a high degree of specificity (Drose and Altendorf, 1997). Because the proton gradient is lost with vacuolar H^+-ATPase blocked in synaptic vesicles, the ability of VGLUT to transport glutamate into synaptic vesicles is also lost. Glutamate thus does not enter synaptic vesicles and cannot be released after such treatment.

Instead of recovery at room temperature, the slices were incubated at 34°C in a miniature submerged incubation chamber (3 ml) (Fig. 2.2) for another 2.5 hour in ACSF containing 4 μM of bafilomycin A1. Slices were then incubated at room temperature before transferring to recording chamber superfused with ACSF without bafilomycin A1. The effect of bafilomycin A1 can last for at least 3 to 4 hours. No recovery of synaptic transmission was observed in this period. The control slices for this set of experiments were incubated in the same conditions but without bafilomycin A1. For testing the effect of bafilomycin A1, whole-cell spontaneous and evoked glutamatergic EPSCs were recorded via whole-cell patch-clamp recording with a holding potential at -70 mV. The evoked synaptic release of glutamate was induced by electrical stimulation of Schaffer collaterals in CA1 area via a bipolar stainless steel electrode more than 200 μm away from the recorded neurons. There were no spontaneous EPSCs and evoked EPSC in the bafilomycin A1-treated slices even with a stimulation current 10 times larger than in control slices (Fig. 3.6).

2.5. Local synaptic stimulation and finding the active spine

Local synaptic stimulation was done with an extracellular glass pipette (2−3 µm tip) filled with 1M NaCl. To monitor the location of the pipette, 5 µM Alexa Fluor 594 was also added to the solution in the pipette. The pipette then was positioned 5 to 20 µm from an apical oblique dendrite of the recorded neuron (Yasuda et al., 2004). The neuron was voltage-clamped at -40 mV in absence of AMPA receptor antagonists. Then we identified spines which responded with Ca^{2+} transients to a train of 5 stimulus pulses (0.2-5 V, 200 µs) at 50 Hz to assure glutamate release (Fig. 4.1). Then the AMPA receptors were blocked. The cells were held in current clamp and three types of measurements were done in the dendrite and the spine: (1) Ca^{2+} transients in response to a bAP; (2) Ca^{2+} response to synaptic stimulation; and (3) a response to the bAP and 'synaptic' stimulation combined. In protocol (3) bAPs were initiated 70 ms after the end of synaptic stimulation.

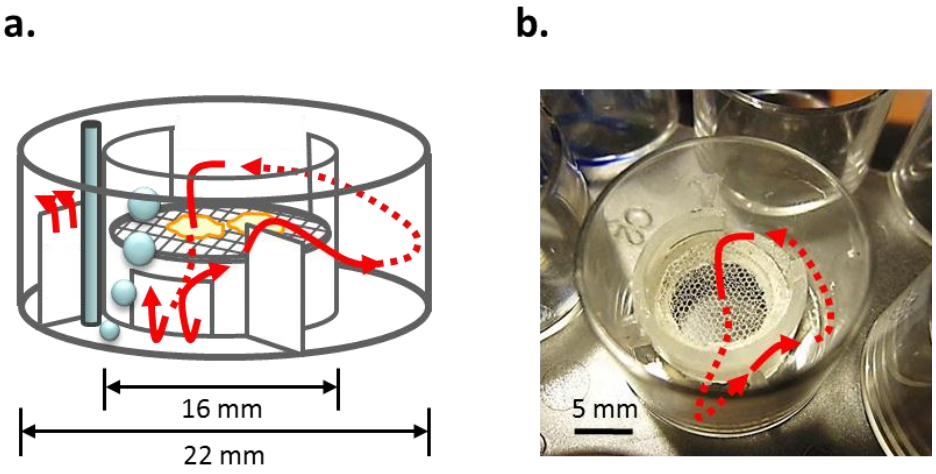

Figure 2.2 Miniature slice incubation chamber

a. The scheme and design of the chamber. The solution flow (indicated with red arrows) was driven by air bubbles. The slices were placed in the middle of the mesh. The top of the chamber was sealed with Para film during the incubation. **b.** The red arrows indicate the solution flow.

2.6. Visualized patch clamp recording

To obtain whole-cell recordings, cells were first visually searched using an Olympus BX-61 microscope equipped with differential interference contrast optics under infrared illumination and a water immersion lens (60x, NA=0.9, Olympus, Japan). The identified neurons were then approached with a patch pipette using motorized manipulators (Luigs & Neumann, Germany). For imaging experiments, whole-cell current-clamp recordings were obtained from CA1 pyramidal neurons with a patch pipette (3 - 6 MΩ) filled with a solution containing (mM): 130 KCH_3SO_3, 8 NaCl, 10 HEPES, 10 Na_2-Phosphocreatine, 0.4 Na_2GTP, 4 MgATP, 3 Na-Ascorbate, pH = 7.2, osmolarity was adjusted to 300 mOsm. The recording solution also

contained a fluorophore Alexa Fluor 594 (50 µM) and the Ca^{2+} sensitive dye Fluo-4 (250 µM) or Fluo-4FF (500µM). Once the whole cell recordings were obtained, the patch amplifier (Multiclamp 700B; Axon Instruments Inc.; Union City, CA, USA) was set to either current- or voltage-clamp mode. Dendritic bAPs were induced in these cells by somatic current injections (2-3 ms, 400 - 1000 pA) and monitored in the soma.

To monitor the effects of NMDAR antagonists and of the glutamate uptake blocker TBOA on the membrane properties of CA1 pyramidal cells, whole-cell voltage clamp recordings were obtained with patch pipettes (3-6 MΩ) filled with a solution containing (mM): 130 $CsCH_3SO_3$, 8 NaCl, 10 HEPES, 10 Na_2-Phosphocreatine, 0.5 EGTA, 0.4 Na_2GTP, 4 MgATP, 3 Na-Ascorbate, pH = 7.2, osmolarity was adjusted to 300 mOsm. Changes in the holding current were measured following 100 µM TBOA application with the membrane potential clamped at -70 mV. The series resistances and input resistance (R_{input}) of the recorded cells were measured by injection of hyperpolarizing pulses (5 mV, 50 -100 ms) and not compensated.

The series resistance was usually < 20 MΩ and data were discarded if its value changed more than by 20% during the recording. In current clamp mode, the series resistance was compensated with “bridge balance” mode. Signals were low-pass filtered at 2.2 kHz and digitized at 4-10 kHz with a NI PCI-6221 card (National Instruments). The data were recorded using WinWCP and WinEDR (supplied free of charge to academic users by Dr. John Dempster, University of Strathclyde, UK).

2.7. Two-photon imaging system

Cells were filled with Alexa Fluor 594 (50 µM) and calcium sensitive dye Fluo-4 (250 µM) or Fluo-4FF (500 µM) for 20 to 30 minutes before the start of acquiring image data to insure reachingsteady-state of both dyes. Two-photon Ca^{2+} imaging was performed using a two-scanner FV1000 microscope (Olympus) equipped with an ultra-fast, pulsed (<140 fs at peak) tunable 720-930 nm laser Chameleon (Coherent) and a near UV (405 nm) LED laser (Fig.. 2.3). The dyes were excited at 810 nm, and their fluorescence was chromatically separated and imaged by two independent photomultipliers (PMTs) separated with a 570nm dichroic mirror followed with two band pass filters (570-625 nm for Alexa Fluor 594 (red channel (R)); 495-540 nm for Fluo-4/Fluo-4FF (green channel (G))) (Fig.. 2.4).

We used the bright Alexa Fluor 594 emission to identify oblique apical dendrites (within 150 µm from the soma) and their spines. Free-line line-scan image acquisition was normally performed to record Ca^{2+} signals in the dendritic shaft and 1-4 spines at 200 – 500 Hz. Image acquisition was synchronized with electrophysiological sweeps. bAPs were induced by brief depolarizing current injections through a patch pipette producing a single action potential in the soma. bAP-evoked Ca^{2+} transients were imaged in dendrites and spines (Fig.. 3.1). We also tested that recorded transients were well below Fluo-4 saturation level achieved by prolonged somatic depolarization causing Ca^{2+} build up in the neurons. We also monitored changes in baseline Ca^{2+} level as the ratio between Fluo-4 and Alexa Fluor 594 fluorescence. If this ratio steadily increased and changed more than

20% during the experiment, the cells were discarded. The dark noise of the PMTs was collected when the imaging laser shutter was closed in every individual recording and subtracted from the baseline fluorescent signal as indicated in Chapter 2.10 Data analysis.

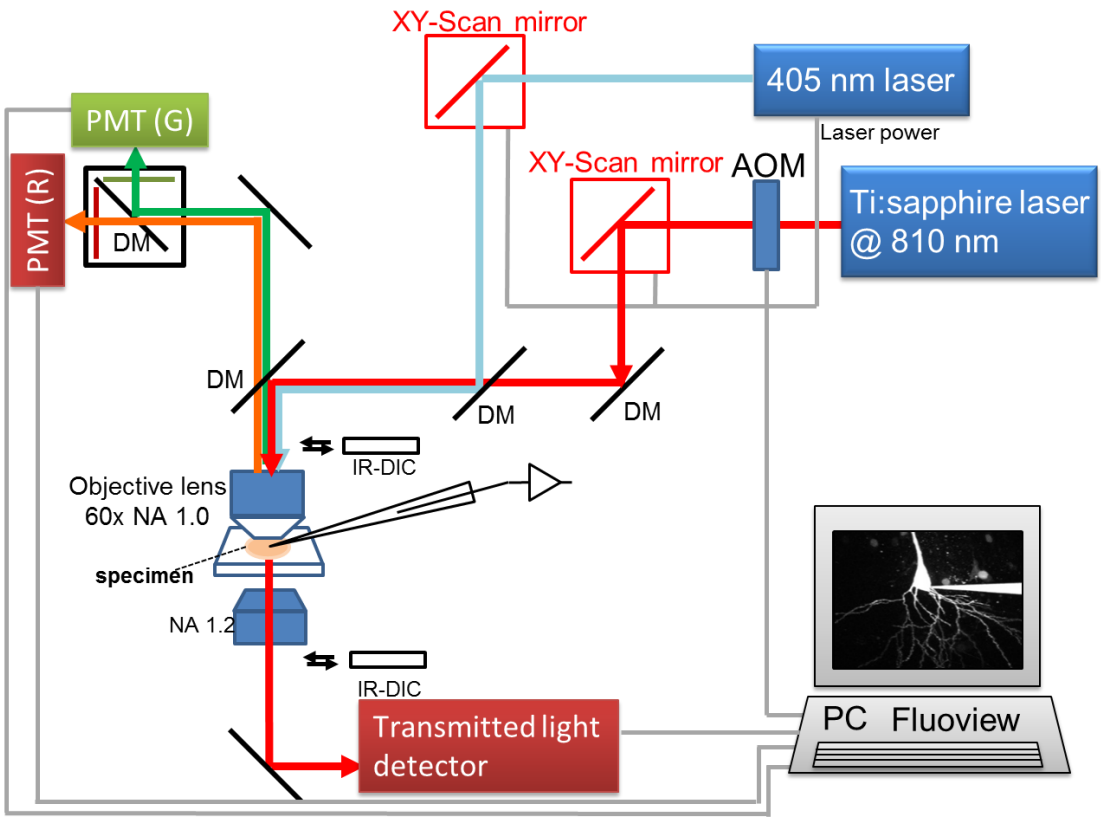

Figure 2.3 Experimental setup (FV1000) for two-photon imaging and single-photon uncaging.

The system includes a Ti:sapphire laser tuned to 810 nm for imaging, and a 405 nm LED laser for glutamate uncaging. The two light paths are connected to the microscopy via their own galvanometer XY-scan mirrors. The 810 nm laser output power was controlled by an acousto-optic-modulator (AOM). Emission light was separated to a green (G) and a red (R) channels with a 570 nm dichroic mirror (DM) followed by two band-pass filters, and then detected with two photomultiplier tubes (PMTs).Gray lines indicate the signal received and sent from the PC.

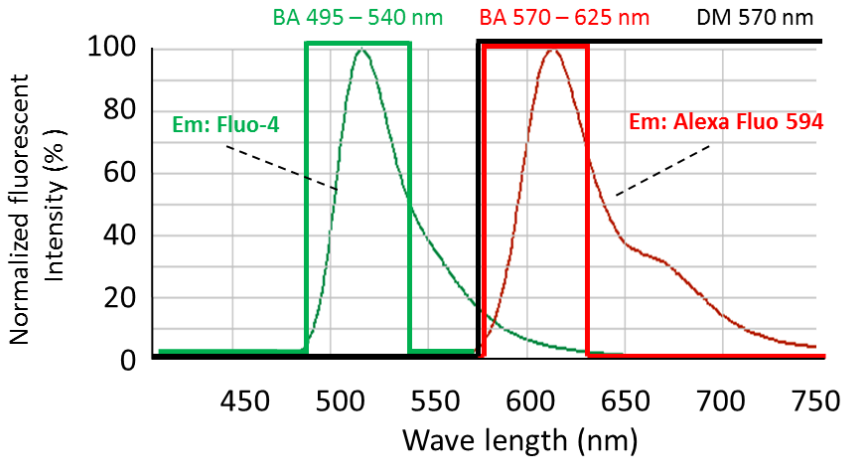

Figure 2.4 Optic design for separating emission light from Alexa Fluor 594 and Fluo-4/Fluo-4FF.

The normalized emission spectra for Alexa Fluor 594 (thin red line) and Fluo-4 (thin green line) are present. The emission light is first separated with a 570 nm dichroic mirror (thick black line) and then filtered with two band-pass filters (495 – 540 nm for Fluo-4 (thick green line) and 570 – 625 nm for Alexa Fluor 594 (thick red line)). The spectra of both dyes are taken from Invitrogen website (http://www.invitrogen.com/site/us/en/home/support/Research-Tools/Fluorescence-SpectraViewer.html).

2.8. Glutamate uncaging

2.8.1. Single photon glutamate uncaging

Single photon uncaging was carried out with a near UV laser (405 nm diode laser; FV5-LD405, Olympus) in the same system mentioned in the previous Chapter (Fig. 2.3). 4-methoxy-7-nitroindolinyl-caged L-glutamate (MNI-glutamate) was applied in the bath (200-250 µM) with a micro-perfusion system containing 4 ml ACSF. The

uncaging spot was located 2-5 µm near an oblique dendrite. Uncaging was carried out using a 405 nm laser line, in 'tornado' circular scan mode with a diameter about 1 µm. To mimic the transient rise of extracellular glutamate concentration, the duration and the power of the uncaging pulse were set to 20 ms and 10-20 % to produce a detectable Ca^{2+} response.

In experiments addressing the physiological effects of TBF-induced plasticity, somatic uEPSPs were obtained by uncaging bath-applied MNI-glutamate (400 µM) using 5-10 ms laser pulses at spots located close to spines on apical dendrites between 100 and 150 µm from the soma.

2.8.2. Two photon glutamate uncaging

In the two-photon uncaging experiments, a two-scanner FV1000-MPE microscope (Olympus) equipped with two ultra-fast, pulsed (<140 fs at peak) tunable 690-1020 nm lasers Mai-Tai (Spectra-Physics) was used. The imaging and uncaging lasers were tuned to 840 nm and 720 nm respectively (Fig. 2.5). Lasers were aligned in XYZ-axis every time before the experiments with 0.5 µm fluorescent beads coated with Alexa Fluor 488 (Fig. 2.6) to ensure the precision of uncaging. MNI-caged glutamate (12 mM) was applied locally via an extracellular glass pipette (1-2 MΩ) with a constant pressure of 1-2 KPa. The uncaging spot was located opposite an oblique dendrite at equal distances (around 1 µm) from the imaged dendritic shaft and spine. Uncaging was carried out under a "point scan" mode in the FV1000-MPE system. To mimic the transient rise of extracellular glutamate concentration, the

duration and the power of the uncaging pulse were set to 5 ms and 2-3 mW (under objective) to produce a just detectable Ca^{2+} response. In control experiments, we also confirmed that illumination of the preparation in absence of MNI-caged glutamate, or the application of MNI-glutamate alone had no effect on either the resting Ca^{2+} or Ca^{2+} transients induced by bAPs.

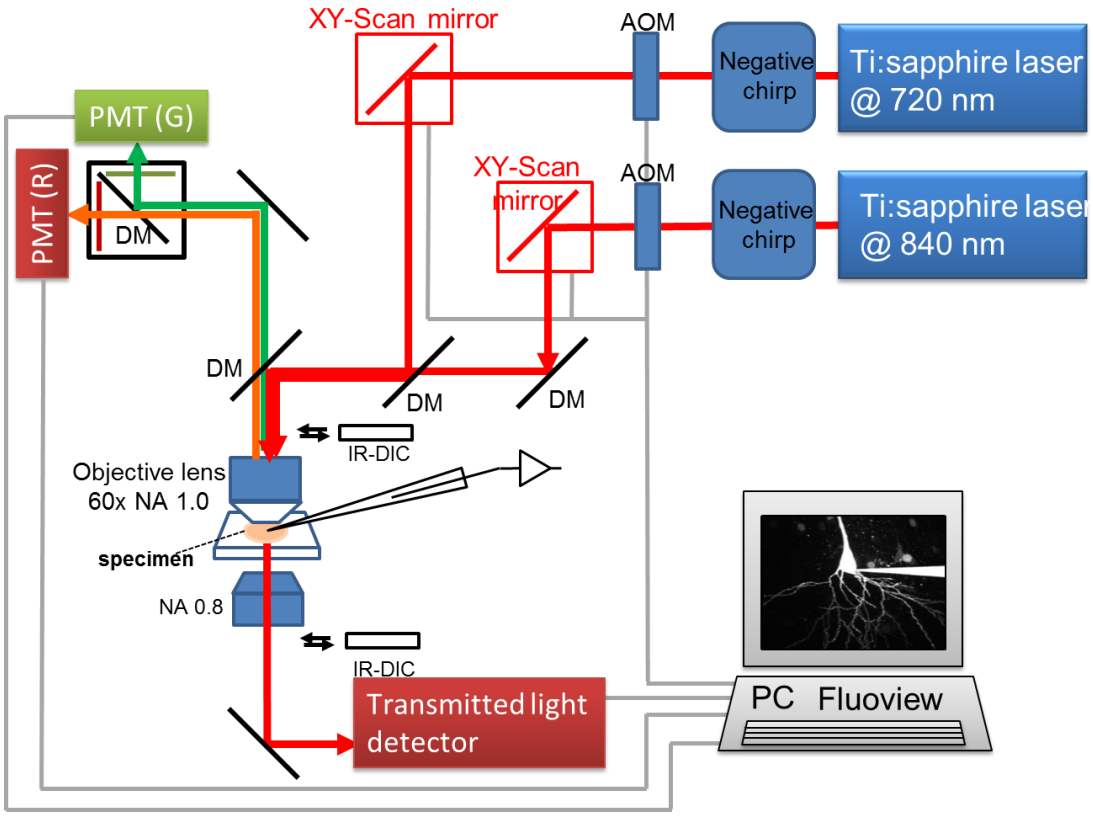

Figure 2.5 Experimental setup (FV1000-MPE) for two-photon imaging and two-photon uncaging.

The system includes two Ti:sapphire laser tuned to 840 nm and 720 nm for imaging and glutamate uncaging respectively. The lasers first pass through the negative pre-chirp optics to correct the dispersion after passing the objectives to maintain a short enough pulse width. The two light paths are connected to the microscopy via their own galvanometer XY-scan mirrors, and the output power was controlled by two independent acousto-optic-modulators (AOMs) via Fluoview software. Emission light was separated to a green (G) and a red (R) channel with a 570 nm dichroic mirror (DM) followed with two band-pass filters, and then detected with two photomultiplier tubes (PMTs). Gray lines indicate the signal received and sent from the PC.

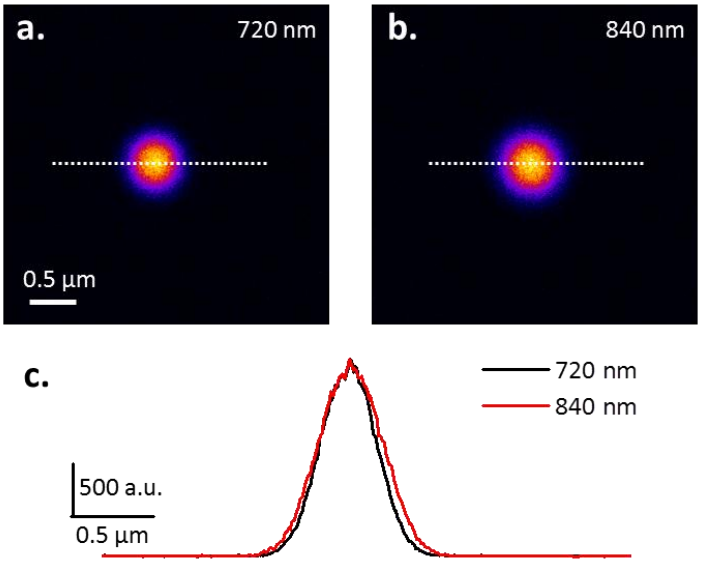

Figure 2.6 Laser alignment for precise glutamate uncaging.

a and b, A fluorescent bead of 0.5 µm diameter coated with Alexa Fluor 488 was imaged with 720 nm and 840 nm lasers with their own scan mirrors separately. **c,** The spatial profiles along the white dash lines in **(a)** and **(b)** were plotted. The peaks of the point spread function were overlaid to each other suggesting that the lasers were well aligned. a.u. represents arbitrary units of fluorescent signal.

2.9. Drugs and chemicals

All drugs were made from stock solutions kept frozen at -20^{o}C in 100-200 µl x1000 concentration aliquots. Picrotoxin (PTX) 100 µM, LY341495 100 µM,S-MCPG 200-400 µM, D-APV 50 µM, NBQX 25 µM, DL-TBOA 100 µM, Ro25-6981 5 µM, ZD7288 20 µM, CGP52432 5 µM, QX-314 3 mM, PPDA 0.5 µM and MNI-caged glutamate (bath-application: 200 or 400 µM; local application 12 mM) were purchased from Tocris Cookson (Bristol, UK). Bafilomycin A1 4 µM was obtained

from Wako Chemicals (Osaka, Japan). Chemicals for solutions were from Sigma (St. Louis, MO, USA).

2.10. Data analysis and software development

2.10.1. Data analysis

Electrophysiological data were analysed by using WinWCP and Clampfit (Axon Instruments Inc.; Union City, CA, USA). Imaging data were analysed using Fluoview (Olympus, Japan), ImageJ (a public domain Java image processing program by Wayne Rasband) and custom software written in LabView (National Instruments, Austin, TX, US). Statistical analysis was performed using Excel (Microsoft, US) and Origin 8 (OriginLab Corp.)

The fluorescent measurements of Ca^{2+} transients were represented as *ΔG/R*: $((G_{peak} - G_{baseline}) / (R_{baseline} - R_{dark\ noise}))$. Baseline Ca^{2+} signals were represented by *baseline G/R*: $((G_{baseline} - G_{dark\ noise}) / (R_{baseline} - R_{dark\ noise}))$, where *G* is the Fluo-4 or Fluo-4FF fluorescence, and *R* is Alexa Fluor 594 fluorescence. $G_{baseline}$ and $R_{baseline}$ are averaged fluorescence 50~100 ms before the stimulation. G_{peak} is averaged fluorescence 30-40 ms after the stimulation. $G_{dark\ noise}$ and $R_{dark\ noise}$ are the dark currents of the corresponding PMTs. For illustration purposes, single traces were processed by 5 point moving average, and then 4-5 sequential traces were averaged.

2.10.2. Statistics

To choose a correct statistic method, I performed Shapiro–Wilk normality test on the distribution of APV effect on bAP-evoked Ca^{2+} entry in the first set of experiments which contained enough sample numbers (Fig. 3.1 c and d), and showed that the data points followed a normal distribution (shafts: n = 13, W = 0.31; spines: n = 22, W = 0.8). Thus, for experiments testing drug effect on bAP-evoked Ca^{2+} entry, the statistical significance was tested using a paired or unpaired Student's t-test. For all the other experiments, Wilcoxon signed-rank test was performed for testing statistical significance. The data are given in mean ± the standard error of the mean (s.e.m.); n – number of recordings. In all figures error bars indicate mean ± s.e.m.

2.10.3. Analysis software development

For data analysis, I developed two LabView programs.

(1), "*Fluo-LineScan Viewer.vi*" is designed to read line-scan image files acquired by Fluoview, and to automatically define region of interests (ROIs) for sub-dendritic structures (spines and shafts). Signals from both G (Fluo-4/Fluo-4FF) and R channels (Alexa Fluor 594) were read into the software. Dark noise was subtracted from the signal first (Fig. 2.7, step b). The morphological profile across the scanning line was built by averaging all the scans from the R channel (Fig. 2.7, step c). The profile was filtered with Savitzky-Golay smoothing (3^{rd} polynomial order, 15 pixel/side points),

and followed by a multiple-peak detection and Gaussian fitting (Fig. 2.7, step d and e). The ROIs were defined as the region within the *f*ull-*w*idth-at-*h*alf-*m*aximum (FWHM) of each Gaussian fitting (Fig. 2.7, step f). Then, the fluorescent time course traces were calculated by averaging signal across the space within ROI (Fig. 2.7, step g). The time course traces were then used for further analysis. The user interface is shown in figure 2.8.

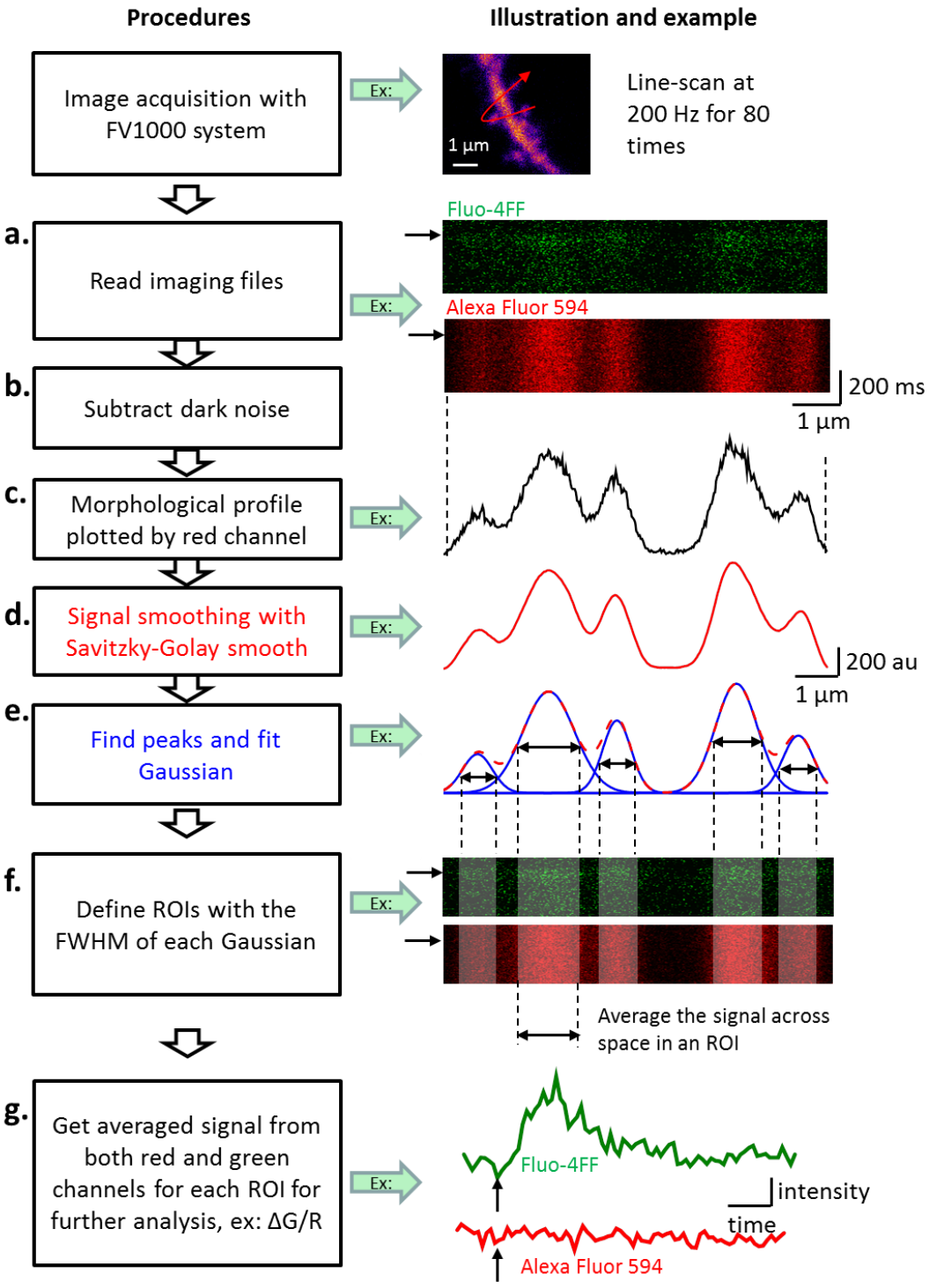

Figure 2.7 The procedures for transferring imaging data to time-course traces

Image data was first acquired with Fluoview. **Step a,** Signals from both G (Fluo-4/Fluo-4FF) and R channels (Alexa Fluor 594) were read into the software. The calcium transient in G channel was induced by bAPs (black arrows). **Step b,**

Subtract dark noise. **Step c,** The morphological profile across the scanning line was built by averaging all the scans from the R channel. **Step d and e,** The profile was filtered with Savitzky-Golay smoothing (3^{rd} polynomial order, 15 pixel/side points), and followed by a multiple-peak detection and Gaussian fitting. **Step f,** The ROIs were defined by the FWHM of each Gaussian fitting. **Step g,** The fluorescent time course traces were calculated by averaging signal across the space within ROI. ROI for region of interest.

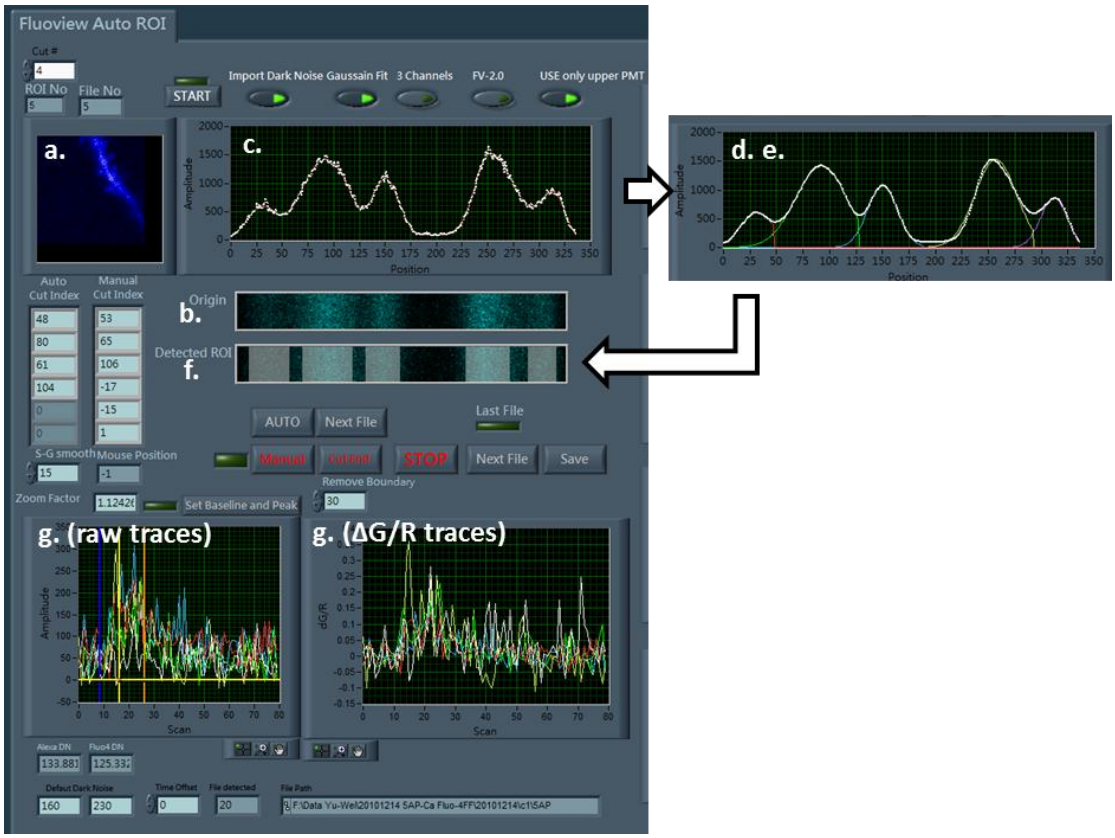

Figure 2.8 User interface of the software, "Fluo-LineScan Viewer.vi".

The user interface of the "Fluo-LineScan Viewer.vi". **Step a,** Images acquired with Fluoview were read into the program. **Step b,** Image with dark noise **s**ubtracted. **Step c,** The morphological profile across the scanning line. **Step d and e,** With one click, the profile was filtered with Savitzky-Golay smoothing, and followed by a multiple-peak detection and Gaussian fitting. **Step f,** The ROIs (marked with gray squares) were then defined by the FWHM of each Gaussian fitting. **Step g,** the fluorescent time course traces were calculated by averaging signal across the space within ROI.

(2), "*Fluo-TimeCourse Viewer.vi*" is designed for automated trial-by-trial calculation of *baseline G/R* and *ΔG/R* from the fluorescent time courses generated by "Fluo-LineScan Viewer.vi". First, the baseline and peak of fluorescent transient were manually defined (Fig. 2.9, step a). After assigning an ROI, the trial-by-trail normalized *G* and *R* of this ROI were plotted (Fig. 2.9, step b). Normalized *baseline G/R*, *ΔG/R* and the variance of *baseline G/R*, *ΔG/R* peak were also plotted in separated graphs (Fig. 2.9, step c and d). Finally the time-course traces were averaged from trials of different experimental treatments and displayed on a graph (Fig. 2.9, step e). All the results were then saved as text files.

Figure 2.9 User interface of the software, "Fluo-TimeCourse Viewer.vi".

Step a, The baseline and peak of fluorescent transient were manually defined. **Step b,** After assigning an ROI, the trial-by-trail normalized G and R were

plotted. **Step c and d,** Normalized baseline G/R, ΔG/R and the variance of baseline G/R, ΔG/R peak were also plotted in separated graphs. **Step e,** The time-course traces were averaged from trials of different experimental treatments and displayed on a graph.

Chapter 3: Detection of ambient glutamate by NMDARs in quiescent slices

3.1. Introduction

It has been shown that there is a tonic current mediated by ambient glutamate-bound extrasynaptic NMDARs in CA1 pyramidal neurons by artificially holding the cell membrane potential to either a more depolarized potential (-35 to -33 mV) (Cavelier and Attwell, 2005; Sah et al., 1989) or positive potential (+40 to 50 mV) (Jabaudon et al., 1999; Le Meur et al., 2007) with the voltage-clamp technique. However, it is not known whether the glutamate pre-bound NMDARs are also activated during a physiological depolarizing event, like a bAP. Since the NMDAR is Ca^{2+} permeable, NMDAR-mediated Ca^{2+} influx was monitored with a Ca^{2+}-sensitive dye by two-photon laser excitation microscopy to test whether NMDARs contribute to Ca^{2+} influx during a bAP (illustrated in Fig. 1.7a) in hippocampal CA1 pyramidal neurons.

Furthermore, because excitatory synapses are shielded by astrocytic processes expressing high densities of glutamate transporters, it has been suggested that ambient glutamate is restricted to the extrasynaptic regions and excluded from synaptic clefts (Featherstone and Shippy, 2008). Based on the fact that glutamatergic synapses in adult hippocampus in rat are mostly sitting on spines (Bourne and Harris, 2011), NMDARs on dendritic shafts are considered to be exclusively extrasynaptic. I

then tested whether there is a different contribution in NMDAR-mediated Ca^{2+} entry in dendritic spines and shafts.

The source of the glutamate tonically bound with NMDARs was also investigated. I tested whether synaptically-released glutamate also contributes to the baseline glutamate concentration either by pharmacologically emptying the synaptic vesicles or by using genetically modified mice in which the synaptic release is shut down in CA3 pyramidal cells.

3.2. Materials and methods

3.2.1. Animals and slice preparation

Transverse slices of hippocampus were prepared from animals as described in Chapter 2.2. Briefly, the majority of the experiments were done using SD rats, aged p21 - p35. Slices from CA1-GluN1 KO mice, aged p42 - p49, were used for control experiments showing the involvement of postsynaptic NMDARs on CA1 pyramidal cells. Slices from CA3-TeTX mice, aged p42 - p49, were used in experiments probing the source of glutamate.

The procedures for slice preparation are described in Chapter 2.3. Briefly, animals were anaesthetised and decapitated. The brain was removed, and chilled with ice-cold cutting solution. Hippocampi from both hemispheres were isolated and placed in an agar block and transverse slices (350 µm) were cut with a vibroslicer (Fig.

2.1e). The slices were left to recover for 20 to 30 min at 34°C in a submerged chamber in cutting or storage solution. Then they were transferred and incubated on either an interface- or submerged-type chamber (mostly submerged-type) at room temperature for at least 1 hour for recovery with storage solution. After that, the slices were transferred to the recording chamber and were continuously superfused at 33-34^{o}C with ACSF. All solutions were saturated with 95% O_2 and 5% CO_2. Osmolarity was adjusted to 298 ± 3 mOsm. The procedures for incubation of slices in bafilomycin A1 are described in Chapter 2.4.

3.2.2. Electrophysiology and two-photon imaging

Whole cell patch-clamp recording and two-photon imaging were performed as described in Chapter 2.5 and 2.6. Briefly, cells in slices were first visually searched using Olympus BX-61 microscope equipped with differential interference contrast optics under infrared illumination and a 60x water immersion lens. For imaging experiments, whole-cell current-clamp recordings were obtained from CA1 pyramidal neurons with a patch pipette (3 - 6 MΩ) filled with solution containing the morphological tracer Alexa Fluor 594 (50 µM) and the Ca^{2+} sensitive dye Fluo-4 (250 µM). Once the whole cell recordings were obtained, the patch amplifier (Multiclamp 700B) was set to either current- or voltage-clamp mode. Dendritic bAPs were induced in these cells by somatic current injections (2-3 ms, 400 – 1000 pA) and monitored in the soma. Two-photon imaging was performed at least 20 -30 min after

rupturing the seal and breaking into the cell to ensure dye equilibration. Imaged dendrites were at least 30 µm (mostly 50 µm) below the slice surface.

3.3. Dendritic shaft-associated NMDARs are enabled by a single bAP

Hippocampal CA1 pyramidal cells were held in whole-cell current clamp mode, filled with the Ca^{2+} indicator Fluo-4 (250 µM) and the morphological tracer Alexa Fluor 594 (50 µM). Line-scan imaging of Ca^{2+} transients were induced by a single bAP in shafts and spines of the apical oblique dendrites (Fig. 3.1a,b) with AMPA/kainate and $GABA_A$ receptors blocked by 25 µM NBQX and 100 µM Picrotoxin respectively. It has been shown that the majority of the Ca^{2+} transients induced by bAPs both in spine and shaft are contributed by VDCC (Bloodgood and Sabatini, 2007b; Sabatini and Svoboda, 2000). The amplitudes of fluorescence Ca^{2+} responses, indicated by *ΔG/R* (see chapter 2.11.1), in the dendritic shafts were reversibly reduced to 89 ± 3% of baseline by the broad-spectrum NMDAR antagonist D-APV (50 µM) (n = 13, p = 0.001; Table 3.1; Fig.3.1c; Fig. 3.2a for trial-by-trial example). Strikingly, no such reduction was detected in the spines on the same dendritic shaft (n = 22, p = 0.31; Table 3.1; Fig.3.1d; Fig. 3.2b for trial-by-trial example). Because the overwhelming majority of excitatory synapses in CA1 pyramidal cells are hosted by spines (Bourne and Harris, 2011), extrasynaptic rather than synaptic NMDARs are activated upon generation of a bAP. The lack of APV effects on the bAP-evoked Ca^{2+} influx in spines also suggests that unblocking NMDARs had no detectable influence on the bAP

waveform (e.g. amplitude or duration) which controls the opening of local voltage-dependent Ca^{2+} channels.

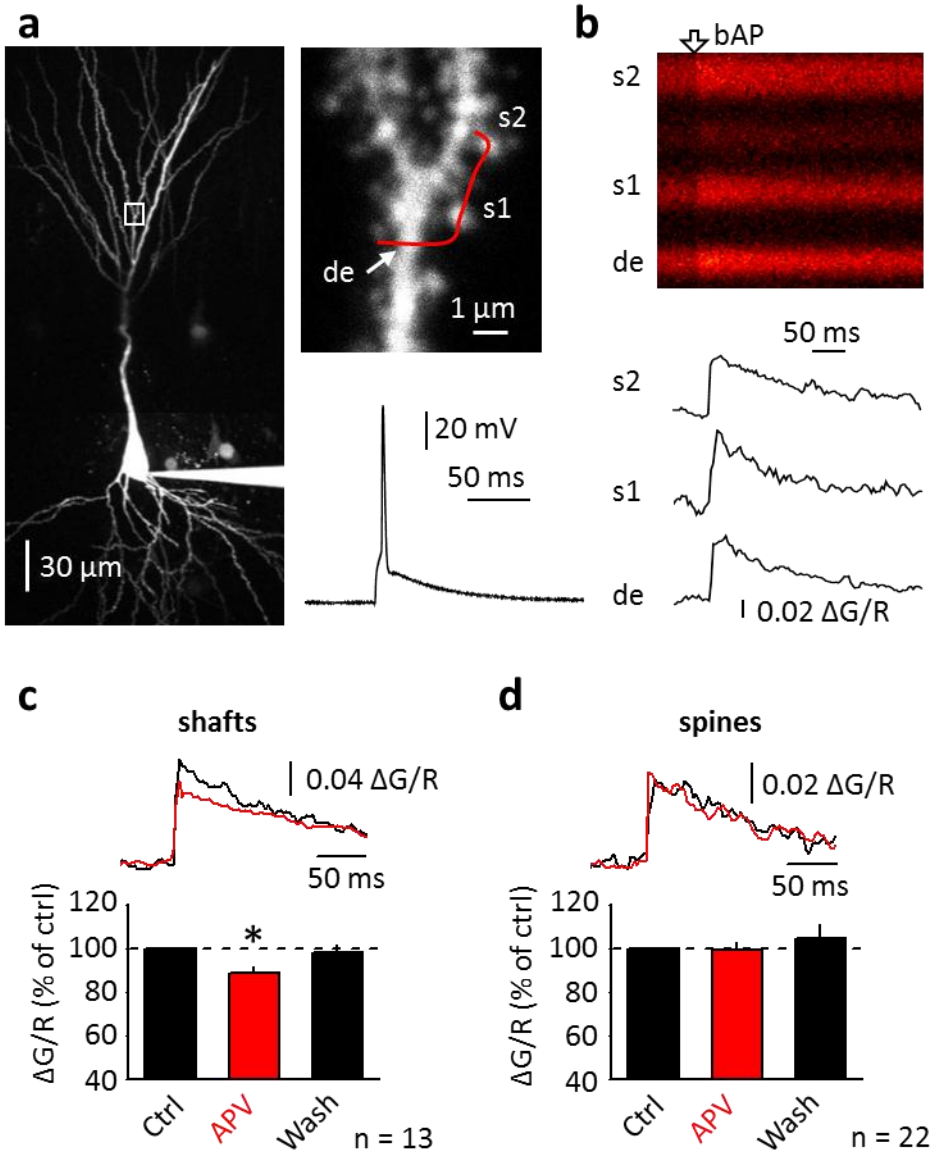

Figure 3.1 Activation of shaft NMDARs is enabled by bAPs

a, *Left panel*, a recorded neuron filled with Alexa Fluor 594. *Upper right*, the boxed region expanded. Red line: the line-scan trajectory through the dendritic shaft (*de*) and spines (*s1*, *s2*). *Lower right*, somatic action potential in response to current injection. **b,** Line-scan Ca^{2+} imaging (*upper*) and average traces (*lower*); notation is as in (a). **c** and **d,** The effect of NMDAR antagonist APV on bAP-evoked Ca^{2+} entry (*ΔG/R*) in shafts (c) and spines (d). Averaged traces in control (black) and in APV (red). Summary data normalized to control (Ctrl). Wash – washout of APV. *, $p < 0.05$.

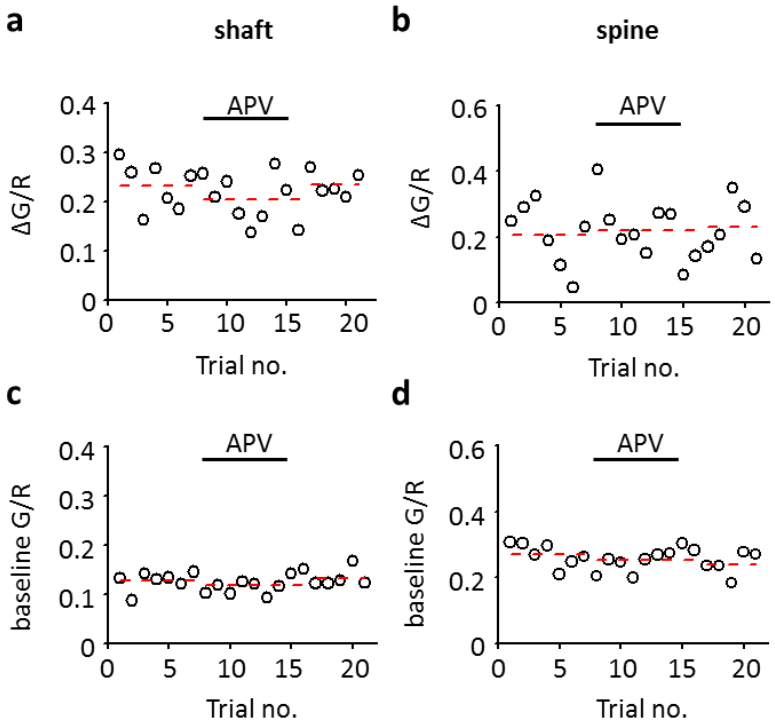

Figure 3.2 A trail-by-trial example of single experiments for APV effect on bAP-evoked Ca^{2+} transients

a and **b**, APV slightly decreases bAP-evoked Ca^{2+} transients (*ΔG/R*) in the dendritic shaft (a) but not in the spine (b). **c** and **d**, Baseline Ca^{2+} indicated by *baseline G/R* is not affected by APV in the shafts (c) and spines (d). Open circles, individual trials. Red dash-lines, averaged values of each condition.

3.4. Shaft NMDARs contribution to bAP-Ca^{2+} entry was occluded in Mg^{2+} free solution

Because NMDARs also exhibit voltage-dependent gating even in the absence of external Mg^{2+} (Clarke and Johnson, 2008), I tested whether this Ca^{2+} influx through dendritic shaft-associated NMDARs is due to the relief of voltage-dependent Mg^{2+} block during AP backpropagating. To separate the effect of depolarization from that

of Mg^{2+} blockade, these experiments were repeated in Mg^{2+} free solution. There was no significant effect of APV (*ΔG/R*; 97 ± 2% of control, n = 6, p = 0.09; Fig. 3.3), which argues against any contribution of the voltage-dependent receptor properties other than the Mg^{2+} block.

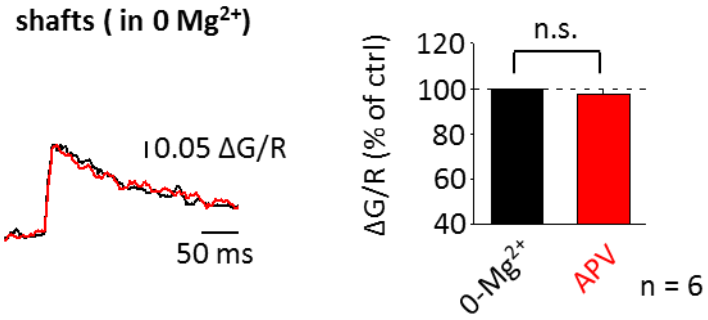

Figure 3.3 Shaft NMDARs contribution to bAP-Ca^{2+} entry was occluded in Mg^{2+} free solution

No significant effect of APV on bAP-evoked Ca^{2+} entry in Mg^{2+}-free ACSF (0-Mg^{2+}) in shafts. *Left panel*, Averaged traces in 0- Mg^{2+} (black) and after adding APV (red). Summary data normalized to control (0-Mg^{2+}). n.s. for no significant difference.

3.5. No shaft NMDAR-mediated bAP-Ca^{2+} entry in CA1-GluN1 conditional knock-out mice

The APV effect on shaft NMDAR could be explained by downregulation of network activity because all NMDARs on other types of cells were also blocked. Thus, I tested whether the above effects depend on the presence of functional dendritic NMDARs in CA1 pyramidal cells or on the network consequences of APV actions. The

bAP-evoked Ca^{2+} entry in shafts and spines in slices prepared from CA1-GluN1 conditional knock-out mice (Tsien et al., 1996) was insensitive to APV application (*ΔG/R*; shafts: 96 ± 5 % of control, n = 6, p = 0.45, Fig. 3.4a). At the same time, APV was effective in the littermates which expressed functional NMDARs (*ΔG/R*; shafts: 87 ± 5% of control, n = 6, p = 0.04, Fig. 3.4b). These results suggest that the APV effect on bAP-evoked Ca^{2+} entry in shafts is due to the activation of functional shaft NMDARs.

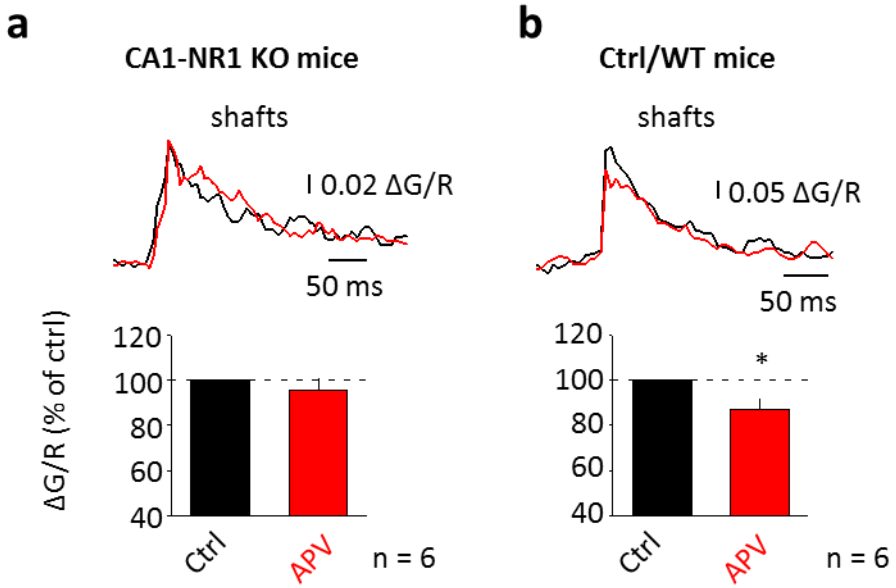

Figure 3.4 No significant shaft NMDAR-mediated bAP-Ca^{2+} entry in CA1-GluN1 conditional knock-out mice

a, No significant effect of APV on bAP-evoked Ca^{2+} entry (*ΔG/R*) in dendritic shafts of CA1-GluN1 KO mice. **b**, APV has effect on bAP-evoked Ca^{2+} entry in the control littermates and wild type mice (Ctrl/WT). Averaged traces in control (black) and in APV (red). Summary data normalized to control (Ctrl). n.s. for no significant difference. Summary data normalized to control (Ctrl). *, $p < 0.05$.

3.6. Activation of background synaptic NMDARs does not contribute to bAP-Ca^{2+} entry

Activation of spine NMDARs by background synaptic release might also generate Ca^{2+} influx, diffusing to dendritic shaft. Thus, I addressed the possibility that the APV sensitivity of bAP-evoked Ca^{2+} entry in dendritic shafts could be due to activation of synaptic NMDARs on a sub-group of neighbouring spines which were not sampled. In baseline conditions the frequency of spontaneous synaptic release detected by whole-cell recording was 1-3 Hz (Fig. 3.6a). Given 5-10 thousand excitatory synapses per CA1 pyramidal cell (Megias et al., 2001), this suggests that spontaneous glutamate release occurs at each individual synapse once every hour or so: indeed, no spontaneous signals were observed in n = 111 documented postsynaptic spines each monitored over several minutes. To further confirm this presumption, I monitored the Ca^{2+} signal on a dendritic branch and the somatic spontaneous EPSPs in low Mg^{2+} ACSF for 5 minutes (fig 3.5). It has been shown that the Ca^{2+} signal generated by synaptic glutamate release is much larger than that generated by a bAP (Yasuda et al., 2004). I tested whether our two-photon Ca^{2+} imaging system was sensitive enough to detect Ca^{2+} influx triggered by spontaneous glutamate release by monitoring bAP-evoked Ca^{2+} influx. Indeed, the imaging system was able to capture bAP-evoked Ca^{2+} entry (Fig. 3.5 b1) which is usually smaller than a typical EPSP-induced Ca^{2+} event (Fig 3.5 b2). The frequency of somatic spontaneous EPSPs was 0.93 Hz, but no spontaneous Ca^{2+} activity was seen in the 11 monitored spines during this period. Altogether, these again suggested infrequent spontaneous Ca^{2+}

activity in an individual spine in acute hippocampal slice preparation. Therefore, any impact of background synaptic NMDARs activation on bAP-evoked Ca^{2+} entry is highly unlikely.

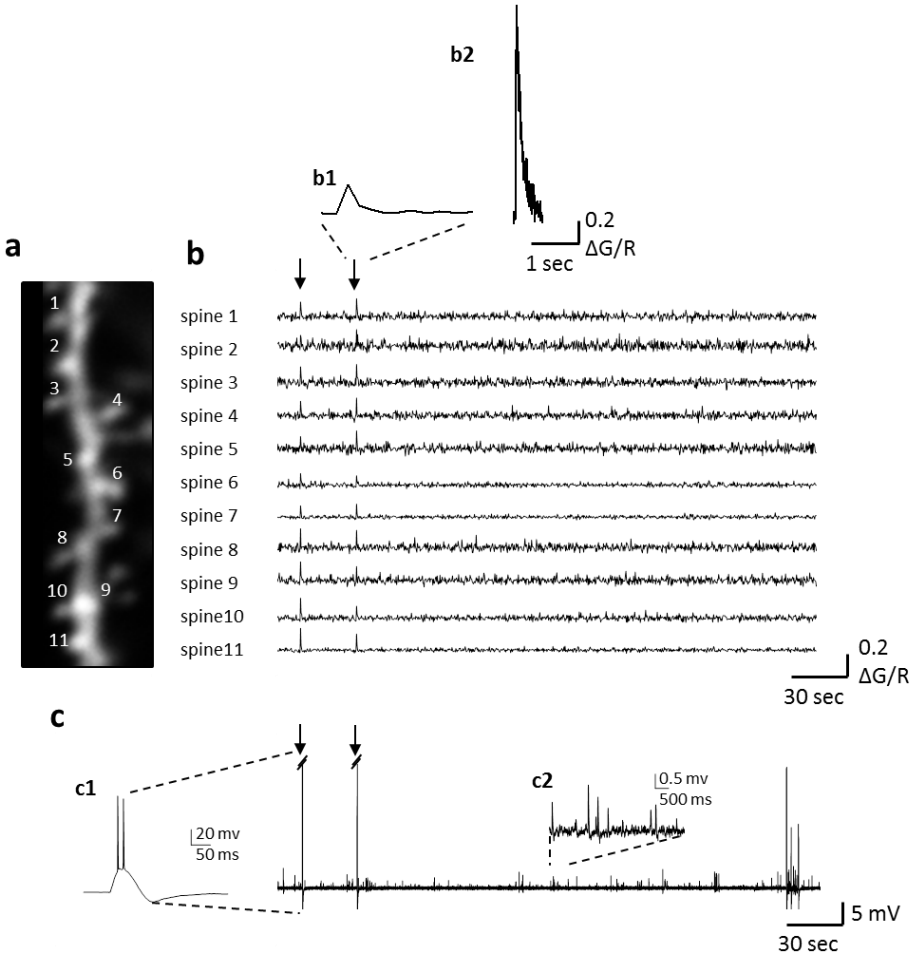

Figure 3.5 Spontaneous Ca^{2+} activity rarely detected in spines of a dendritic branch in acute hippocampal slice

a, A CA1 pyramidal cell was filled with Alexa Fluor 595 and Fluo-4 with a whole-cell patch pipette in low Mg^{2+} (0.05 mM) ACSF containing CGP52432 (5 µM) and PTX (100 µM). 11 spines on an oblique dendritic branch were imaged for 5 minutes. **b**, No Ca^{2+} activities were observed except bAP-activated Ca^{2+} transients induced by somatic current injection (arrows). **Insert b1,** Enlarged bAPs-induced Ca^{2+} transient. **Insert b2,** A typical trace of a single synaptic stimulation induced Ca^{2+} transient in a dendritic spine recorded in a separated experiment. Note that the Ca^{2+} transient induced by synaptic stimulation is significantly larger than the bAP-induced one. **c**, Membrane potential recording simultaneously with Ca^{2+} imaging in **b**. Many spontaneous EPSPs could be seen during the 5 minutes. **Insert c1,** APs triggered by somatic current injection. **Insert c2,** Enlarged spontaneous EPSPs waveforms.

3.7. Glutamate that binds to shaft NMDAR has non-synaptic origin in quiescent slices

Next, I examined whether synaptically-released glutamate participates in binding to shaft NMDARs in the baseline conditions. Synaptic release was blocked with 4 μM bafilomycin A1 (a specific inhibitor of vacuolar-type H^+-ATPase; Chapter2 2.4). Indeed, this treatment completely abolished both spontaneous and evoked glutamatergic synaptic responses (Fig. 3.6; for method see chapter 2.4). Strikingly, the effect of APV on bAP-evoked Ca^{2+} entry in these slices compared to control conditions was qualitatively identical (Table 3.1; Fig. 3.7).

Finally, I confirmed this finding in a more specific way in a mouse line (CA3-TeTX mouse line) in which CA3 to CA1 glutamatergic synaptic transmission was specifically shut down (Nakashiba et al., 2008). Because the apical oblique dendrites of CA1 pyramidal neurons receive excitatory inputs mostly from CA3 Schaffer collaterals (Jones and McHugh, 2011), in CA3-TeTX mice there should be no or at least considerably fewer frequent glutamatergic synaptic events targeting to the imaged dendritic branches. In agreement with the results shown in bafilomycin A1 treated slices, no qualitative difference of the APV effect on bAP-evoked Ca^{2+} entry was found in CA3-TeTX mice compared to control conditions (Table 3.1; fig 3.8).

These observations indicated that activation of synaptic NMDARs does not contribute significantly to the APV sensitivity of bAP-evoked Ca^{2+} entry in the shafts in baseline condition. This was also consistent with previous reports demonstrating

that ambient glutamate in quiescent slices has a non-synaptic origin under basal conditions (Cavelier and Attwell, 2005; Fleming et al., 2011a; Fleming et al., 2011b; Jabaudon et al., 1999; Le Meur et al., 2007).

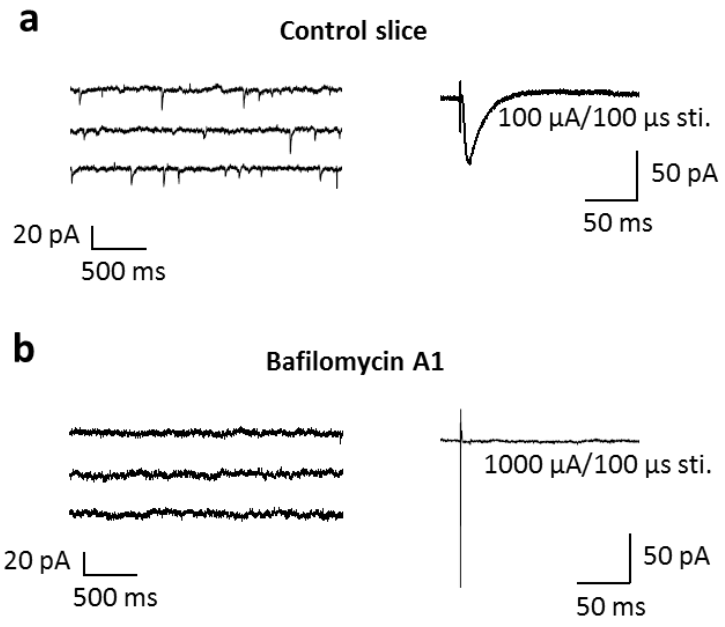

Figure 3.6 Spontaneous and evoked EPSC were completely blocked in bafilomycin A1 treated slice

a, The spontaneous (left) and evoked (by stainless-steel bipolar electrodes) (right) synaptic activity in a control slice. Many spontaneous EPSCs were observed. **b,** No spontaneous EPSCs (left) were observed. No evoked (right) synaptic activity was seen even stimulated with 10 times stronger current in a bafilomycin A1 treated slice.

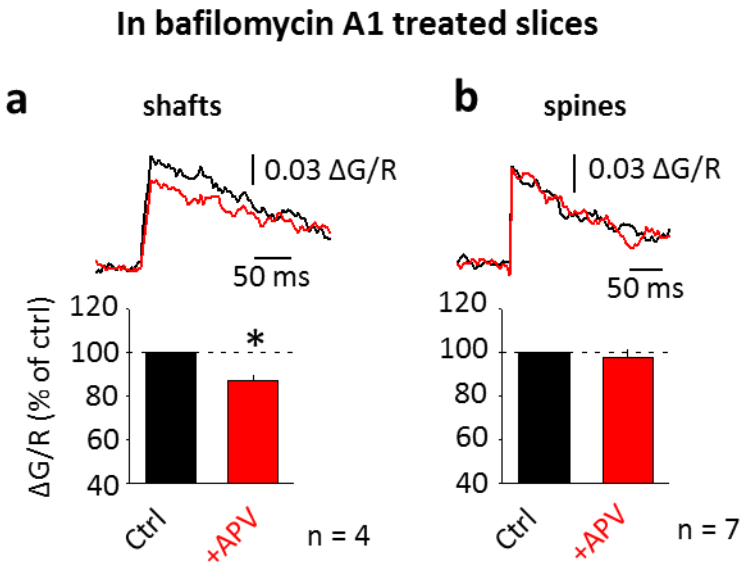

Figure 3.7 bAP triggers detection of ambient glutamate by shaft NMDARs.

a and **b,** The effect of APV on bAP-evoked Ca^{2+} entry (*ΔG/R*) in shafts (a) and spines (b) of CA1 pyramidal neurons from bafilomycin A1 treated slices. *Upper panels*, averaged traces of bAP-evoked Ca^{2+} transients in control (black trace) and after adding APV (red trace) in one characteristic dendritic shaft and spine, respectively. *Lower panels*, summary data normalized to "Ctrl"– control condition in bafilomycin A1 treated slice. *, $p < 0.05$.

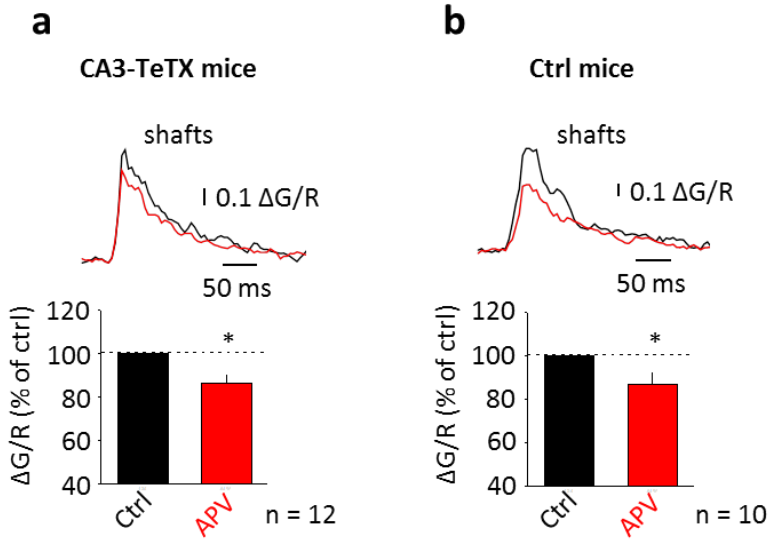

Figure 3.8 bAP triggers detection of glutamate by shaft NMDARs in mice without CA3 to CA1 excitatory synaptic transmission

a and **b,** The effect of APV on bAP-evoked Ca^{2+} entry (*ΔG/R*) in shafts of CA1 pyramidal neurons in CA3-TeTX mice (a) and in control littermates (b). *Upper panels*, averaged traces of bAP-evoked Ca^{2+} transients in control (black trace) and after adding APV (red trace) in one characteristic dendritic shaft and spine, respectively. *Lower panels*, summary data normalized to control (Ctrl). *, $p < 0.05$.

3.8. Glutamate uptake protects synaptic NMDARs from exposure to ambient glutamate

Electron microscopy suggests that astrocytic processes, which are enriched in high-affinity glutamate transporters (Lehre and Danbolt, 1998) and provide > 90 % of the glutamate uptake in area CA1 (Danbolt, 2001), tend to occur in the vicinity of

postsynaptic spines (Lehre and Rusakov, 2002). While this transporter shield provides a powerful buffer for glutamate which escapes the adjacent synaptic cleft (Bergles et al., 1999; Diamond and Jahr, 1997), it could also protect local synaptic NMDARs from extracellular glutamate originating from outside the immediate synapse. To test this hypothesis, I asked whether blocking glutamate uptake would affect the differential contribution of postsynaptic (associated with dendritic spines), as opposed to dendritic- shaft NMDARs, to the bAP-evoked Ca^{2+} entry.

3.8.1. Glutamate uptake prevents contribution of spine NMDARs to bAP-evoked Ca^{2+} entry

Glutamate transporters were blocked with the potent non-selective glutamate transporter blocker DL-threo-β-Benzyloxyaspartic acid (TBOA) (100 µM). TBOA was added on the presence of the blockers of AMPA/kainate receptors and mGluRs to avoid the involvement of other types of glutamate receptors after extracellular glutamate built up.

Under TBOA treatment, several phenomena were observed. First, TBOA increased the effect of APV on bAP-evoked Ca^{2+} entry in dendritic shafts (Ca^{2+} transients were reduced to 79 ± 3 % of baseline, n = 9; $p < 0.001$; Table 3.1; Fig. 3.9a) indicating that shaft NMDARs are not saturated under basal conditions. Secondly, in the presence of TBOA APV also reduced Ca^{2+} transients in dendritic spines (Table 3.1; Fig. 3.9b; $p < 0.001$). These results provide evidence that the shaft NMDARs sense

concentrations of extracellular glutamate, whereas spine receptors are relatively 'protected' by local transporters (Lozovaya et al., 2004a; Scimemi et al., 2004).

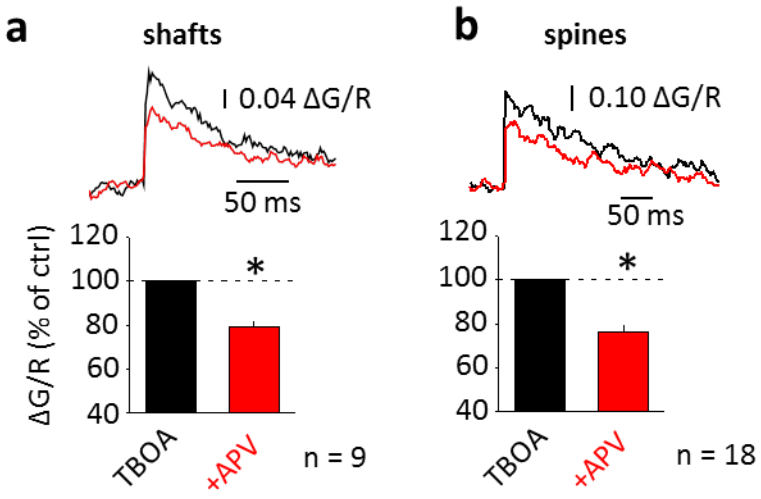

Figure 3.9 Blockade of glutamate uptake unveils the NMDAR contribution to bAP-evoked Ca^{2+} transients in dendritic spines.

a, The glutamate transporter blocker TBOA increases the effect of APV on bAP-evoked Ca^{2+} transients (*ΔG/R*) in shafts. **b,** TBOA reveals a APV-sensitive component in Ca^{2+} transients in spines. **a** and **b**, *Upper panels*, averaged traces of bAP-evoked Ca^{2+} transients in TBOA (black trace) and in TBOA + APV (red trace) in one characteristic dendritic shaft and spine, respectively. *Lower panels*, summary data normalized to the Ca^{2+} transient in TBOA. *, $p < 0.05$.

Table 3.1 Effect of APV on bAP-evoked Ca^{2+} transients

	Normal ACSF	**Bafilomycin A1**	**CA3-tetanus mice**	**In TBOA**
		p, for difference with 'Normal ACSF'		
Shafts	89 ± 3 (13)	87 ± 4 (4)	86 ± 4 (12)	79 ± 3 (9)
		p = 0.36	p = 0.56	*p = 0.011
Spines	98 ± 4 (22)	93 ± 5 (7)	93 ± 6 (11)	77 ± 3 (18)
		p = 0.22	p = 0.43	*p < 0.001

* *ΔG/R*; mean ± SEM (n) - % of bAP-evoked Ca^{2+} transients in its control condition

3.8.2. The concomitant effects of TBOA application

Although the blockade of glutamate uptake resulted in a relatively larger contribution of NMDARs to bAP-evoked Ca^{2+} transients, the baseline amplitude of these transients was decreased by TBOA both in shafts and spines (*ΔG/R*; 80 ± 3 % of control; n= 9, $p < 0.001$ in shafts; 80 ± 5 % of control; n = 18, $p < 0.001$ in spines; Fig. 3.10a,b). Possible explanations for this effect of TBOA are (1) depolarization which leads to recruitment or inactivation of some voltage dependent Ca^{2+} channels (Magee and Johnston, 1995) (thus their insensitivity to bAP), and (2) shunting of bAPs due to an increase in membrane conductance.

Indeed, TBOA notably increased Ca^{2+} baseline level (*baseline G/R*; 117 ± 3% of control, n = 9, p = 0.002 in shafts; 117 ± 4% of control, n = 18, p = 0.001 in spines; Fig. 3.10c,d). TBOA induced a significant shift in the holding current (ΔI_{hold} = -35 ± 8 pA, n = 6, Wilcoxon signed-rank test p = 0.016; Fig. 3.11a) in CA1 pyramidal cells held at -70 mV, which was completely reversed by APV (50 μM). The shift in the holding current was accompanied by an irreversible decrease in the R_{input} (83 ± 7 % of control, n = 6, p = 0.016; Fig 3.11b). The changes in holding current and R_{input} in TBOA were blocked when the slices were pre-incubated in APV (ΔI_{hold} = 2.5 ± 13 pA, n = 5, p = 1; R_{input} : 100 ± 2 % of control, n = 5, p = 0.59; Fig 3.11c,d). These results suggest that TBOA induced an NMDAR-dependent modulation of non-NMDAR conductance (e.g. h-channels (Fan et al., 2005) or Kv channels (Mulholland et al., 2008; Mulholland and Chandler, 2010) following extracellular buildup of glutamate in the presence of TBOA. This also suggests that some NMDARs could be activated at physiological Mg^{2+} near

the cell resting membrane potential (Kovalchuk et al., 2000), and furthermore it highlights the importance of local transporters to protect synaptic NMDARs from globally increased glutamate concentration produced from outside the immediate synapse, which leads to concomitant side-effects including increase in baseline Ca^{2+} concentration, depolarization, and change in cell membrane R_{input}.

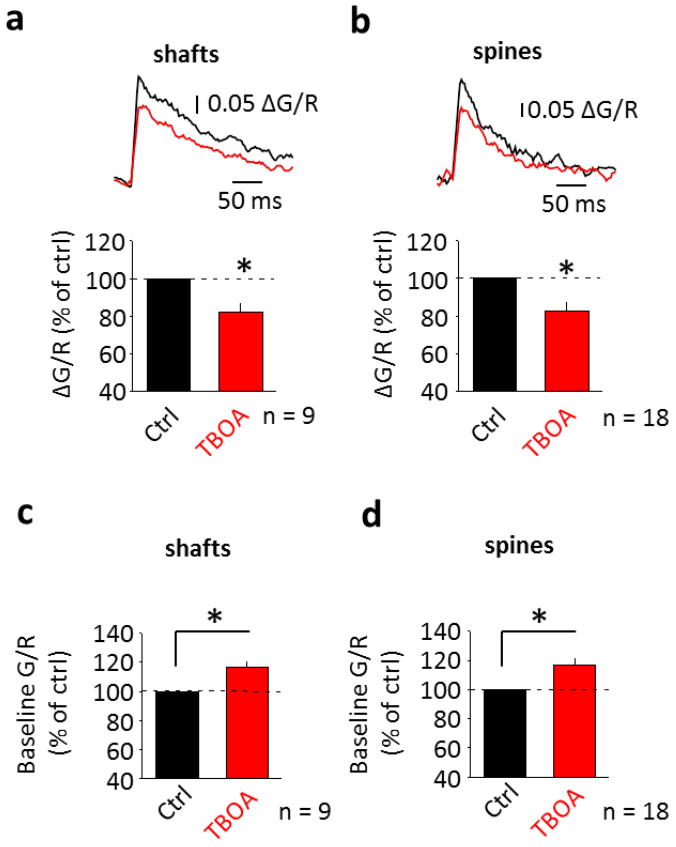

Figure 3.10 The glutamate uptake blocker TBOA reduces bAP-evoked Ca^{2+} transients.

a and **b**, TBOA reduces bAP-evoked Ca^{2+} transients(*ΔG/R*) in dendritic shafts (**a**) and spines (**b**). *Upper panels*, Ca^{2+} transients in control (black line) and in TBOA (red line) in shafts (**a**) and spines (**b**). *Lower panels*, summary data normalized to control ('Ctrl'). c and d, TBOA increases baseline Ca^{2+} (*baseline G/R*)both in in dendritic shafts (c) and spines (d). *, $p < 0.05$.

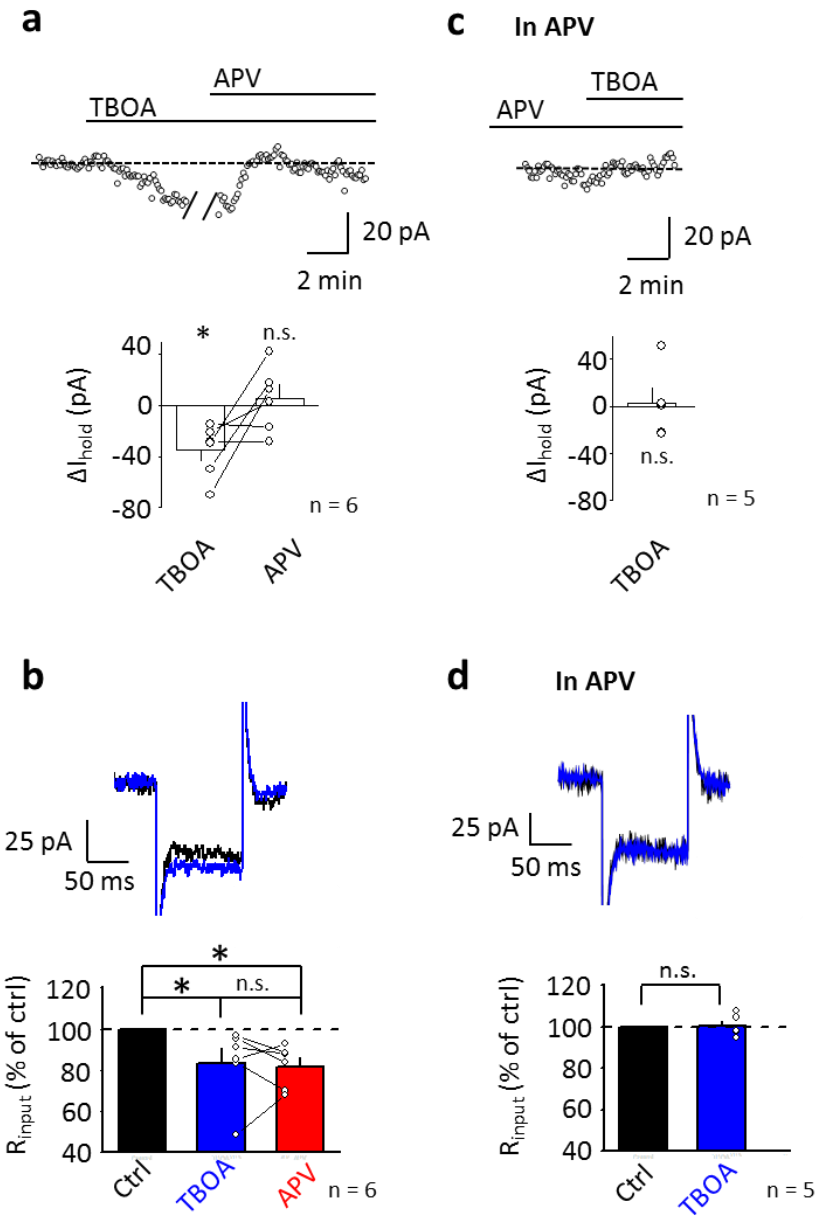

Figure 3.11. Blockade of glutamate uptake induces an NMDAR-dependent decrease of membrane R_{input}.

a and **b**, TBOA induced an NMDAR-dependent shift in the holding current (ΔI_{hold}) in CA1 pyramidal neurons voltage clamped at -70 mV. *Upper panels*, sample traces showing holding current time-course. *Lower panels*, summary data. **c** and **d**, TBOA induced an irreversible decrease in membrane R_{input}. *Upper panels*, the membrane current response to a -5 mV pulse in control (black) and after TBOA (blue). *Lower panels*, summary data. Open circles, individual experiments. *, $p < 0.05$. "n.s.", $p > 0.05$.

Therefore, next I tested the potential effects of TBOA application, namely (a) shunting and (b) depolarization, to see whether they could reproduce the effect of TBOA on bAP-evoked Ca^{2+} entry. First, a shunting effect was mimicked by applying 30 - 50 µM extracellular GABA (with AMPA, NMDA, $GABA_B$ receptors blocked). Extracellular GABA successfully induced a 17 ± 3 % decrease in R_{input} (n =7, $p < 0.008$; Fig 3.12a) which was reversed by $GABA_A$ receptor blocker PTX (100 µM) (104 ± 2 % of control, n = 7, p = 0.625; Fig 3.12a). However, bAP-evoked Ca^{2+} entry was not affected by extracellular GABA (*ΔG/R*; 96 ± 4 % of control, n = 8, p = 0.12 in shafts; and *ΔG/R*; 100 ± 8 % of control, n = 10, p = 0.16 in spines; Fig 3.12c,d) which suggested that the decrease of bAP-evoked Ca^{2+} entry upon TBOA application was not due to an accompanied shunting effect. (At least bAP-evoked Ca^{2+} entry was not affected in proximal oblique dendrites which were imaged). Next, the depolarization effect was mimicked by raising extracellular K^+ to 3.5 mM. It induced 3.6 ± 0.5 mV depolarization and decreased the bAP-evoked Ca^{2+} entry in both shafts and spines (*ΔG/R*; 83 ± 5 % of control; n= 6, $p < 0.009$ in shafts; 79 ± 4 % of control; n = 11, $p < 0.001$ in spines; Fig. 3.13). Therefore, the decrease of bAP-evoked Ca^{2+} entry upon TBOA application could be due to membrane depolarization.

However, neither (a) shunting nor (b) depolarization could explain an increase of the APV effect on bAP-induced Ca^{2+} entry in dendritic spines. Although these data are thus consistent with the hypothesis that glutamate transporters protect synaptic NMDARs from exposure to glutamate, it was important to demonstrate this using less invasive physiological manipulations.

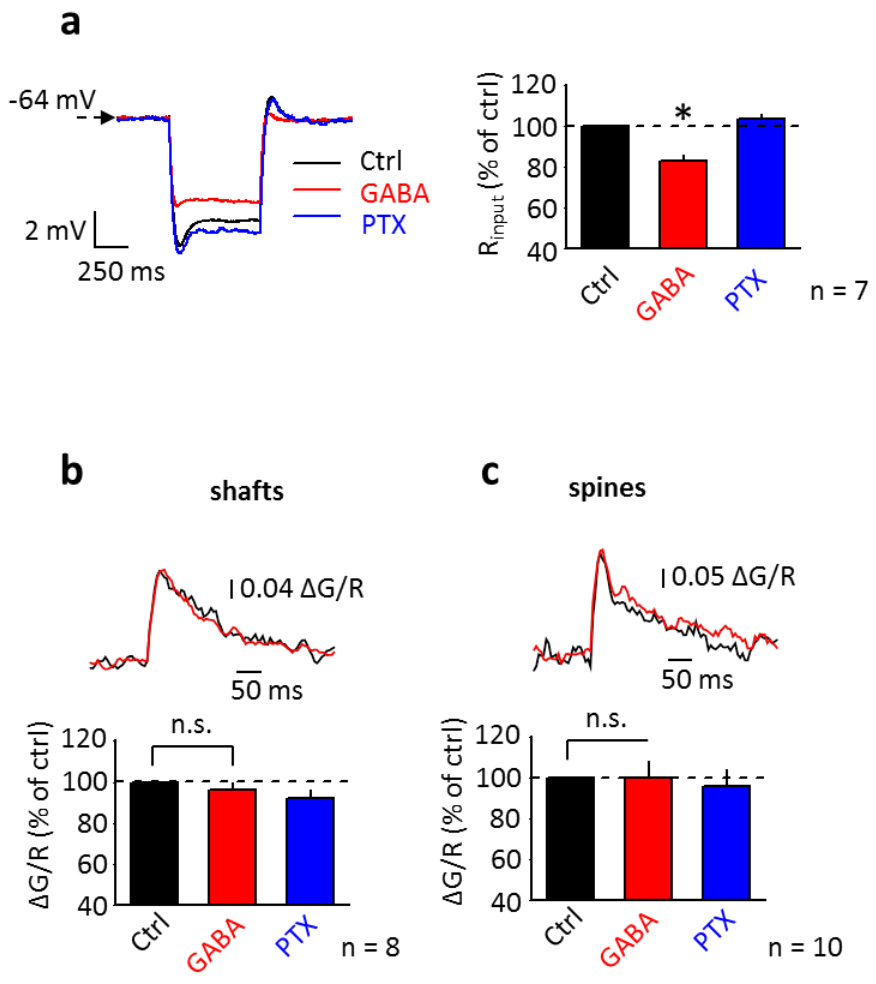

Figure 3.12. Shunting generated by activation $GABA_A$ receptor does not affect bAP-evoked Ca^{2+} transients.

a, GABA (50 µM) induced $GABA_A$ receptor mediated shunting (decrease in R_{input}) in CA1 pyramidal neurons. *Left panel*, the membrane potential responses to a 800 ms/-60 pA current injection in control (black), GABA (red), and PTX (Red). *Right panel*, summary data. **b** and **c**, Shunting induced by $GABA_A$ receptor activation is not accompanied by a decrease of bAP-evoked Ca^{2+} transient. *Upper panels*, bAP-evoked Ca^{2+} transients in control (black line) and in GABA (red line) in shafts (b) and spines (c). *Lower panels*, summary data normalized to control ('Ctrl'). *, $p < 0.05$.

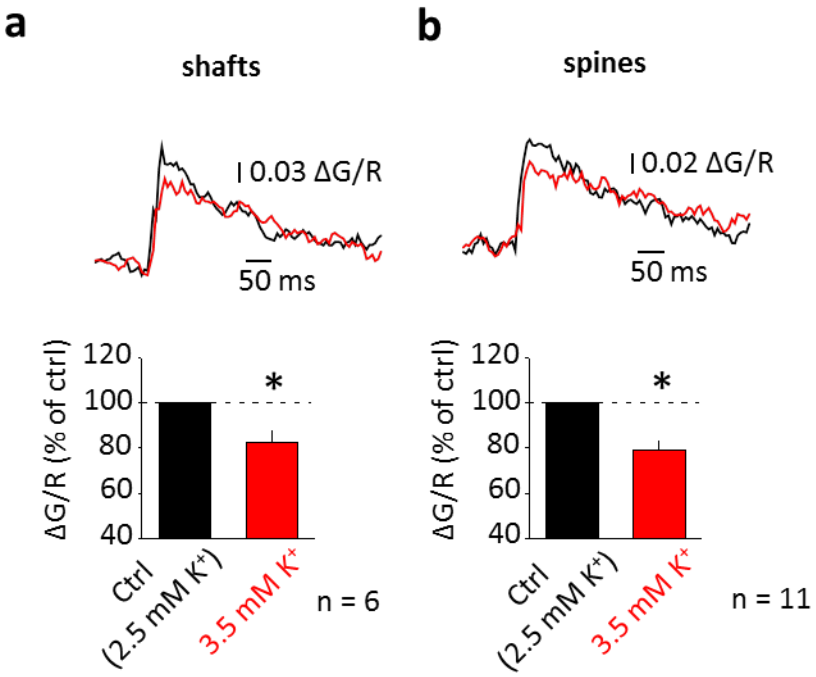

Figure 3.13. Raising external K^+ reduces bAP-evoked Ca^{2+} transients.

a and **b**, Raising external K^+ from 2.5 to 3.5 mM reduced bAP-evoked Ca^{2+} transients(*ΔG/R*) in dendritic shafts (**a**) and spines (**b**) which partially mimics the effect of TBOA. *Upper panels*, Ca^{2+} transients in control (black line) and in 3.5 mM external K^+ (red line) in shafts (**a**) and spines (**b**). *Lower panels*, summary data normalized to control ('Ctrl'). *, $p < 0.05$.

3.9. Discussion

These results demonstrate that NMDARs located in dendritic shafts, but not spines, are bound to glutamate under baseline condition. A bAP relieves the Mg^{2+} block of the receptors providing 'readout' for the ambient glutamate. Because glutamatergic synapses on CA1 pyramidal neurons occur mainly on dendritic spines, shaft NMDARs exist overwhelmingly as extrasynaptic receptors (Petralia et al., 2010). Dendritic spines however may host both synaptic and extrasynaptic NMDARs. Because it may be difficult to distinguish between the two, I have focused on the physiological role of shaft NMDARs as almost exclusively extrasynaptic. The mechanism behind the distinction between spine and shaft NMDARs is likely to be the differential expression of high-affinity neuronal and glial glutamate transporters. The relatively tight glial coverage of dendritic spines and efficient postsynaptic transporters appear to maintain a negligible background glutamate concentration inside the synaptic cleft in the absence of synaptic events (Fig. 1.7a) (Danbolt, 2001; Danbolt et al., 1998; Diamond, 2001).

Indeed, the blockade of glutamate uptake with TBOA revealed contribution of spine NMDARs in Ca^{2+} entry induced by a bAP. Such isolation of the synaptic cleft from baseline ambient glutamate may serve not only the purpose of separation of the signalling mediated by synaptic and extrasynaptic NMDARs, but could also be important for minimizing the desensitization of synaptic AMPA receptors by ambient glutamate (Trussell and Fischbach, 1989). The concomitant effects of blocking

glutamate transporters further suggest the importance of maintaining the compartmentalization of synaptic and extrasynaptic receptors.

Moreover, these results also demonstrate that, in quiescent slices, the extrasynaptic glutamate which binds to shaft NMDARs originates from non-vesicular release, because shaft NMDAR-mediated Ca^{2+} entry enabled by bAP was not affected when the vesicular glutamate release was blocked by bafilomycin A1 or in the transgenic mice without synaptic release from CA3 pyramidal neurons. This finding is consistent with previous reports that baseline ambient glutamate originates from non-vesicular astrocytic release (Cavelier and Attwell, 2005; Jabaudon et al., 1999; Le Meur et al., 2007).

Actually, the majority of the bAP-evoked Ca^{2+} influx in dendrite of CA1 pyramidal neuron is mediated by VDCCs both in spine and shaft (Bloodgood and Sabatini, 2007b; Sabatini and Svoboda, 2000). Specifically, Bloodgood and colleagues performed two-photon Ca^{2+} imaging approaches combining pharmacological tools which sensitively block different types of VDCCs, and show that the T-type, L-type, and N-type VDCCs contribute to bAP-evoked Ca^{2+} entry both in shafts and in spines, whereas R-type VDCCs are specifically presented in spines (Bloodgood and Sabatini, 2008). However, the glutamate-bound NMDAR-mediated Ca^{2+} entry during bAP was not discussed because the NMDAR antagonist was always present in their recording solution. Another work by Herman and colleagues, however, suggested no contribution of Ca^{2+} entry through NMDARs during a single bAP (Herman et al., 2011). In their work, the lower sensitive Ca^{2+} dye, Fluo-5F (Kd = 1.3 μM), was used for

monitoring bAP-evoked Ca^{2+} entry, whereas in my work the ~4-fold more sensitive calcium dye, Fluo-4 (Kd = 0.3μM), was used. This difference in dye sensitivity might be critical for observing the small changes, here 13 ± 4%, of a single bAP-evoked Ca^{2+} entry.

Chapter 4: Detection of extrasynaptic glutamate concentration rises by NMDARs during bAPs

4.1. Introduction

In chapter 3, I have shown that a bAP can provide 'readout' for the baseline ambient glutamate bound to shaft NMDARs, whereas spine NMDARs could be protected from ambient glutamate by the powerful transporter shield. The extracellular glutamate concentration in a quiescent brain slice can be thought of as a 'floor' level of ambient glutamate which is independent of the synaptic network activity. In addition to ambient non-vesicular glutamate, extrasynaptic NMDARs potentially can also be bound to glutamate escaping from the synaptic cleft when synaptic network activity increases, as well as from transient astrocytic release. In this chapter, I tested whether the same readout mechanism also applies to the detection of rises of extracellular glutamate concentration in these conditions (illustrated in Fig. 1.6e and 1.7b).

4.2. Materials and methods

4.2.1. Animal and slice preparation

Procedures for preparing transverse slices (350 μm) of hippocampus from SD rats aged p21 - p35 are described in Chapter 2.2 and 2.3. Briefly, rats were anaesthetised and decapitated. The brain was removed, chilled with ice-cold cutting solution. Hippocampi from both hemispheres were isolated and placed in an agar block and transverse slices (350 μm) were cut with a vibroslicer (Fig. 2.1e). The slices were left to recover for 20 to 30 min at 34°C in a submerged chamber in cutting or storage solution. Then they were transferred and incubated on either an interface- or submerged-type chamber (mostly submerged-type) at room temperature for at least 1 hour for recovery with storage solution. After that, the slices were transferred to the recording chamber and were continuously superfused at 33-34^{o}C with ACSF. All solutions were saturated with 95% O_2 and 5% CO_2. Osmolarity was adjusted to 298 ± 3 mOsm.

4.2.2. Electrophysiology and two-photon imaging

Whole cell patch-clamp recording and two-photon imaging were performed as described in Chapter 2.5 and 2.6. Briefly, cells in slices were first visually identified using Olympus BX-61 microscope equipped with differential interference contrast optics under infrared illumination and a 60x water immersion lens. For imaging experiments, whole-cell current-clamp recordings were obtained from CA1

pyramidal neurons with a patch pipette (3 - 6 MΩ) filled with a solution containing the morphological tracer Alexa Fluor 594 (50 µM) and the Ca^{2+} sensitive dye Fluo-4 (250 µM). Once the whole cell recordings were obtained, the patch amplifier (Multiclamp 700B) was set to either current- or voltage-clamp mode. Dendritic bAPs were induced in these cells by somatic current injections (2-3 ms, 400 - 1000 pA) and monitored in the soma. Two-photon imaging was performed at least 20 -30 min after rupturing the seal and breaking into the cell to ensure dye reaching steady-state. Imaged dendrites were at least 30 µm (mostly 50 µm) below the slice surface.

4.2.3. Local synaptic stimulation and finding the active spine

Local synaptic stimulation was done with an extracellular glass pipette (2–3 µm tip) filled with 1M NaCl. To monitor the location of the pipette, 5 µM Alexa Fluor 594 was also added to the solution in the pipette. The pipette then was positioned 5 to 20 µm from an apical oblique dendrite of the recorded neuron (Yasuda et al., 2004). The neuron was voltage-clamped at -40 mV in absence of AMPA receptor antagonists. Then we identified spines which responded with Ca^{2+} transients to a train of 5 stimulus pulses (0.2-5 V, 200 µs) at 50 Hz to assure glutamate release (Fig. 4.1). Then the AMPA receptors were blocked. The cells were held in current clamp and three types of measurements were done in the dendrite and the spine: (1) Ca^{2+} transients in response to a bAP; (2) Ca^{2+} response to synaptic stimulation; and (3) a response to the bAP and 'synaptic' stimulation combined. In protocol (3) bAPs were initiated 70 ms after the end of synaptic stimulation.

4.2.4. Uncaging of caged glutamate

Single-photon and two-photon glutamate uncaging were performed as described in Chapter 2.6 and Chapter 2.7 respectively. Briefly, experiments were performed by using a two-scanner FV1000-MPE microscope (Olympus) equipped with two ultra-fast pulsing lasers, Mai-Tai (Spectra-Physics) tuned to 810 – 830 nm and 720 nm for imaging and for glutamate uncaging, respectively (Fig. 2.5). MNI-caged glutamate (12 mM) was applied locally via an extracellular glass pipette (1-2 MΩ). The uncaging spot was located opposite an oblique dendrite at equal distances (around 1 µm) from the imaged dendritic shaft and spine (Fig 4.1). To mimic the transient rise of extracellular glutamate concentration, the duration and the power of the uncaging pulse were set to 5 ms and low power (2-3 mW) to produce a just detectable Ca^{2+} response.

4.2.5. Pairing protocols for two-photon uncaging

For the 'pairing' protocol, the three types of recordings were carried out: (1) Ca^{2+} transients in response to a bAP; (2) a Ca^{2+} response to glutamate uncaging; and (3) a response to the bAP and uncaging combined. In protocol (3) bAPs were induced 70 ms after the uncaging pulse to avoid the involvement of another voltage-gated conductance.

4.3. Detection of glutamate spillover

To test whether such protection withstands increased network activity, a brief train of stimuli to Schaffer collaterals was applied (5 at 50 Hz, Chapter 2.9). This stimulation is compatible with physiological discharges of CA3 pyramidal cells, thought to be sufficient to produce detectable glutamate escape (Lozovaya et al., 2004b; Min et al., 1999; Min et al., 1998; Scimemi et al., 2004; Semyanov and Kullmann, 2000). When the cell was held at -70 mV with AMPA receptors not blocked, this stimulus evoked clear Ca^{2+} responses in a proportion of dendritic spines, but not in dendritic shafts (Fig. 4.1). This pattern of responses has routinely been associated with spines activated by glutamate released at the immediate synapse (Sabatini et al., 2002). Next we depolarized the cell to -40 mV to relieve the Mg^{2+} block of NMDARs. Under these conditions synaptic stimulation did evoke a detectable APV-sensitive Ca^{2+} response in a proportion of the previously unresponsive spines, as well as in the dendritic shaft (Fig. 4.1). The most plausible explanation is that removing the Mg^{2+} has boosted the response of spine and shaft NMDARs to glutamate escaping from active synapses. An alternative explanation involving activating NMDAR-only ('silent') synapses (Kerchner and Nicoll, 2008) is unlikely because the 'mature' spine types which were routinely imaged in adult animals are thought to host synapses equipped with AMPA receptors (Beique et al., 2006; Busetto et al., 2008).

To understand the role of signals mediated by synaptic glutamate escape, I therefore focused on the spines showing small (indirectly activated) NMDAR-mediated Ca^{2+} responses, termed here as spillover-activated spines (SASs). In the presence of AMPA/kainate, mGluRs, $GABA_A$ and $GABA_B$ receptor blockers, the stimulation induced a small and slow somatic depolarization (2.3 ± 0.6 mV). It was shown that bAP itself can be boosted when it coincides with an EPSP due to many voltage-dependent ion channels within a narrow time window (4-6 ms) (Stuart and Hausser, 2001b). To avoid the effect of the depolarization itself on the amplification of bAP, the bAP was paired with a very long delay (70 ms) after the last synaptic stimulation. When the synaptic stimulation was paired with a bAP (Fig. 4.2b), a relatively small, but highly significant, supra-linear summation of Ca^{2+} entry was observed both in the shafts (*ΔG/R*; 115 ± 3 % of the sum, n = 10, $p < 0.001$; Fig. 4.2c,e) and in the spines (*ΔG/R*; 115 ± 5 % of the sum, n = 19, p = 0.001; Fig. 4.2d,f; cells were held in current clamp mode). If anything, the supra-linear effect is likely to be underestimated under these conditions, as any partial saturation of the fluorescence indicator would produce a smaller fluorescence increment in response to the same Ca^{2+} entry. Importantly, the effect was completely abolished by APV (*ΔG/R*; shafts: 100 ± 2 % of the sum, n = 7, p = 0.49; spines: 104 ± 4 % of the sum, n = 13, p = 0.17; Fig. 4.2e,f) suggesting that bAPs can provide a readout mechanism for the detection of a glutamate rise by both shaft and spine NMDARs.

Interestingly, no supra-linear boost was found in directly activated spines (DASs) (*ΔG/R*; 98 ± 4 % of the sum, n = 4, p = 0.65), which indicates that either the subunit

compositions of synaptic NMDARs are different from extrasynaptic ones (Harney et al., 2008; Lozovaya et al., 2004b), or they had already desensitized due to binding with a higher concentration of glutamate.

Finally, because the depolarization caused by the synaptic stimulation protocol could also induce a direct amplification of the pairing bAP even with a 70 ms delay (although unlikely), a different way of synaptic stimulation was applied to test this possibility. Instead of local stimulation, synaptic stimulation was applied with a bipolar electrode placed > 200 μm from the recorded neurons in stratum radiatum. The stimulation intensity was set to produce similar somatic depolarization as with local stimulation. Then spines and shafts of an apical oblique dendritic branch were scanned to monitor the Ca^{2+} transients induced by the pairing protocols. In this set of experiments no supra-linear summation of bAP-evoked Ca^{2+} entry was observed (*ΔG/R*; 103 ± 7 % of the sum, n = 8, p = 0.42 in shafts; 99 ± 4 % of the sum, n = 8, p = 0.32 in spines) which ruled out the possibility of direct amplification of bAPs by depolarization. These results also suggested that bAPs readout the local glutamate concentration rise and produce supra-linear Ca^{2+} entry locally.

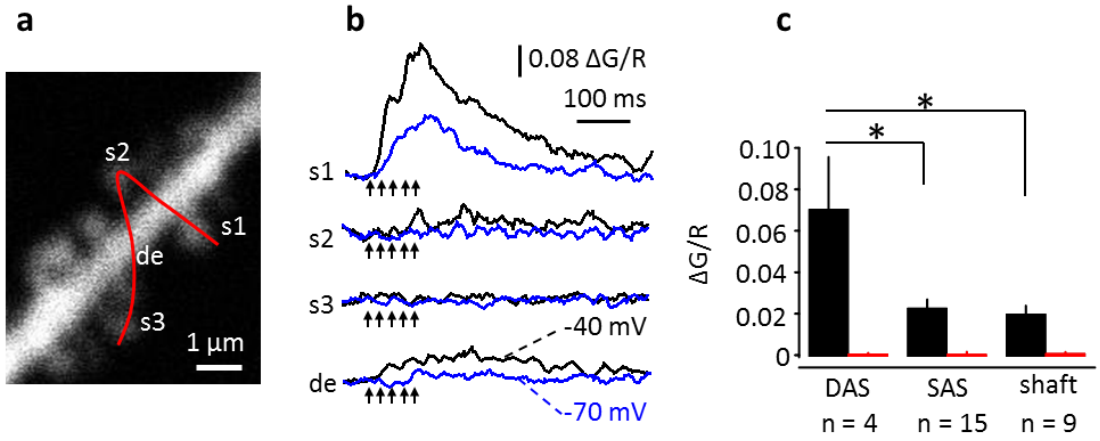

Figure 4.1. Ca^{2+} response to synaptically released glutamate in dendritic shafts and spines.

a, A recorded dendrite. Red line: line-scan position through the spines (*s1-3*) and the shaft (*de*). **b**, Ca^{2+} transients (*ΔG/R*) in corresponding shaft and spines induced by 5 x 50 Hz electric stimulation (black arrows) when the cell was voltage-clamped at -70 mV (blue line) or at -40 mV (black line). Large responses were detected in *s1* (directly activated spine - *DAS*); a small response in *s2* (spillover activated spine - *SAS*) and *de*; no response in *s3* (inactive spine). **c**, Averaged amplitude of Ca^{2+} transients (*ΔG/R*) at -40 mV from different cells in *DASs* (n=4), *SASs* (n=15) and shafts (n=9) in control conditions (black bars) and in the presence of APV (red bars) *, $p < 0.05$.

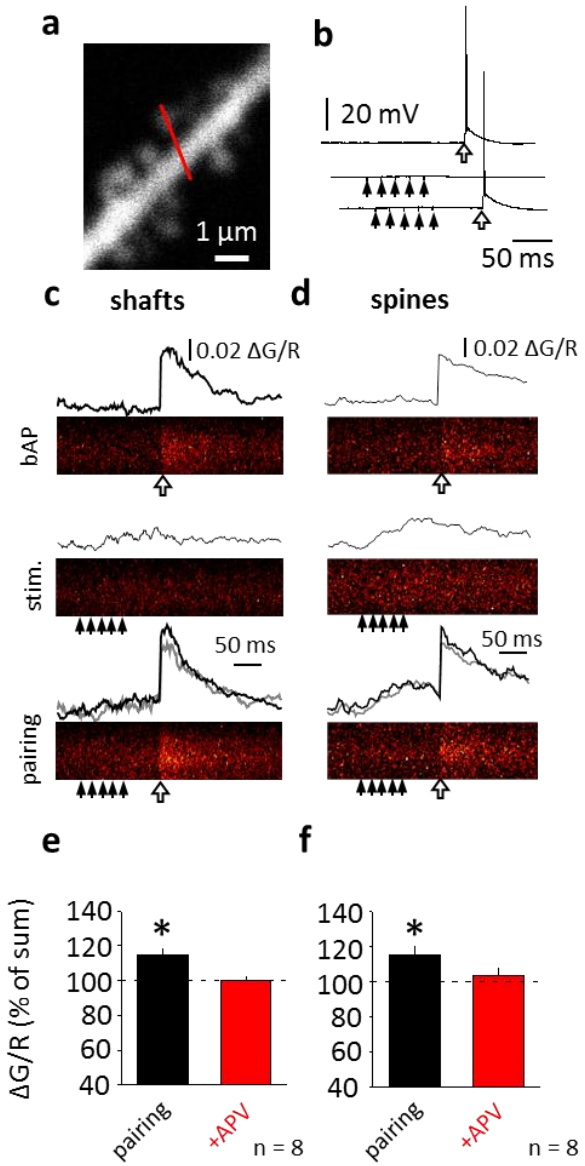

Figure 4.2. bAP triggers detection of synaptic glutamate spillout by both shaft and spine NMDARs .

a, A recorded dendrite with line-scan positions (red line). **b**, Somatic response to current injection (open arrow), local synaptic stimulation (black arrows) and their combination. **c** and **d**, Line-scan images and the corresponding traces (black) of Ca^{2+} transients in shafts (**c**) and spines (**d**) induced by a *bAP* (top), synaptic stimulation (‘*stim.*’; middle), and synaptic stimulation paired with a *bAP* (*‘pairing’*; bottom). Grey line, arithmetic sum of *bAP* and *‘stim.’* traces. **e** and **f**, Summary data of pairing response normalized to the sum of *bAP* and ‘*stim.*’ responses in shafts (**e**) and spines (**f**) in normal ACSF (pairing) and in APV (+ APV). *, $p < 0.05$.

4.4. Detection of extracellular glutamate released from a volume-limited source

Stimulation of afferent fibers activates multiple sources of glutamate in the neuropil in a relatively indiscriminate manner, making it impossible to gauge typical distances between the source and the detected Ca^{2+} signal. To control glutamate release in space and time we employed two-photon uncaging of extracellular glutamate. To test the sensitivity of the bAP-evoked Ca^{2+} entry to local glutamate rises, we uncaged glutamate at a single point 1 µm away from both the spine and the parent shaft (5 ms pulse), a distance exceeding the average nearest-neighbor distance between synapses in the hippocampus (~0.5 µm) (Rusakov and Kullmann, 1998) (Fig. 4.3). The uncaging of glutamate in the presence of an AMPAR antagonist produced small Ca^{2+} transients (*ΔG/R*; 0.093 ± 0.030 in spines and 0.020 ± 0.006 in shafts, n = 7), which are likely to reflect the fraction of NMDARs with Mg^{2+} unblocked at resting conditions (Kovalchuk et al., 2000); these transients were completely blocked by APV (Fig. 4.3). However, when uncaging was paired with a bAP, the resulting Ca^{2+} signals were again substantially higher than the sum of the Ca^{2+} signals evoked by either uncaging or a bAP alone (*ΔG/R*; shafts: 122 ± 4 % of the sum, n = 7, $p < 0.001$; Fig. 4.3c,e and spines: 129 ± 10 % of the sum, n = 7, p = 0.015; Fig. 4.3d, f). Again, the supra-linearity was completely abolished by APV (*ΔG/R*; shafts: 102 ± 3 % of the sum, n = 7, p = 0.28; Fig. 4.3e and spines: 99 ± 1 % of the sum, n = 7, p = 0.19; Fig. 4.3f). This result is therefore consistent with our suggestion that bAPs can provide a readout of local extrasynaptic glutamate rises, be it from synaptic activity

(Rusakov and Kullmann, 1998; Zheng et al., 2008), or through astrocytic (Jabaudon et al., 1999) or ectopic dendritic (Duguid et al., 2007; Shin et al., 2008a) release.

Next the Ca^{2+} entry purely contributed by NMDARs ($\Delta G/R_{NMDARs}$) during the pairing protocol was calculated by subtracting the $\Delta G/R$ values of the arithmetic sum from the pairing. Although the surface density of spine-associated NMDARs is much higher than that of shaft-associated NMDARs (Aoki et al., 1994; Racca et al., 2000; Sans et al., 2000), these experiments failed to show a larger contribution of the Ca^{2+} entry from spine-associated NMDARs compared to the shaft-associated receptors ($\Delta G/R_{NMDAR}$; shaft: 0.018 ± 0.003, n = 7; spine: 0.039 ± 0.012, n = 7; p = 0.12 for difference). This finding suggests that glutamate generated from extrasynaptic sources can access and bind to extrasynaptic NMDARs on dendritic shafts easier. It is also consistent with our previous finding (Fig. 3.1c,d) that extracellular glutamate is more likely to be taken up by high-affinity glutamate transporters in the synaptic vicinity before it binds to synaptic or perisynaptic NMDARs.

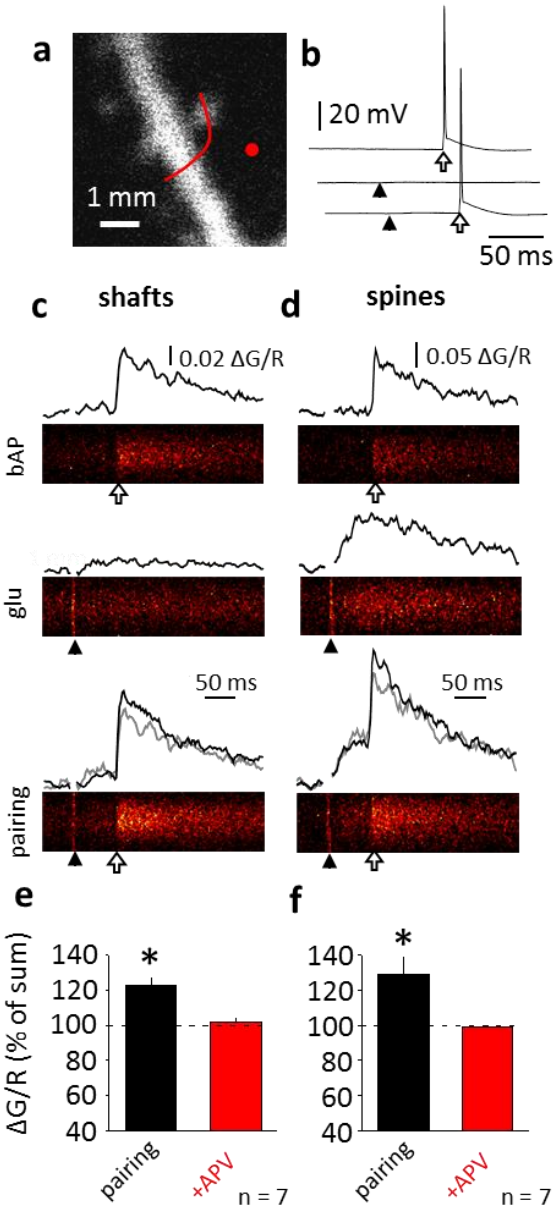

Figure 4.3 bAP triggers detection of photolysis-induced local rises in extracellular glutamate by both shaft and spine NMDARs.

a, A recorded dendrite depicting line-scan positions (red lines). Red circle: the uncaging spot. **b**, Somatic response to current injection (open arrow), local glutamate uncaging (black arrow) and their combination. **c** and **d**, Line-scan images and the corresponding traces (black) of Ca^{2+} transients in shafts (**c**) and spines (**d**) induced by a *bAP* (top), uncaging (‘*glu*’; middle), and uncaging paired with a *bAP* (*‘pairing’*; bottom). Grey line, arithmetic sum of *bAP* and ‘*glu*’ traces. **e** and **f**, Summary data of pairing response normalized to the sum of *bAP* and ‘*glu*’ responses in normal ACSF (pairing) and in APV (+ APV). *, $p < 0.05$.

4.5. NMDAR subtypes that sense extrasynaptic glutamate rise

The results indicate that although in baseline conditions only shaft NMDARs are bound with ambient glutamate, spine NMDARs are recruited when the concentration of glutamate is raised due to glutamate spillover and uncaging. Next, I investigated the subunit compositions of NMDARs that sense the rises of extracellular glutamate. Specifically, because the extrasynaptic NMDARs in hippocampal pyramidal cells were shown to be GluN2B- and GluN2D-containing NMDARs, I tested the effect of GluN2B selective blocker, Ro25-6981, and the GluN2C/D selective blocker, PPDA, on NMDAR-mediated Ca^{2+} influx.

CA1 pyramidal cells were filled with Alexa 594 (50 µM) and Fluo-5F (300 µM) with a patch pipette for at least 20 min. Glutamate uncaging was performed in Mg^{2+} free (or low Mg^{2+} (0.05 mM)) ACSF while voltage clamping the neuron at -70 mV. 200 to 250 µM of MNI-caged glutamate was added to the bath solution. NMDAR-mediated Ca^{2+} entry was induced in the dendritic spines and shafts by single photon glutamate uncaging 1-2 µm away from the dendrite in the presence of AMPA/kainate, mGluR, $GABA_A$, and $GABA_B$ receptor blockers. The GluN2B-containing NMDAR selective blocker, Ro25-6981 5 µM (Ro25) (Fischer et al., 1997), significantly decreased the Ca^{2+} entry in spines (*ΔG/R*; 79 ± 6 % of control, n = 15 spines p = 0.002) but failed to show effect on dendritic shafts (*ΔG/R*; 89 ± 10 % of control, n = 8 spines p = 0.156; Fig 4.4a,b). The GluN2C/D-containing NMDARs selective blocker, PPDA 0.5 µM, further decreased the Ca^{2+} entry both in spines and shafts (*ΔG/R*; 39 ± 5 % of control, n = 15 spines, p < 0.001; 42 ± 7 % of control, n = 8 shafts, p = 0.004). Adding

APV then abolished the remaining Ca^{2+} responses in both shafts and spines, only the artefacts of uncaging, producing auto-fluorescence were left (*ΔG/R*; 10 ± 2 % of control, n = 15 spines, $p < 0.001$; 11 ± 2 % of control, n = 8 shafts, $p = 0.004$). Because it has been shown that the GluN2C subunit does not express in hippocampal neurons (Ishii et al., 1993; Wenzel et al., 1997), the PPDA sensitive component was due to the activation of GluN2D-containing NMDARs. These results suggest that Ca^{2+} entry through spine NMDARs activated by extrasynaptic uncaging are composed of 23 ± 7 % of GluN2B subunits and 45 ± 6 % of GluN2D subunits. However, in dendritic shaft, Ca^{2+} entry through NMDARs was not contributed by GluN2B-containing NMDARs, but 55 ± 9 % of which was contributed by GluN2D-containing NMDARS. Both in spines and shafts, the residual 30 % of Ca^{2+} response was insensitive to Ro25 and PPDA, but blocked by APV. Presumably, it was partially mediated by GluN2A subunit-containing NMDARs but this needs to be further confirmed by the GluN2A selective blocker.

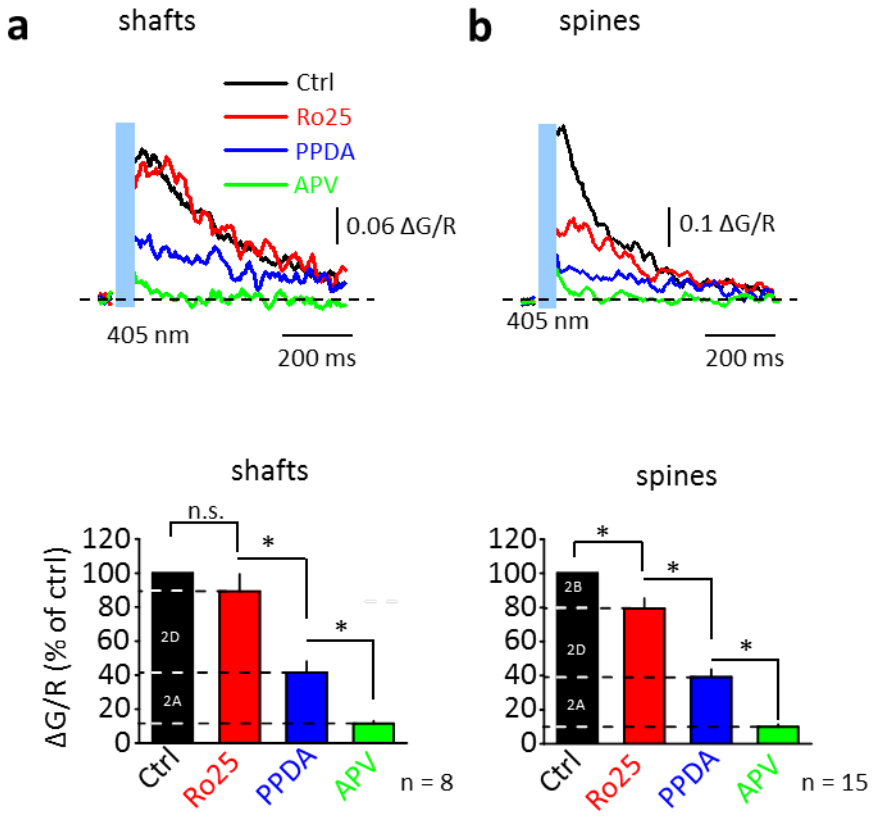

Figure 4.4 NMDAR subtypes that sense extrasynaptic glutamate rise

a and **b**, The uncaging induced Ca^{2+} transients (*ΔG/R*) in zero-Mg^{2+} solution can be reduced by GluN2B selective blocker, Ro25-6981 (Ro25), and GluN2C/D selective blocker, PPDA, in both shafts (**a**) and spines (**b**). *Upper panels*, averaged traces of Ca^{2+} transients in control (Ctrl; black), Ro25 (red), PPDA (blue), and APV (green). *Lower panels*, bar charts of summary data normalized to control (Ctrl). '2D, '2B' and '2A' indicate the portions of Ca^{2+} entry that is possibly contributed by GluN2B and GluN2D subunits, respectively. *, $p < 0.05$. "n.s.", $p > 0.05$.

4.6. Discussion

These results demonstrated that in addition to ambient non-vesicular glutamate, presumably the 'floor' level of extracellular glutamate, extrasynaptic NMDARs can also bind glutamate escaping from the synaptic cleft when synaptic network activity increases. They can also bind glutamate released from astrocytes. I found that synaptic discharges (or local glutamate uncaging mimicking this) paired with bAPs boost Ca^{2+} entry in both shafts and spillover-activated spines (Fig. 4.1 and 4.2). Thus both shaft and spine NMDARs can also sense extracellular glutamate, which is transiently elevated as a result of local synaptic activity, but they require a 'readout' signal such as the bAP to be activated. Importantly, the coincidence detection interval for glutamate release and bAPs extends beyond the duration of individual glutamate rises, reflecting the fact that glutamate molecules can remain bound to dendritic NMDARs for hundreds of milliseconds. The NMDAR-mediated enhancement of bAP-evoked dendritic Ca^{2+} signals could therefore act as an integrating detector of glutamate release events.

It is also worth noting that the experiments were performed in the presence of AMPA/kainate receptor blocker, NBQX, which reduces the depolarization during synaptic stimulation. However, there is still NMDAR-Ca^{2+} entry observed without the 'readout' provided by bAP, suggesting that NMDARs were partially activated by massive glutamate release during high frequency synaptic stimulation at the resting membrane potential. The depolarization triggered by NMDARs can provide 'readout'

by themselves and recruit more NMDARs to become active, which works as a positive feedback loop. Such positive feedback has been shown to mediate NMDAR spikes triggered by clustered synaptic inputs in cortical pyramidal neurons (Schiller et al., 2000). On the other hand, unlike glutamate release triggered by high frequency synaptic stimulation, which still directly activates synaptic NMDARs due to the high concentration of glutamate in the synaptic cleft, the extrasynaptic glutamate uncaging can preferentially activate extrasynaptic NMDARs with a relatively lower glutamate concentration. Indeed, glutamate uncaging triggered less depolarization (less than 1 mV) than when it was induced by synaptic stimulation, while it generated larger Ca^{2+} entry during the 'readout' period, suggesting that the 'readout' signal is more important for pure extrasynaptic signalling which by itself cannot produce sufficient depolarization to relieve the magnesium block.

The results also demonstrate that a large portion (more than 50% in the shafts and more than 40% in the spines) of NMDAR-mediated Ca^{2+} entry induced by extrasynaptic glutamate uncaging is sensitive to selective blockers of GluN2B- and GluN2C/D-containing NMDARs (Ro25-6981 and PPDA respectively). Especially the PPDA sensitive component contributes more than 40% of Ca^{2+} entry. Since GluN2C-containing NMDARs are expressed highly confined to cerebellum, thalamus, and olfactory bulb (Ishii et al., 1993; Wenzel et al., 1997), it is unlikely that GluN2C-subtyes contribute to the Ca^{2+} entry which I observed. Although it has also been shown that in adult hippocampus only a very low level of GluN2D mRNA was detected (Dunah et al., 1996), evidence demonstrated that functional GluN2D-

containing NMDARs are located on the extrasynaptic membrane(Costa et al., 2009; Harney et al., 2008; Lozovaya et al., 2004b), and contributes about 60% of the tonic NMDAR-mediated current in CA1 hippocampal neurons (Le Meur et al., 2007). Therefore, my results suggest that besides GluN2B, GluN2D-containing NMDAR might be another major subtype that mediates the detection of rise of extrasynaptic glutamate concentration.

It has been shown that the Mg^{2+} unblocking from GluN2A and GluN2B-containg NMDARs has a prominent slow component in cultured cells (Clarke and Johnson, 2006) and in cortical pyramidal neurons (Vargas-Caballero and Robinson, 2003). The slow unblocking time constants during rapid depolarization pulses are around 5 ms for GluN2A and 9 ms for GluN2B whereas the Mg^{2+} unblocking rate from GluN2D-containing receptors is extremely fast (unblocking time constant: 0.25 ms) without any slow unblock (Clarke and Johnson, 2006). Thus during rapid depolarization, such as a bAP, the Mg^{2+} block might be preferentially relieved from GluN2D-containing NMDARs than from other subtypes.

Chapter 5: Computational simulation of tonic NMDAR-mediated Ca^{2+} entry during bAPs

5.1. Introduction

I next addressed the question of whether even short durations of depolarization during a single bAP, approximately 2 ms half duration, could relieve the Mg^{2+} block efficiently and produce a large enough Ca^{2+} influx to be observed by 2-photon Ca^{2+} imaging (Fig. 3.1). It has been shown that NMDAR has a slow fraction of Mg^{2+} unblock (i.e. unblocking τ = 4 – 10 ms weights 35 -45 % of total unblocking) and a rapid reblock (reblocking τ < 0.2 ms) (Kampa et al., 2004; Vargas-Caballero and Robinson, 2003). In order to confirm the experimental results and also to further evaluate the Ca^{2+} influx from tonic NMDAR conductances (i.e. tonic glutamate-bound NMDARs) during different firing modes, I built a mathematical model of tonic NMDAR conductance which takes subunit-specific kinetics of Mg^{2+} unblocking into consideration (Clarke and Johnson, 2006; Kampa et al., 2004; Le Meur et al., 2007). This NMDAR conductance then was inserted onto a modelled CA1 pyramidal cell built previously (Poirazi et al., 2003), and simulated with the NEURON simulation environment (Hines and Carnevale, 1997).

5.2. Methods for computational simulation

First, I constructed a modelled tonic NMDA conductance with channel gating properties both obtained from experimental data and from a previous report (Kampa et al., 2004) (Chapter 5.2.1 – 5.2.3). Then the constructed tonic conductance was inserted into a modelled neuron with morphology reconstructed from a biocytin-filled CA1 pyramidal cell and biophysical properties built by Poirazi and colleagues (Poirazi et al., 2003) (Chapter 5.2.4). The simulation was performed with the NEURON simulation environment (version 7.1) (Hines and Carnevale, 1997) using a desktop PC equipped with 4-core 64-bit processor (Intel Core i7). The detailed procedures are described below.

5.2.1. Obtaining the I-V relation of tonic NMDAR-mediated current

To obtain the I-V relation of tonic NMDAR-mediated currents in CA1 pyramidal neurons, whole-cell voltage clamp recordings were performed using the same $CsCH_3SO_3$ based internal solution as described above with additional 3 mM QX-314. The cell was voltage clamped to +50 mV to inactivate voltage-dependent conductances. After the holding current stabilized, a 4-second voltage ramp (from -70 mV to + 50 mV) was applied to the soma every 10 sec (Fig. 5.1a). The tonic NMDAR-mediated current was isolated by subtracting the holding current before and after D-APV (100 μM) application. After offline series resistance compensation, the I-V relation of tonic NMDAR-mediated current was obtained (Fig 5.1b).

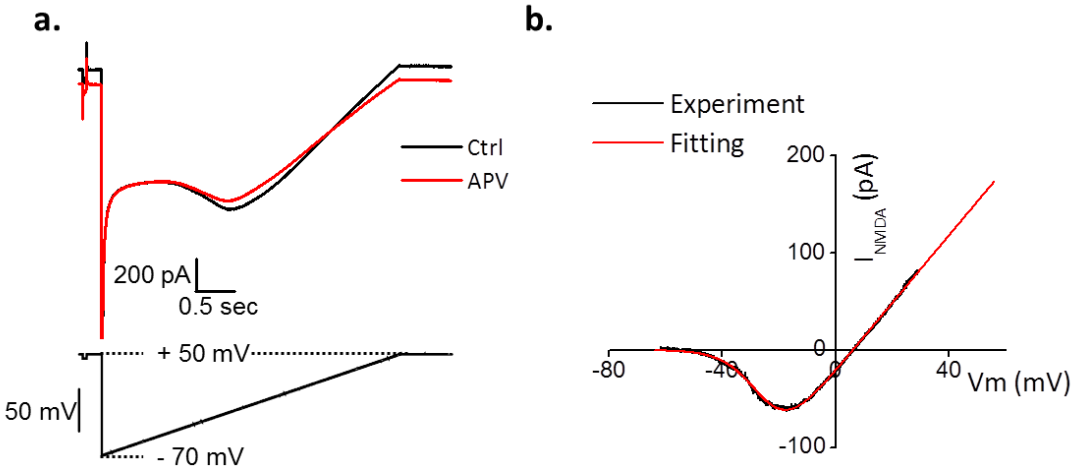

Figure 5.1 I-V curve of tonic NMDAR–mediated conductance

a. The cell was voltage clamped at +50 mV followed by a voltage ramp from -70 mV to + 50 mV at 34°C. Upper panel, the holding current in control (Ctrl; black) and after applying 100 µM D-APV (APV; red). Lower panel, the voltage command. **b.** The I-V curve of tonic NMDAR-mediated current isolated by D-APV (black).The I-V curve was fitted with a Boltzmann equation (red).

5.2.2. NMDAR channel property: open-channel Ionic flux

The open-channel ionic fluxes of tonic NMDAR are composed of sodium, potassium, and calcium fluxes. The ionic fluxes are described by Goldman-Hodgkin-Katz flux equations (Hille, 2001):

$$I_{Na^+}(V_m) = P_{Na}(V_m) * {Z_{Na}}^2 * \frac{V_m F^2}{RT} * \frac{[Na^+]_i - [Na^+]_0 * exp(-Z_{Na} V_m F/RT)}{1 - exp(-Z_{Na} V_m F/RT)} \quad (1)$$

$$I_{Ca^{2+}}(V_m) = P_{Ca}(V_m) * {Z_{Ca}}^2 * \frac{V_m F^2}{RT} * \frac{[Ca^{2+}]_i - [Ca^{2+}]_0 * exp(-Z_{Ca} V_m F/RT)}{1 - exp(-Z_{Ca} V_m F/RT)} \quad (2)$$

$$I_{K^+}(V_m) = P_K(V_m) * {Z_K}^2 * \frac{V_m F^2}{RT} * \frac{[K^+]_i - [K^+]_0 * ex\square(-Z_K V_m F/RT)}{1 - exp(-Z_K V_m F/RT)} \quad (3)$$

where *F*, *R*, and *T* are Faraday constant, gas constant, and absolute temperature (here *T* = 307 degrees Kelvin), respectively; V_m is the membrane potential; P_{Na}, P_{Ca}, and P_K are the ionic permeability; Z_{Na}, Z_{Ca}, and Z_K are valence for sodium, calcium, and potassium, respectively. The ratio of $P_{Na} : P_{Ca} : P_K$ is set to be 1 : 10.6 : 1 according to the ionic permeability of NMDAR (Mayer and Westbrook, 1987). Therefore, the open channel ionic flux of NMDAR, $I_{NMDAR\text{-}open}$ is simply the summation of three different ionic currents:

$$I_{NMDAR-open}(V_m) = I_{Na^+}(V_m) + I_{Ca^{2+}}(V_m) + I_{K^+}(V_m) \quad (4)$$

5.2.3. NMDAR channel property: voltage-dependent Mg^{2+} unblocking

The voltage-dependent Mg^{2+} unblocking properties described here are based on several previous findings. First, the tonic NMDAR-mediated current was shown to be mainly contributed by around 40% of GluN2A and 60% GluN2D containing NMDARs (Le Meur et al., 2007). Second, NMDARs exhibit a GluN2 subunit-dependent slow component of Mg^{2+} unblock (Clarke and Johnson, 2006). The slow component of Mg^{2+} unblock is absent in the GluN1/2D receptor (i.e. instantaneous unblocking), while GluN1/2A has a prominent slow component (delayed unblocking). Therefore the voltage-dependent channel conductivity (from 0 to 1; 0 = close; 1 = fully open) of NMDAR caused by Mg^{2+} block was described by combining instantaneous and delayed Mg^{2+} unblocking mechanisms:

$$G_{NMDAR}(V_m) = G_{NMDAR\_delay}(V_m) + G_{NMDAR\_inst}(V_m), \quad (5)$$

where $G_{NMDAR\_delay}(V_m)$ is the voltage-dependent conductivity of delayed Mg^{2+} unblock, and was modified from a 10-state kinetic model (Kampa et al., 2004). $G_{NMDAR\_inst}(V_m)$ is the voltage-dependent conductivity of instantaneous Mg^{2+} unblock, and is characterized by fitting the APV isolated tonic NMDAR current obtained from whole-cell recording of a CA1 pyramidal cell with the Boltzmann equation (Fig. 5.1b). The $G_{NMDAR\_inst}(V_m)$ is described as:

$$G_{NMDAR\_inst}(V_m) = 1/(1 + exp(-(V_m + 22.55)/6.41)) \quad (6)$$

Then the ionic permeabilities (P_{Na}, P_{Ca}, and P_K in equation (1), (2), and (3)) were adjusted so that tonic NMDAR current contributed 40% from delayed and 60% from instantaneous Mg^{2+} unblocking mechanisms when the cell is voltage-clamped at +50 mV. Therefore, the final NMDAR-mediated current is:

$$I_{NMDAR}(V_m) = G_{NMDAR}(V_m) * I_{NMDAR-open}(V_m) \quad (7)$$

Thus, we could get a modelled NMDAR I-V curve and its ionic compositions (Fig. 5.2).

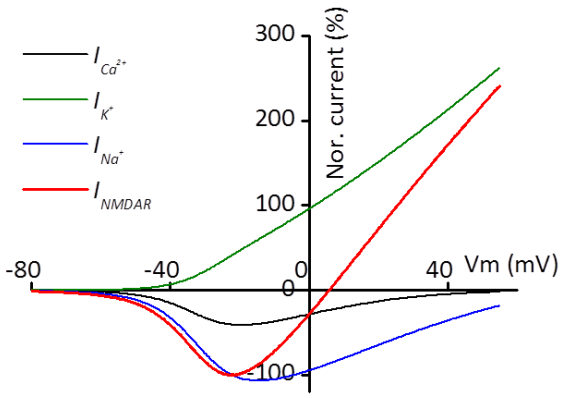

Figure 5.2. I-V curve and ionic fluxes of modelled tonic NMDAR–mediated conductance

The I-V curve of modelled tonic NMDAR-mediated current (red) and the compositions of its ionic fluxes (black: I_{Na^+}; green: I_{Ca2+}; blue: I_{K^+}).

5.2.4. Tonic NMDAR-mediated conductance in a modelled CA1 pyramidal cell.

Simulations were performed with the NEURON simulation environment (Hines and Carnevale, 1997). The modelled CA1 pyramidal cell was imported from the website of Laboratory for Neural Computation at USC (http://www-lnc.usc.edu/CA1-pyramidal-cell-model/). The modelled cell has a realistic morphology of dendritic branching, location-dependent Rm (membrane resistance) and Ra (axial resistance), and subcellular distribution of sodium, DR-, A-, M-type, Ca^{2+}-activated potassium, and h-type currents; as well as L-, R-, and T-type voltage-dependent calcium channels (VDCCs) (Poirazi et al., 2003) (Fig 5.3). The detailed gating properties of the listed channels and their subcellular distribution and density can be found in the online supplemental information of the report published by Poirazi et al. (2003). The modelled cell has also been validated and compared with several experimental

findings. The modelled neuron has the pronounced rectifying sag of the electrotonic potential when injecting a hyperpolarizing current pulse (Magee, 1998; Poirazi et al., 2003). Furthermore, the bAP properties, i.e. time-, frequency- and distance-dependent attenuate, of the modelled neuron are similar to experimental reports (Hoffman et al., 1997; Stuart et al., 1997). Therefore, this modelled neuron can be a good plate form to test the potential biophysical impacts of the tonic NMDAR-mediated conductance.

In order to have a physiological range of the modelled tonic NMDAR-mediated conductance, the current density obtained from the ramp voltage-clamp experiment (0.6 pA/pF; V-clamp at + 50 mV; Chapter 5.2.1, Fig. 5.1) was inserted into this modelled CA1 pyramidal cell homogeneously. Then, the model was used to simulate the contribution of Ca^{2+} entry from tonic NMDAR-mediated conductance during action potential back propagation.

5.3. Simulated bAP-induced NMDAR-mediated Ca^{2+} entry is comparable to experimental results

First, to confirm the experimental findings, bAP-evoked Ca^{2+} entry was monitored in an apical oblique dendrite (around 50 μm from soma) of the modelled neuron (Fig. 5.3a). A short pulse of current was injected in the soma to make the modelled neuron fire a single action potential, and the membrane potential and Ca^{2+} current in the dendrite were monitored during bAP (Fig. 5.3b). The Ca^{2+} current during the bAP was integral to Ca^{2+} charge transfer, and was compared before and after tonic NMDAR conductance was removed (Fig. 5.3d,e). After removing tonic NMDAR conductance, there was only negligible change in AP shapes (Half-width: 99.74 %, and amplitude: 99.80 % of "with NMDAR"; Fig. 5.3c), but a significant reduction of Ca^{2+} charge transfer (90 ± 3 % of Ctrl, n = 9 positions along the dendrites, p = 0.003; Fig. 5.3d,e,f). This result is consistent with the APV effect on bAP-evoked Ca^{2+} entry in real neurons, which further confirmed the experimental findings that a single bAP can enable ambient glutamate bound NMDARs.

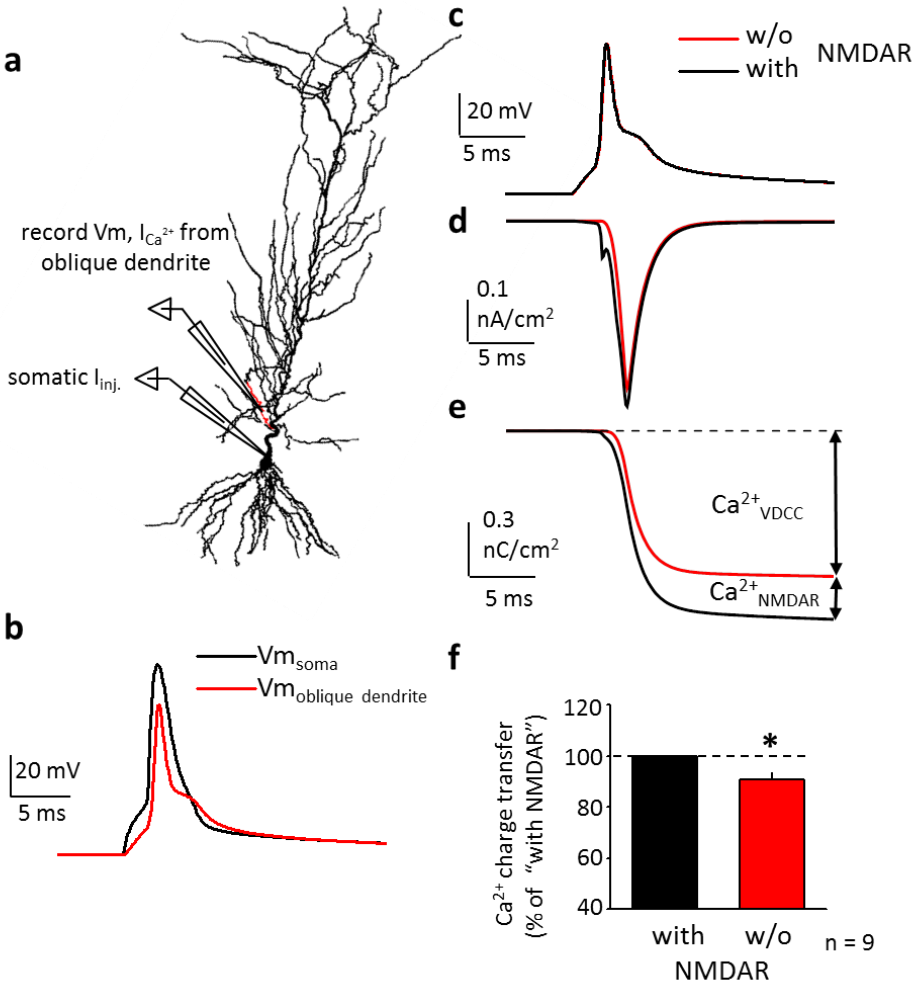

Figure 5.3. Ca^{2+} influx through tonic NMDAR during a single bAP in an apical oblique dendrite of a modelled CA1 pyramidal neuron

a, A 3D reconstructed CA1 pyramidal neuron. bAP was triggered in soma; Vm and Ca^{2+} current were monitored in a proximal apical oblique dendrite. **b,** The action potential waveforms in the soma and dendrite. **c,** bAP waveforms were not changed with (black) or without (w/o; red) tonic NMDAR conductance. **d,** Ca^{2+} current density in the oblique dendrite with and w/o tonic NMDAR conductance. **e,** Ca^{2+} charge transfer density in the oblique dendrite with and w/o tonic NMDAR conductance. **f,** Summary Ca^{2+} charge transfer data normalized to "with NMDAR". *, $p < 0.05$.

5.4. Burst firing induces supra-linear Ca^{2+} entry through tonic NMDAR conductance

Next, burst-firing induced tonic NMDAR-mediated Ca^{2+} entry (NMDAR-Ca^{2+}) was simulated to see how Ca^{2+} enters the dendrite during each bAP of a burst. The simulation was performed by changing the number of AP from 1 to 5 at 100 Hz to mimic the burst in TBF (Fig. 5.4a). Total NMDAR-Ca^{2+} charge transfers during different number of APs were then monitored (Fig. 5.4b). The result showed that NMDAR-Ca^{2+} summated supra-linearly compared to the arithmetic sum of NMDAR-Ca^{2+} induced by a single AP (Fig. 5.4c). 5 APs burst produced 164 ± 19 % (n = 9 places on the branch) of NMDAR-Ca^{2+} entry when compared to the arithmetic sum of 5 single AP (Fig. 5.4d). The NMDAR-Ca^{2+} entry for each bAP in a burst correlated with the half-width of the bAP, which was prolonged during the burst (R^2 = 0.90; ANOVA, $p < 0.01$) (Fig. 5.4e). Therefore, broadening of the bAP might be the underlying mechanisms for such supra-linearity.

This result not only confirmed the finding that burst-firing enhances Ca^{2+} entry through extrasynaptic NMDARs, but also proposed that burst-firing of APs might be more efficient in triggering NMDAR-Ca^{2+} entry than a single AP.

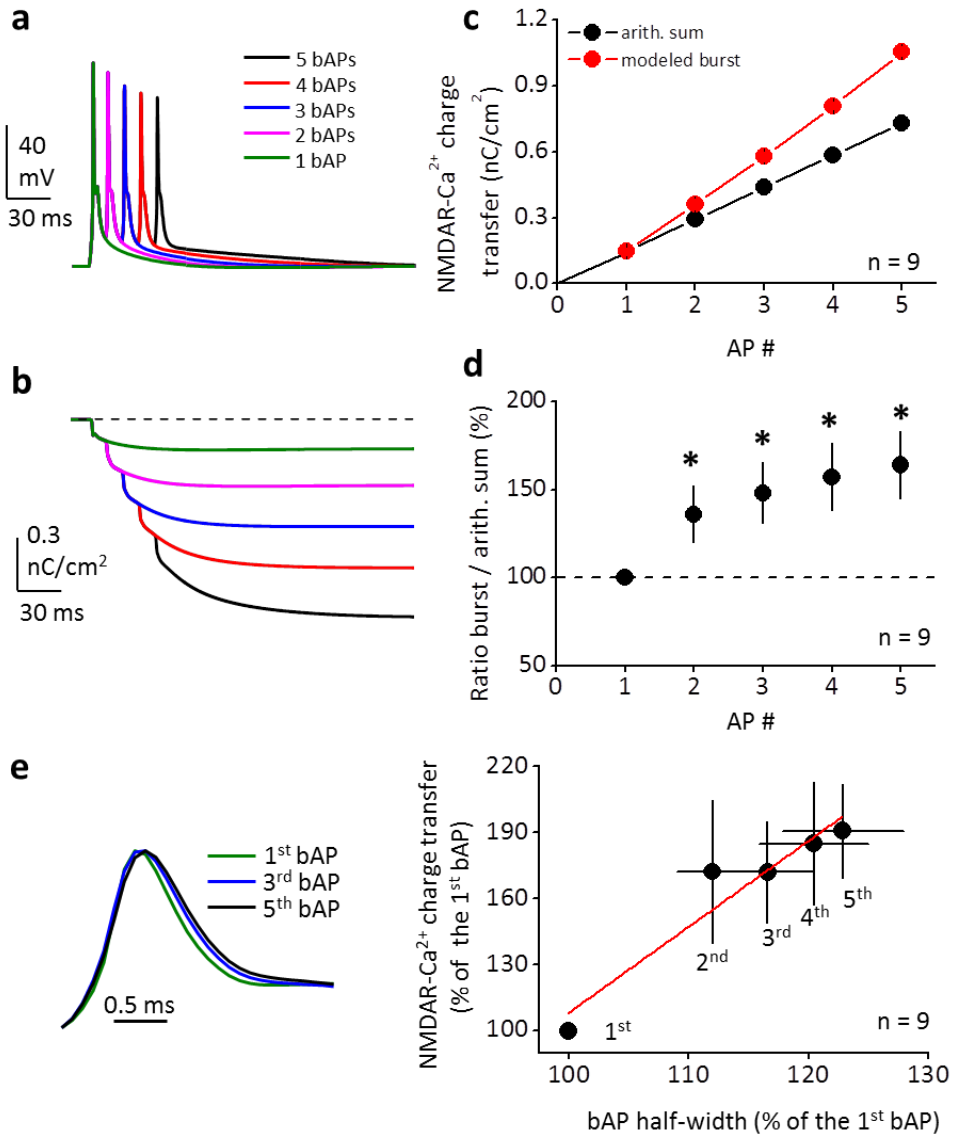

Figure 5.4 Supra-linear Ca^{2+} influxes through tonic NMDAR during burst-firing

a, bAP waveforms of burst-firing at 100 Hz in a modelled oblique dendrite triggered by somatic current injection. **b,** Ca^{2+} charge transfer density traces in the oblique dendrite during a different number of bAPs. The colour code for different number of AP is the same as in **a**. **c,** Ca^{2+} charge transfer showed a supra-linear summation (red) comparing to the arithmetic sum of single bAP (black). **d,** The supra-linear summation ratio of Ca^{2+} charge transfer for different number of bAP. "AP #" - number of AP within a burst. *, $p < 0.05$. **e,** The amount of NMDAR-mediated Ca^{2+} entry correlates to the bAP duration. *Left panel*, Example traces of bAP waveform for the 1st, 3rd and 5th bAP in a burst. *Right panel*, The NMDAR-mediated Ca^{2+} entry correlates to the duration of the half-width of bAPs which prolonged in a burst.

5.5. Discussions

These simulation results first confirmed my experimental finding that a tonic NMDAR conductance with a physiological conductance density is able to generate about 10 % of total Ca^{2+} entry during a single bAP. The results also demonstrated that tonic NMDAR conductance has a limited effect on shaping bAP waveform but contributes to Ca^{2+} influx. Furthermore, the simulation also showed that during a burst firing of APs (5 x 100 Hz), tonic NMDAR-mediated Ca^{2+} entry increases with the number of bAP in a supra-liner manner. Thus the results proposed a way to enhance 'readout' for the ambient glutamate via burst firing of APs.

Chapter 6: Plasticity triggered by extrasynaptic NMDARs

6.1. Introduction

The results so far indicate that a bAP can recruit glutamate-bound extrasynaptic NMDARs and generate NMDAR-mediated Ca^{2+} entry, depending on the level of extrasynaptic glutamate. Therefore I asked whether there is also room for signal modulation depending on the 'readout'. If a bAP can promote some amount of NMDAR-mediated Ca^{2+} entry, burst firing of the cell should produce more because of repeated dendritic depolarization, as it is demonstrated by the simulation results in the previous chapter. Here, I tested this hypothesis experimentally using whole-cell patch clamp recording and two-photon Ca^{2+} imaging in CA1 pyramidal neurons.

Furthermore, because in many cases postsynaptic Ca^{2+} elevation triggers various forms of cellular plasticity, I asked whether activation of glutamate-bound extrasynaptic NMDARs also triggers neuronal plasticity. *In vivo*, the common firing pattern of CA1 pyramidal cells has two classical features. First, they usually fire short burst consisting of 3 to 5 action potentials at 50 to 100 Hz (Kandel and Spencer, 1961; Ranck, 1973; Suzuki and Smith, 1985). Second, the burst repeats at a slower 4 to 12 Hz frequency, which is defined as the theta rhythm (Rose, 1983; Rose and Dunwiddie, 1986). This theta oscillation occurs when animals are exploring and performing attentive behaviours (Bland, 1986; Grastyan et al., 1959; Vanderwolf, 1969). Furthermore, the burst stimulation repeated at theta rhythm has also been shown to

effectively induce synaptic plasticity in the hippocampal CA1 area (Larson and Lynch, 1986; Larson et al., 1986). Such a firing pattern is usually termed as theta-burst firing (TBF). It has previously been shown that activation of glutamate-bound synaptic NMDARs during TBF (Fig. 6.1) can reduce input resistance and excitability of CA1 pyramidal neurons though upregulation of G_h (conductance mediated by *h*-channel) (Fan et al., 2005). The *h*-channel is a hyperpolarization-activated channel that plays an important role in modulating neuronal resting membrane potential and membrane excitability (Biel et al., 2009). Here, I tested whether activation of glutamate-bound extrasynaptic NMDARs during the same burst activity also triggers lasting consequences for cell excitability.

6.2. Materials and methods

6.2.1. Animal and slice preparation

Procedures for preparing transverse slices (350 µm) of hippocampus from SD rats aged p21 - p35 are described in Chapter 2.2 and 2.3. Briefly, rats were anaesthetised and decapitated. The brain was removed and chilled with ice-cold cutting solution. Hippocampi from both hemispheres were isolated and placed in an agar block and transverse slices (350 µm) were cut with a vibroslicer (Fig. 2.1e). The slices were left to recover for 20 to 30 min at 34°C in a submerged chamber in cutting or storage solution. Then they were transferred and incubated on either an interface- or submerged-type chamber (mostly submerged-type) at room

temperature for at least 1 hour for recovery with storage solution. After that, the slices were transferred to the recording chamber and were continuously superfused at 33-34^{o}C with ACSF. All solutions were saturated with 95% O_2 and 5% CO_2. Osmolarity was adjusted to 298 ± 3 mOsm.

6.2.2. Electrophysiology and two-photon imaging

Whole cell patch-clamp recording and two-photon imaging were performed as described in Chapter 2.5 and 2.6 Briefly, cells in slices were first visually identified using an Olympus BX-61 microscope equipped with differential interference contrast optics under infrared illumination and a 60x water immersion lens. For imaging experiments, whole-cell current-clamp recordings were obtained from CA1 pyramidal neurons with a patch pipette (3 - 6 MΩ) filled with a solution containing the morphological tracer Alexa Fluor 594 (50 μM) and the Ca^{2+} sensitive dye Fluo-4 (250 μM). Once the whole cell recordings were obtained, the patch amplifier (Multiclamp 700B) was set to either current- or voltage-clamp mode. Dendritic bAPs were induced in these cells by somatic current injections (2-3 ms, 400 - 1000 pA) and monitored in the soma. Two-photon imaging was performed at least 20 -30 min after rupturing the seal and breaking into the cell for dye reaching steady-state. Imaged dendrites were at least 30 μm (mostly 50 μm) below the slice surface.

6.2.3. Monitoring the apparent R_{input} with current-clamp recording

To monitor the plasticity of apparent R_{input} in current clamp mode, cells were recorded with pipette solution containing (mM): 130 K gluconate, 8 NaCl, 10 HEPES, 10 Na_2-Phosphocreatine, 0.5 EGTA, 0.4 Na_2GTP, 4 MgATP, 3 Na-Ascorbate, pH = 7.2, osmolarity was adjusted to 290 mOsm. R_{input} was determined by 700 ms current injections (ranging from -50 to +50 pA in steps of 10 pA every 3 sec). The steady-state voltage shifts versus the injected currents were plotted and fitted with a linear regression line (Fig. 6.1). The slope of the line then was assigned as the R_{input} of the cell at at steady-state.

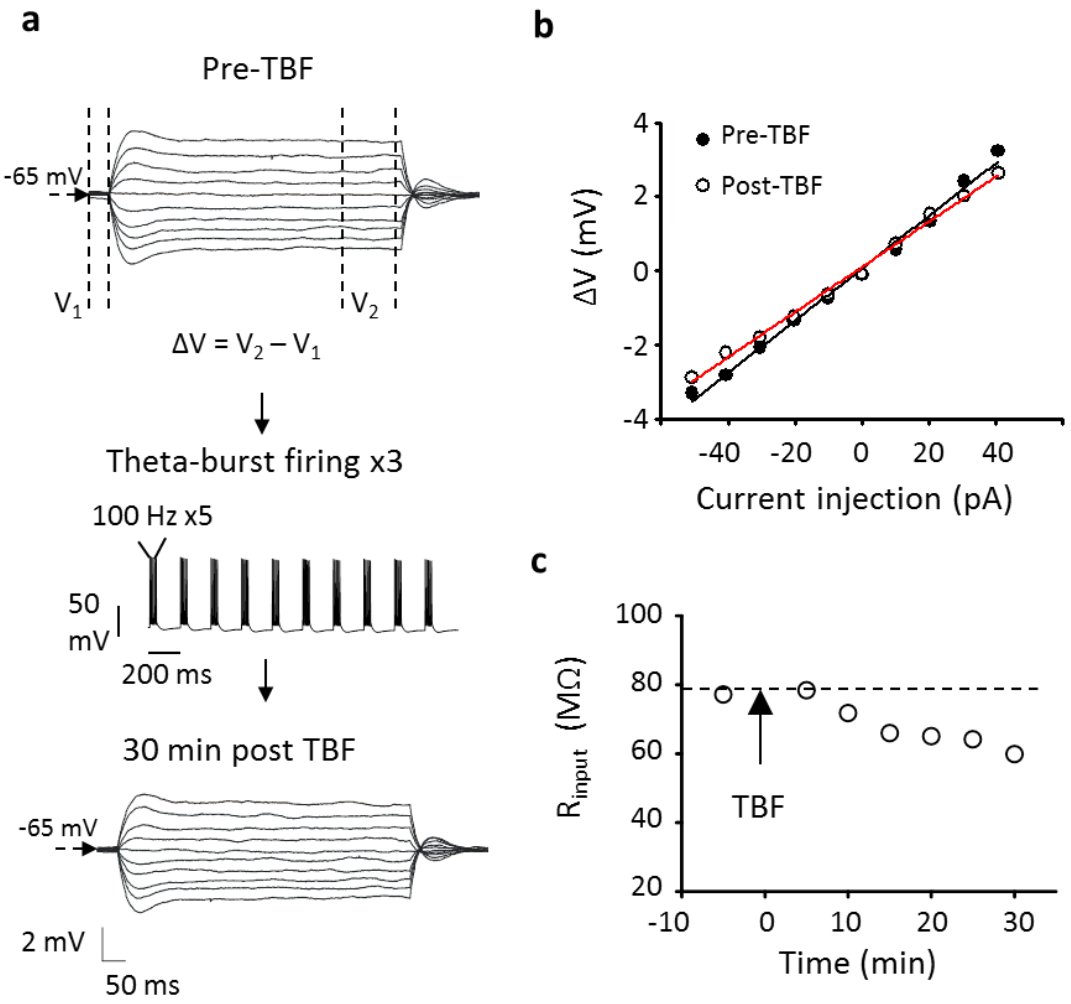

Figure 6.1 Protocol for measurement of cell R_{input} by steps of current injection.

a, A demonstration of the measurement of steady-state cell R_{input} and the protocol to induce R_{input} plasticity. ΔV is the membrane potential change upon 700 ms current injection. **b**, R_{input} is determined by fitting the linear I-V relation (current injection v.s. ΔV) upon current injections. Here shows an example of the fitting pre- and post-TBF. **c**, An example of a single experiment of R_{input} plasticity after TBF, with synaptic glutamate release intact.

6.2.4. Protocol for inducing theta-burst firing (TBF)

The plasticity of R_{input} was induced by somatic current injection to trigger neuron firing in theta frequency (theta-burst firing; TBF). TBF consisted of 30 trains of 5 action potentials firing at 100 Hz (10 trains at 5 Hz repeated three times with a 10 sec interval) (Fig 6.2). Each AP is triggered by current injection (1.5-2 nA; 2-3 ms) to ensure the fidelity of AP initiation.

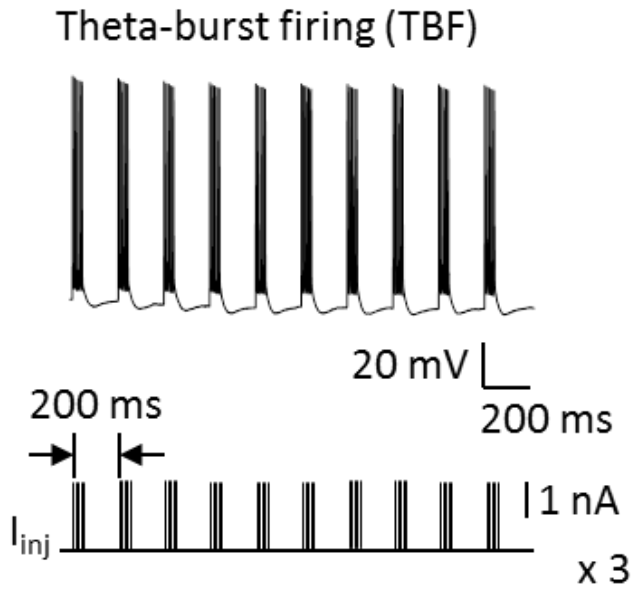

Figure 6.2 Protocol of theta-burst firing (TBF) stimulation

TBF stimulation consists of 30 trains of 5 action potentials firing at 100 Hz (10 trains at 5 Hz repeated three times with a 10 sec interval. *Upper trace*, an example of somatic membrane potential during TBF stimulation. *Lower trace*, the amplitude of the injected current during TBF.

6.3. Burst firing of bAPs increases readout for activation of ambient glutamate bound extrasynaptic NMDARs

The results so far indicate that a bAP can recruit glutamate-bound extrasynaptic NMDARs and generate NMDAR-mediated Ca^{2+} entry. Therefore I asked whether there is room for signal modulation. If a bAP can promote some amount of NMDAR-mediated Ca^{2+} entry, burst firing of the cell should produce more because of repeated dendritic depolarization. To address this, I monitored Ca^{2+} entry mediated by the burst of bAPs. Fluo-4 has a high Ca^{2+} affinity (Ca^{2+} Kd = 0.35 µM), it easily saturates and goes beyond linear range (Fig. 6.3a); therefore, a low-affinity Ca^{2+} dye, Fluo-4FF (Ca^{2+} Kd = 6.7 µM), was used instead. I then could use the linear sensitivity range to estimate the amount of Ca^{2+} entry during burst stimulation (Fig. 6.3b). It was found that the relative effects of APV on Ca^{2+} entry were similar for 5x100 Hz bursts and single bAPs ($\Delta G/R$; shafts: 93 ± 3 % of control, n = 10, p = 0.02; and spines: 103 ± 7 % of control, n = 10, p = 0.35; Fig. 6.4a, b). However, because of increased depolarization, burst firing can also enhance the contribution of VDCCs to Ca^{2+} entry. Therefore, I measured the APV-sensitive response on each stimulus in the burst (NMDAR mediated bAP-Ca^{2+}; $\Delta G/R_{NMDAR}$) and normalized it to the amplitude of the total Ca^{2+} response to the first bAP. This measurement indicated that either (1) a larger number of NMDARs is indeed recruited with more bAPs or (2) repeated Ca^{2+} entry was triggered during each bAP in a burst ($\Delta G/R_{NMDAR}$: 5^{th} vs 1^{st} bAP, n = 10, p = 0.04; Fig. 6.3c). Strikingly, a similar result was obtained in slices pre-treated with bafilomycin A1 ($\Delta G/R$; shafts: 90 ± 2 % of control, n = 8, p = 0.002; spines: 97 ± 4 % of

control, n = 7, p = 0.21; Fig. 6.4a,b). Thus synaptically released glutamate does not contribute to activation of extrasynaptic NMDARs in the slice even during the burst firing of the postsynaptic cell.

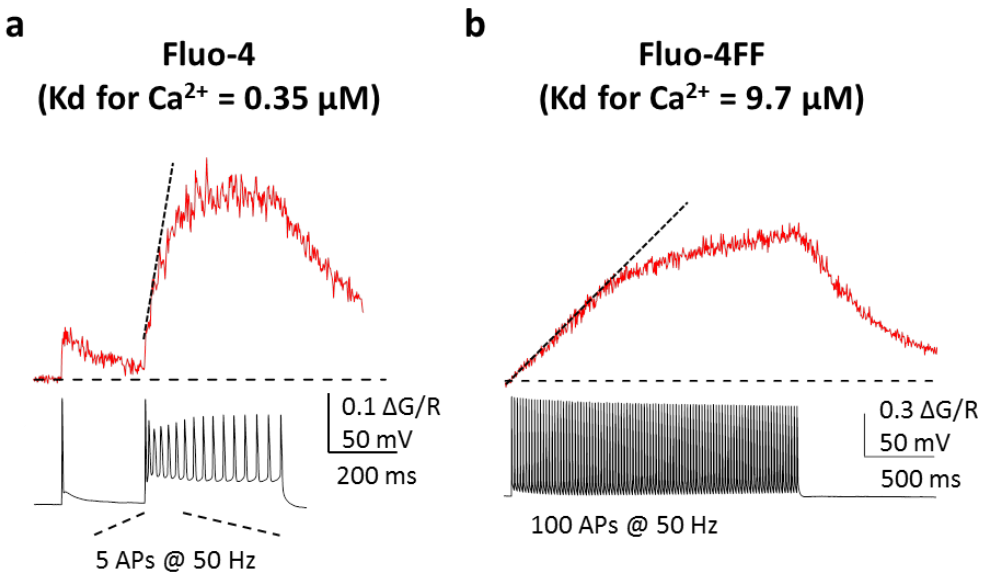

Figure 6.3 Using the low-affinity Ca^{2+} dye Fluo-4FF to approach the linear sensitivity

a, Imaging bAPs-induced Ca^{2+} entry in an apical oblique dendrite with high affinity Ca^{2} dye, Fluo-4 (250 µM). The Ca^{2+} signal (*ΔG/R*) went beyond the linear range for more than 3 APs at 50 Hz. **b**, When imaged with low affinity Ca^{2} dye, Fluo-4FF (500 µM), the Ca^{2+} signal (*ΔG/R*) stayed linear up to 30 APs at 50 Hz. *Upper panels*, *ΔG/R* traces. *Lower panels*, membrane potential traces recorded via whole-cell patch pipettes in soma.

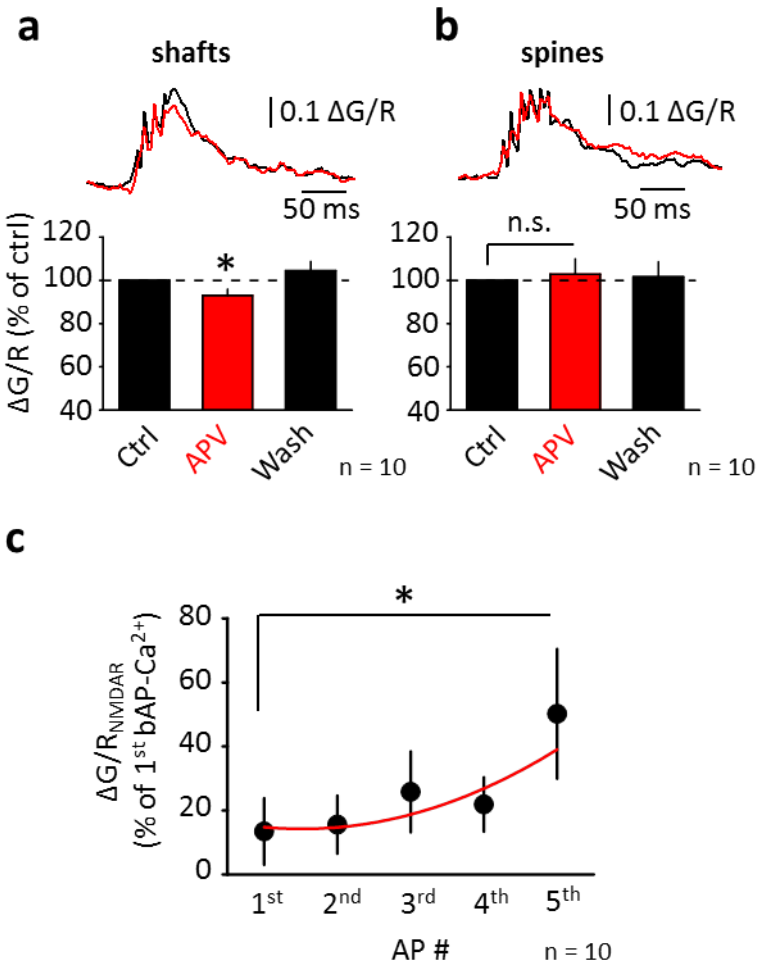

Figure 6.4 Burst firing triggers detection of ambient glutamate and induces more shaft NMDAR-mediated Ca^{2+} entry.

a and **b,** The effect of APV on burst bAPs-evoked Ca^{2+} transients (*ΔG/R*) in shafts (**a**) and spines (**b**). *Upper panels*, averaged traces of burst bAPs-evoked Ca^{2+} transients in ACSF (black trace) and in APV (red trace) in one characteristic dendritic shaft and spine, respectively. *Lower panels*, summary data normalized to the burst bAPs-evoked Ca^{2+} transient in control (Ctrl). **c**, More NMDAR-mediated Ca^{2+} entry is triggered with increased number of bAPs within a burst. "$\Delta G/R_{NMDAR}$"- NMDAR-mediated Ca^{2+} entry ;"AP #" - sequential number of AP within a burst. *, $p < 0.05$.

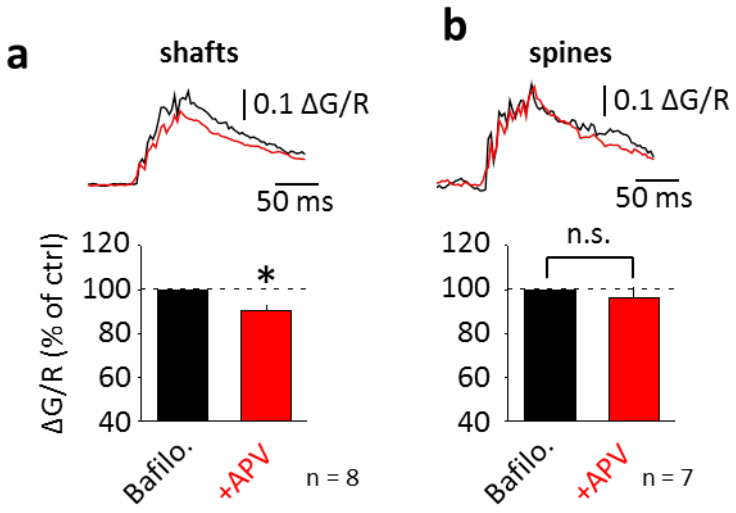

Figure 6.5 Burst firing triggers detection of ambient glutamate by shaft NMDARs in bafilomycin A1 treated slice.

a and **b,** The effect of APV on burst bAPs-evoked Ca^{2+} entry (*ΔG/R*) in shafts (b) and spines (c) of CA1 pyramidal neurons from bafilomycin A1 treated slices. *Upper panels*, averaged traces of burst bAPs-evoked Ca^{2+} transients in control (black trace) and after adding APV (red trace) in one characteristic dendritic shaft and spine, respectively. *Lower panels*, summary data normalized to "Bafilo."– control state in Bafilomycin A1 treated slice. *, $p < 0.05$.

6.4. Bidirectional modulation of G_h by activation of synaptic and extrasynaptic NMDARs during TBF

To test whether activation of glutamate-bound extrasynaptic NMDARs during burst activity also triggers lasting changes in cell excitability, these experiments were performed in control slices and in slices pre-treated with bafilomycin A1. The slices pre-incubated in bafilomycin A1 had no vesicular release (Fig 3.6), but the ambient glutamate concentration remained intact (Cavelier and Attwell, 2005; Le Meur et al., 2007). In this condition, bAPs can only activate shaft extrasynaptic NMDARs which are already bound by ambient glutamate but not synaptic ones (Fig. 3.1c,d). In control slices, TBF led to a gradual decrease in the cell input resistance (to 90 ± 4 % of baseline 30 min post-TBF, n = 8; p = 0.011, Fig. 6.6) consistent with the previously reported upregulation of G_h that is mediated by synaptic NMDARs (Fan et al., 2005). In striking contrast, similar stimulation in slices treated with bafilomycin A1 increased input resistance (to 124 ± 9 % of baseline 30 min post-TBF, n = 6; p = 0.031) whereas bafilomycin A1 alone had no effect (to 101 ± 5 % of baseline 30 min post-TBF, n = 5; p = 0.82) (Fig. 6.6). The effect of TBF in bafilomycin A1 treated-slices was completely abolished either by the NMDAR antagonist APV (98 ± 3 % of baseline in 30 min after TBF, n = 5; p = 0.187, Fig. 6.7); by the *h*-channel blocker ZD7288 (Harris and Constanti, 1995) (20 μM, 96 ± 2 % of baseline in 30 min after TBF, n = 5; p = 0.313, Fig. 6.7); or by chelating intracellular Ca^{2+} with 10 mM BAPTA (97 ± 7 % of baseline in 30 min after TBF, n = 7, p = 0.47 , Fig. 6.7) . These experiments suggest that Ca^{2+} entry during activation of shaft extrasynaptic NMDARs by bursts of bAP is

responsible for the downregulation of G_h. This finding demonstrates a form of neuronal non-synaptic plasticity induced by extrasynaptic glutamate signalling.

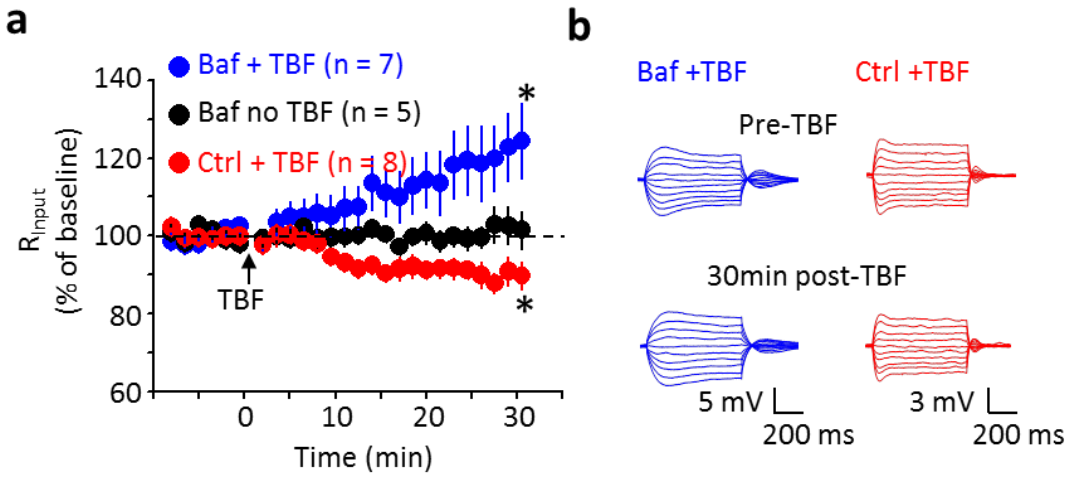

Figure 6.6 Activation of extrasynaptic NMDARs during TBF increased cell R_{input}

a, The changes in cell R_{input} induced by TBF in bafilomycin A1 treated slice (blue circles) and control slice (red circles). No gradual change in R_{input} was detected in bafilomycin A1 treated slice without TBF (black circles). **b**, Traces for voltage response to current injections before (pre-TBF) and 30 min after (post-TBF) TBF in bafilomycin A1 treated (blue traces) and control (red traces) slices. *, $p < 0.05$.

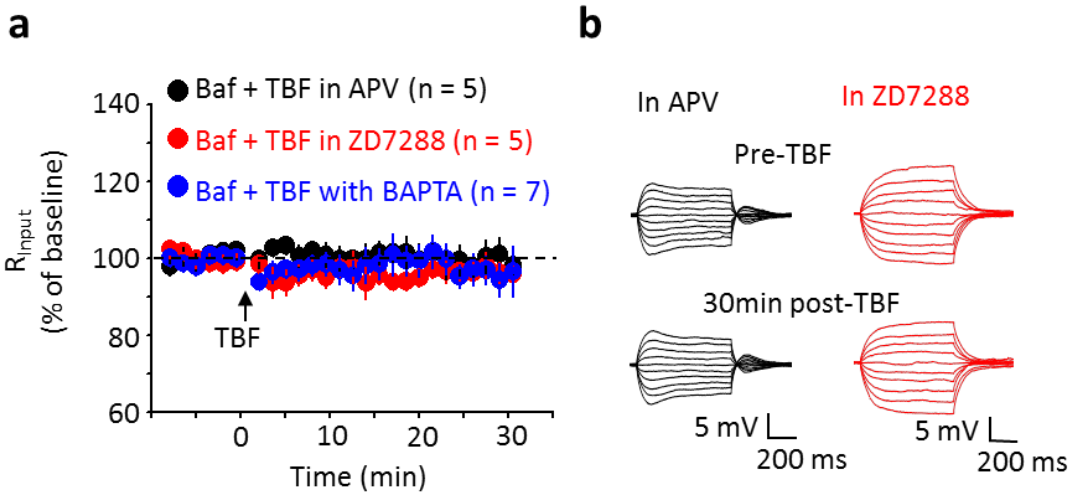

Figure 6.7 Increase of cell R_{input} induced by TBF was due to downregulation of G_h

a, TBF did not produce detectable change in the R_{input} in bafilomycin A1 treated slice in the presence of APV (black circles)or 20 µM ZD7288 (red circles) or dialysing the cell with BAPTA (blue circles). **b,** Traces for voltage response to current injections before (pre-TBF) and 30 min after (post-TBF) TBF in the presence of APV (black traces) and ZD7288 (red traces). *, $p < 0.05$.

6.5. Plasticity in G_h in turn regulates dendritic input

Changes in G_h and associated changes in input resistance can affect the synaptic input into cell dendrites (Campanac et al., 2008; Fan et al., 2005). Local spot uncaging near identified dendritic spines produced an EPSP-like potential (uEPSP) in the cell soma (Fig. 6.8). Consistent with previous reports, upregulation of G_h in control slices did not significantly affect the amplitude of the uEPSP (amplitude after TBF was 101 ± 3 % of control, n = 12, p = 0.85), however it significantly reduced the half-duration of the uEPSP (half-duration after TBF was 82 ± 2 % of control, n = 12, p

< 0.001) (Fig. 6.8a) (Magee, 1998; Poolos et al., 2002). TBF in bafilomycin A1 treated slices increased both the amplitude (amplitude after TBF was 121 ± 4 % of control, n = 18, p < 0.001) and the half-duration of the uEPSP (half-duration after TBF was 113 ± 4 % of control, n = 18, p < 0.001) (Fig. 6.8b). This finding demonstrates a form of neuronal non-synaptic plasticity induced by the read out of extrasynaptic glutamate by bAPs, which in turn affects integration of synaptic inputs in the postsynaptic cell.

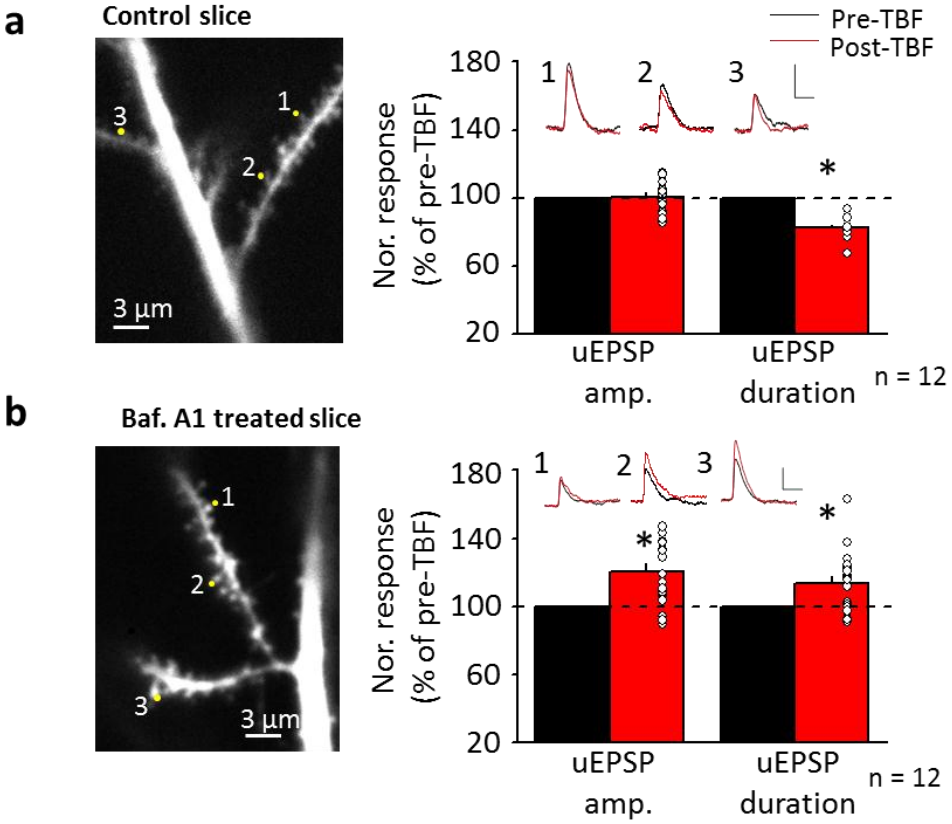

Figure 6.8 Activation of extrasynaptic NMDARs during TBF enhances uEPSPs

a, *Left panel*, Glutamate was uncaged on spines of apical dendrites of CA1 pyramidal neuron in control slices. *Right panel*, The summarized results of the amplitudes and half-durations of uEPSP before (black) and after (red) TBF. *Inserts*, The uEPSP traces recorded via a somatic whole-cell patch pipette before (black) and 30 min after (red) the induction of TBF. Calibration: 50 ms, 1 mV. **b,** The experimental settings were similar to those in (a) but performed in bafilomycin A1 treated slices.

6.6. Discussions

In this chapter, the results demonstrate that burst firing of bAP induces significantly larger NMDAR-Ca^{2+} entry than that induced by a single bAP; although the result did not show a supra-liner increase with the number of bAPs as it was shown by the simulation (Fig. 5.4). This might be explained by the low signal to noise ratio of low affinity Ca^{2+} dye (Fluo-4FF) for detecting single bAP-evoked Ca^{2+} entry. Hence, this dye might not be sensitive enough to see the supra-liner Ca^{2+} entry during a burst. Nevertheless, the data indicate that Ca^{2+} entry through glutamate-bound NMDARs can be enhanced not only by increased extracellular glutamate, but also by increasing the number of the 'readout'.

The results also show that recruitment of ambient glutamate-bound shaft NMDARs (activated by non-vesicular supply of glutamate) by theta-bursts of bAPs increased the R_{input} of the cell. The change is mediated by downregulation of G_h by triggered Ca^{2+} entry from shaft NMDARs (Fig. 6.7). The present results, however, do not show specifically the extrasynaptic NMDAR-dependent downstream signalling pathway that links to G_h, leaving open the possibility that it shares the same pathway as synaptic NMDARs. The G_h in CA1 pyramidal neurons has been shown to be mediated by HCN channels (hyperpolarization-activated cyclic nucleotide-gated channel) (Lorincz et al., 2002; Nolan et al., 2004). It has also been shown that activation of synaptic NMDARs during TBF upregulates G_h. The Ca^{2+} entry through synaptic NMDARs during TBF activates calcium/calmodulin-dependent protein kinase II (CaMKII) and enhances protein synthesis of HCN1 (Fan et al., 2005). CaMKII

can indirectly trigger protein synthesis through activation of extracellular signal-regulated kinases 1 and 2 (ERK1/2) (Greer and Greenberg, 2008), which is oppositely regulated by synaptic and extrasynaptic NMDARs (Ivanov et al., 2006). Therefore, the downregulation of G_h might be due to a decrease in new HCN1 protein synthesis, resulting in reduced total HCN1 proteins. This also explains that the slow change in R_{input} after TBF was introduced, because it required time for protein turnover of HCN1 on the cell membrane.

However, this does not rule out the possibility that the downregulated G_h was due to a change in gating properties of HCN channels, which was strongly modulated by p38 mitogen-activated protein kinase (p38 MAPK) (Poolos et al., 2006). It has been shown that inhibition of p38 MAKP activity downregulates G_h by a hyperpolarizing shift of the activation curve of HCN channels in CA1 pyramidal neurons (Jung et al., 2010). Furthermore, p38 MAPK was shown to be bidirectionally controlled by different NMDAR subtypes (Waxman and Lynch, 2005). Specifically, extrasynaptic NMDARs downregulate p38 MAPK through the activation of phosphoinositide 3-kinase (PI3K), whereas synaptic NMDAR upregulates p38 MAPK through the activation of calcineurin, a Ca^{2+}-dependent phosphatase (Waxman and Lynch, 2005). Therefore, these findings, together with my results, suggest a possible molecular mechanism in bidirectional modulation of G_h through synaptic and extrasynaptic NMDARs.

Chapter 7: General discussion

7.1. Conclusions

1. The dendritic shaft NMDARs, but not spine NMDARs, bound with glutamate released from non-vesicular origin are enabled during bAPs serving as a 'readout' signal.

2. An effective glutamate transporter shield protects synaptic NMDARs from ambient glutamate and extrasynaptic NMDARs from glutamate released in the synapse.

3. The extrasynaptic NMDARs detect local transient rises of glutamate generated either by glutamate spillover or extrasynaptic glutamate uncaging. The consequent Ca^{2+} entry is also boosted by a 'readout' signal, bAPs.

4. bAP-evoked Ca^{2+} entry mediated by ambient glutamate-bound extrasynaptic NMDARs can be enhanced during burst firing of APs.

5. Activation of extrasynaptic NMDARs during repeated bAPs (theta-burst firing) can increase neuronal R_{input} via downregulation of G_h (h-channel conductance).

7.2. Compartmentalized synaptic and extrasynaptic NMDARs

Evidence in this study indicates that synaptic and extrasynaptic NMDARs can form different compartments. First, a proportion of NMDARs in dendritic shafts, but not spines, is bound by ambient glutamate at basal conditions enabling receptor activation upon generation of a bAP (Fig. 3.1c). The relatively tight glial coverage of dendritic spines appears to maintain a negligible glutamate concentration inside the synaptic cleft when there is no synaptic release. This phenomenon could be important for minimizing the desensitization of synaptic AMPA receptors by the ambient glutamate (Trussell and Fischbach, 1989). Secondly, blockade of glutamate transporter by TBOA removed the barriers between synaptic and extrasynaptic compartments. Therefore application of TBOA revealed a portion of Ca^{2+} entry through spine-associated NMDARs during bAPs (Fig. 3.10). Thirdly, the spine- and shaft-associated NMDARs activated by extrasynaptic glutamate uncaging share the same pharmacological profile which distinguish them from synaptic NMDARs. This indicated that the synaptic NMDARs, which are compartmentalized from the extrasynaptic region, cannot sense the glutamate rise generated from extrasynaptic sources (Fig. 1.7a). Finally, activation of ambient glutamate-bound extrasynaptic, but not synaptic NMDARs during TBF downregulates the I_h channels (Fig. 6.6). This further indicates the compartmentalized downstream signalling cascades between synaptic and extrasynaptic NMDARs. Based on these findings, a hypothetical functional architecture of the compartmentalized synaptic and extrasynaptic regions is summarized in Figure 7.1.

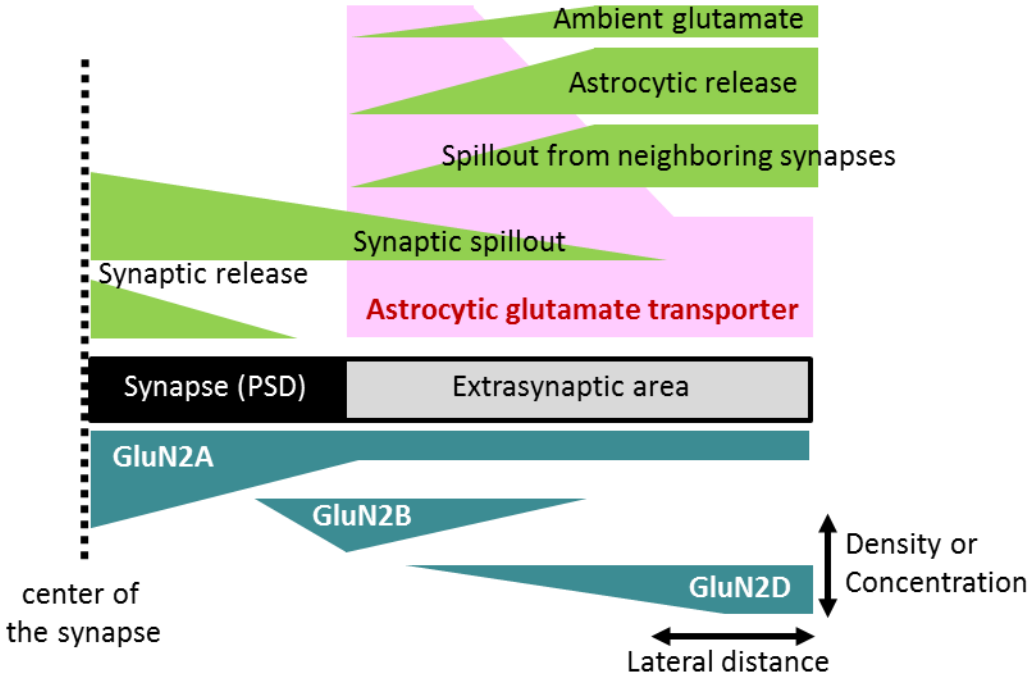

Figure 7.1 The hypothetical functional architecture of the compartmentalized synaptic and extrasynaptic areas

The synaptic area is defined by the region of PSD. The concentration and the spatial distribution of glutamate are indicated in green. The density and the distribution of the astrocytic glutamate transporter are indicated in pink. The relative density and spatial distribution of NMDAR subtypes are indicated in blue. Note the barrier between synapse and extrasynaptic area is the presence of the high density glutamate transporter.

The reasonable explanations for such compartmentalization can be either that ambient glutamate is more likely present in the extrasynaptic region rather than in the synaptic cleft, or that the occupancy of NMDARs for glutamate is higher in the extrasynaptic than synaptic region. The higher density of glutamate transporters on the perisynaptic membrane (Danbolt, 2001; Danbolt et al., 1998), a significantly

higher surface to volume ratio of astrocytic processes which are closer to the synapses (our unpublished data), and the reduction of diffusion due the macromolecular obstacles and the narrower extracellular space inside the synaptic clefts than extrasynaptic regions (Rusakov and Kullmann, 1998; Rusakov et al., 2011) might be the underlying mechanisms. Therefore, in order to understand how ambient glutamate interacts with NMDARs in a complex extracellular microenvironment, the compartmentalized synaptic and extrasynaptic receptors should be taken into consideration.

7.3. Compartmentalized Ca^{2+} signalling mediated by extrasynaptic NMDARs and VDCCs

Although I have demonstrated that blocking shaft NMDAR-mediated Ca^{2+} entry during TBF prevents downregulation of G_h, the residual Ca^{2+} entry through VDCCs still accounts for about 90% of total Ca^{2+} entry of control condition. How such small reduction in Ca^{2+} entry could have profound effects is still questionable. The answer might relate to the highly local nature of Ca^{2+}-dependent signalling mechanisms: Ca^{2+} concentration drops orders of magnitudes 10-50 nm away from the source due to 3D diffusion and endogenous buffering (Bucurenciu et al., 2008; Weber et al., 2010; Yamashita et al., 2010). In particular, it has been shown that NMDAR-mediated postsynaptic Ca^{2+} entry triggers CAMKII-dependent molecular cascades in the immediate vicinity of the NMDAR channel, possibly within nanoscopic Ca^{2+} hotspots

(Lee et al., 2009; Thalhammer et al., 2006). Therefore, extrasynaptic NMDAR- and VDCC-mediated Ca^{2+} signals might be compartmentalized in the dendritic cytoplasm. Although there is no direct evidence for such nanodomains in this work, this has been demonstrated to exist for at least different VDCCs (Hudmon et al., 2005; Wheeler et al., 2012). For example, activation of CaMKII-mediated signalling is ~10-fold more effective by Ca_v1- than by Ca_v2-type VDCCs for the same bulk Ca^{2+} increase, because CaMKIIs are located within nanometer-range to Ca_v1. Furthermore, Ca_v2-mediated Ca^{2+} increase rises are favorably restricted by Ca^{2+} uptake machinery. In a similar context, triggering downregulation of G_h might require Ca^{2+} rises to a substantial concentration in the vicinity of extrasynaptic NMDARs. Therefore, only a 10% reduction in bulk Ca^{2+} transient might reflect a profound decrease of Ca^{2+} within the Ca^{2+} nanodomain of extrasynaptic NMDARs preventing their downstream signalling, whereas the residual VDCC-mediated Ca^{2+}, although accounting for 90% of bulk Ca^{2+} rises, is not efficient enough to activate the same signalling pathway.

7.4. Synaptic and non-synaptic sources of extracellular glutamate

I found that the average NMDAR occupancy by glutamate in quiescent slices does not depend on its vesicular release, which is fully consistent with previous reports (Cavelier and Attwell, 2005; Jabaudon et al., 1999; Le Meur et al., 2007). The resulting space-and-time average extracellular glutamate concentration can be

thought of as a 'floor' level of ambient glutamate, which is independent of the synaptic network activity. In addition to ambient non-vesicular glutamate, extrasynaptic NMDARs can also bind glutamate escaping from the synaptic cleft when synaptic network activity increases. I found that synaptic discharges (or local glutamate uncaging mimicking such) paired with bAPs boost Ca^{2+} entry in both shafts and spillover-activated spines (Fig. 4.1 and 4.2). Thus, both shaft and spine NMDARs can also sense extracellular glutamate which is transiently elevated as result of local synaptic activity, but require a readout signal such as the bAP to be activated. Importantly, the coincidence detection interval for glutamate release and bAPs extends beyond the duration of the individual glutamate rise, reflecting the fact that glutamate molecules can remain bound to dendritic NMDARs for hundreds of milliseconds. The NMDAR-mediated enhancement of bAP-evoked dendritic Ca^{2+} signals could therefore act as an integrating detector of glutamate release events that occurred nearby over an extended period of time.

7.5. Local transient versus global tonic rise of extracellular glutamate

My results suggest that a transient, rather than long-term, rise in extrasynaptic glutamate could boost bAP-induced Ca^{2+} signals. Indeed, although NMDARs contribute to the bAP-evoked Ca^{2+} entry in basal conditions (Fig. 3.1c), the uniform increase in the ambient glutamate level following application of TBOA does not enhance but decrease the Ca^{2+} signals (Fig. 3.11). This is likely because a small

proportion of NMDARs, both extrasynaptic and synaptic, which are activated by the accumulated ambient glutamate at resting membrane potential (Kovalchuk et al., 2000) may already trigger long-term changes in cell membrane properties, which is consistent to previous reports (Mulholland et al., 2008; Mulholland et al., 2009; Mulholland and Chandler, 2010). Such changes might represent an important mechanism to limit a cytotoxic effect of extracellular glutamate rises. This also indicates the importance of glutamate transporters to maintain the compartmentalized synaptic and extrasynaptic regions in neurons.

7.6. Extrasynaptic signalling is tunable

In the current study, I examined different possible ways to modulate extrasynaptic signalling. Here, the NMDAR-Ca^{2+} for each condition during the 'readout' process is normalized to the Ca^{2+} influx of a single bAP and summarized in Figure 7.2. There are two ways to enhance the extrasynaptic signalling sensed by a neuron, namely increased 'readout' (Fig. 7.2 blue region) and a rise of the concentration of extrasynaptic glutamate (Fig. 7.2 pink region). The proportion of Ca^{2+} entry from spines and shafts is different between stimulation paradigms. The 'readout' triggered by burst firing tends to have larger Ca^{2+} entry through shafts than spines, suggesting a novel way for specifically recruiting shaft NMDARs. On the other hand, elevating extracellular glutamate concentration by different stimulation, i.e. blockage of glutamate uptake, glutamate spillover, and extrasynaptic glutamate

uncaging, also results in distinct Ca^{2+} entry, both in terms of the amount and the proportion contributed by spine and shaft. Given that both the 'readout' and the level of extrasynaptic glutamate can be dynamic, the extrasynaptic signal sensed by a neuron can also be dynamic and depends on the activities of the neuron itself and those of the local network. This suggests a complexity of extrasynaptic signalling that was not fully considered.

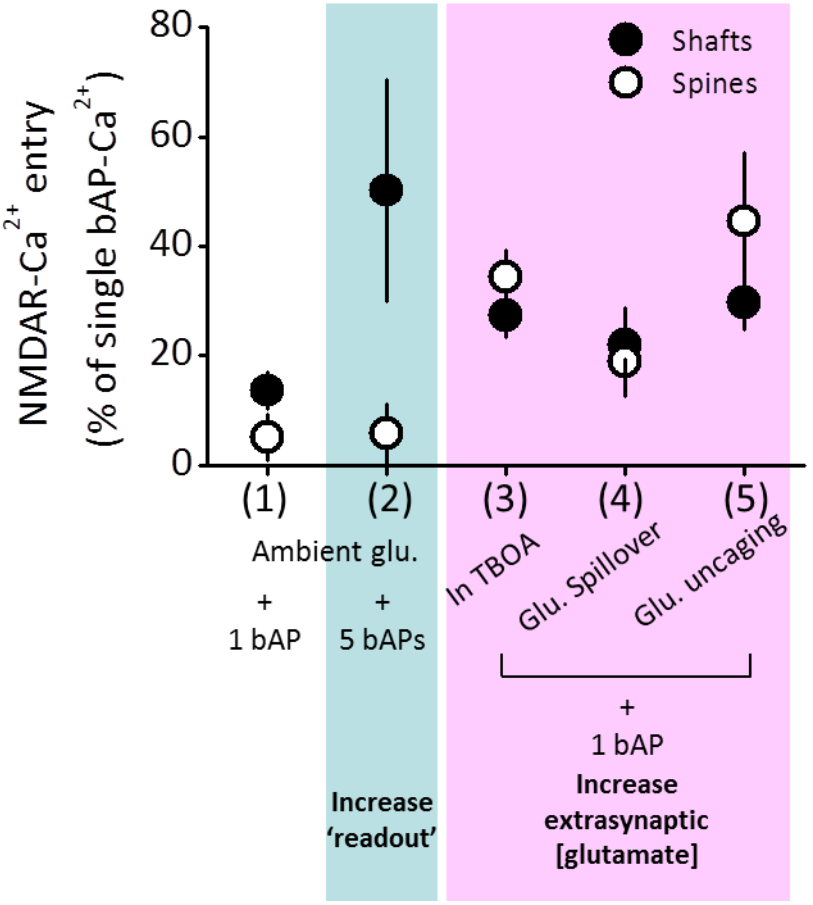

Figure 7.2 Tunable extrasynaptic signalling

The NMDAR-Ca^{2+} for each condition during the 'readout' process is normalized to the Ca^{2+} entry of a single bAP: (1) NMDAR-Ca^{2+} evoked by a single bAP (from Fig. 3.1); (2) NMDAR-Ca^{2+} evoked by burst of bAPs (from Fig. 6.4); (3) NMDAR-Ca^{2+} evoked by a single bAP in TBOA (from Fig. 3.9); (4) NMDAR-Ca^{2+} evoked by glutamate spillover paired with a single bAP (from Fig. 4.2); (5) NMDAR-Ca^{2+} evoked by glutamate uncaging paired with a single bAP (from Fig. 4.3). They can be categorized into two ways of enhancement of the extrasynaptic signalling. Firstly, increase 'readout' (blue region; (2)) and a rise of the concentration of extrasynaptic glutamate (pink region; (3)-(5)).

7.7. Possible roles of extrasynaptic glutamate signalling in neuronal synchronization

The activation of extrasynaptic NMDARs by the astrocytic release of glutamate has been suggested to act as a mechanism for neuronal synchronization (Angulo et al., 2004; Fellin et al., 2004), and a recent discovery of the use-dependent release of the NMDAR co-agonist D-serine from astrocytes provides a potential regulating mechanism for this 'diffuse' form of signalling (Henneberger et al., 2010). The present study suggests that such (slow) extracellular glutamate signals, by acting predominantly on dendritic shaft NMDARs, may trigger downregulation of G_h in a group of neurons in a synchronized fashion. The latter could in principle provide a mechanism for meta-plasticity changes that help to handle information in the network.

7.8. Synaptic versus extrasynaptic communication

The results in this study together suggest that synaptic and extrasynaptic NMDARs could be thought of as destined to receive and process different types of signalling. Synapses are tuned for fast point-to-point communication whereas extrasynaptic NMDARs appear to sense slower, volume-averaged rises of glutamate. Correspondingly, individual synapses can operate at relatively high frequencies to

resolve closely timed events whereas extrasynaptic NMDARs respond to integrated signals reflecting activity of local network and astrocytes.

The results also demonstrated that recruitment of shaft NMDARs (activated by non-vesicular supply of glutamate) by theta-bursts of bAPs downregulates G_h. In contrast, the recruitment of synaptic NMDARs (activated by vesicular glutamate release) by bAPs upregulates G_h. Thus, the net effect of bAPs on the cell's input resistance depends on the balance between glutamate-bound synaptic versus extrasynaptic NMDARs (Fig. 7.3). In this way, increased synaptic network activity can tip the balance in favour of synaptic NMDARs, whereas decreased synaptic activity shifts it back to the extrasynaptic NMDARs. Similar to synaptic potentiation and depression, this bi-directional plasticity mechanism prevents the cell from progressive runaway excitation, thus providing a theoretically plausible basis for information coding in the network.

Recent reports suggest that dendritic branches rather than individual synapses are the primary functional units for long term memory storage (Govindarajan et al., 2011; Losonczy et al., 2008; Makara et al., 2009). These studies used synaptic stimulation to demonstrate that dendritic branches operate as single computational units. The present results suggest therefore that extrasynaptic glutamate signalling acting via the dendritic shaft NMDARs could play a potentially important part in such integration. For example, when a dendrite receives more extrasynaptic inputs than synaptic ones, it suggests that the activity of the dendrite is low compared to the surrounding tissue, because extrasynaptic input reflects the local network activity. In

this case, shaft NMDARs can trigger the downregulation of G_h to increase dendritic excitability and let the dendrite be involved in local network (Fig. 6.6).

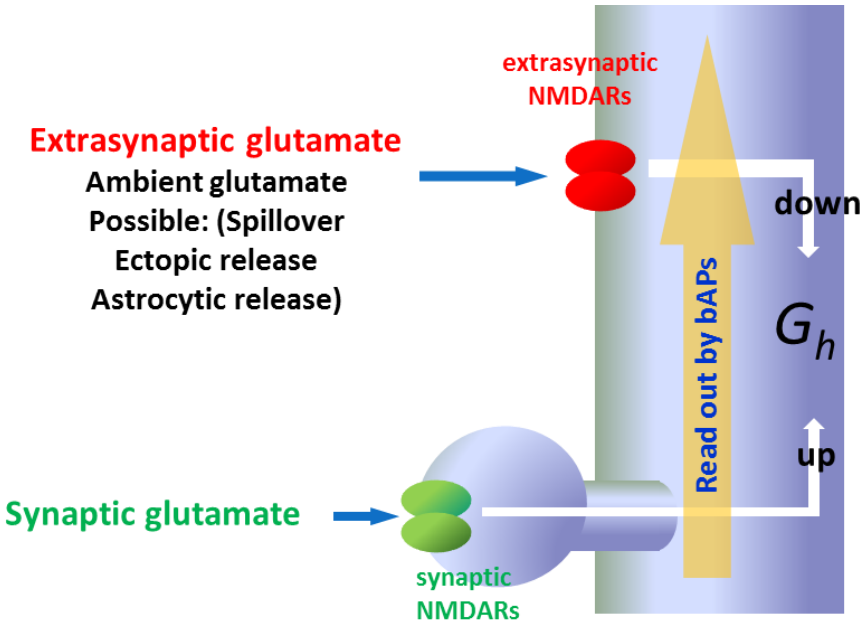

Figure 7.3 Synaptic and extrasynaptic NMDARs differentially regulate G_h

Extrasynaptic glutamate-bound shaft NMDARs enabled by 'readout' provided by bAPs. Repetitive activation of these receptors triggers downregulation of *h*-channels (G_h). In contrast, when synaptic NMDARs are activated by bAP during synaptic events, G_h becomes upregulated.

7.9. Brain-state dependent extrasynaptic NMDAR-mediated signalling

It has been shown that acetylcholine release and activation of muscarinic cholinergic receptors (mAChRs) enhance NMDAR-mediated synaptic transmission in synapses between CA3 and CA1 pyramidal neurons (Marino et al., 1998; Markram and Segal, 1990). The effect is mediated by postsynaptically expressed M1-type mAChRs that mobilize Ca^{2+} from intracellular stores (Shinoe et al., 2005). In addition, extracellular acetylcholine levels were shown to be altered between different brain states, *i.e.* awaking, slow-wave sleep, and rapid-eye-movement (REM) sleep (Kametani and Kawamura, 1990; Marrosu et al., 1995). During awake and REM sleep, the extracellular acetylcholine levels in hippocampus can be three-times higher than during slow-wave sleep (Kametani and Kawamura, 1990). It is, therefore, reasonable to speculate a wake state-dependent modulation of NMDARs by M1-type mAChRs. However, more recent findings have suggested that M1-type mAChRs promote NMDAR-mediated EPSPs (NMDAR-EPSPs) not via direct modulation of NMDARs but by downregulating small conductance Ca^{2+}-activated potassium (SK) channels and thus disinhibiting NMDAR-EPSPs (Giessel and Sabatini, 2010). SK channels have been shown to be co-localized with synaptic NMDARs on individual spine heads and are activated only when intracellular Ca^{2+} rises within a nanodomain through synaptic NMDARs but not extrasynaptic ones (Bloodgood et al., 2009; Bloodgood and Sabatini, 2007b; Ngo-Anh et al., 2005). These findings suggest that the dynamics of ambient

acetylcholine levels in different brain states can specifically modulate synaptic NMDAR-mediated signalling.

On the other hand, as described in Chapter 1.3.2, extracellular glutamate levels are also altered between brain states (Baker et al., 2002; Dash et al., 2009; Del Arco et al., 2003; Mattinson et al., 2011; Rutherford et al., 2007). In the cortex of freely moving rats, extrasynaptic glutamate concentration increased during the awaking and REM sleep state whereas it decreased during non-REM sleep (Dash et al., 2009). Because of the powerful glutamate uptake system, the dynamics of extrasynaptic glutamate across brain states are only sensed by extrasynaptic NMDARs rather than synaptic ones. Altogether, these data further suggest that the modulation of synaptic and extrasynaptic NMDAR signalling can be brain state-dependent but still be compartmentalized.

7.10. Future work

7.10.1. Detection of transient glutamate release from astrocytes by extrasynaptic NMDARs depends on neuronal activity

My results demonstrate that extrasynaptic glutamate generated by glutamate uncaging is sensed by neurons during bAPs. What is not known is that whether such uncaged glutamate indeed mimics the astrocytic release. Therefore, it is important to show that 'readout' is also required for detecting astrocytic glutamate release.

The activation of extrasynaptic NMDARs by the astrocytic release of glutamate has been suggested to promote synchronized firing of a proportion of neurons (Angulo et al., 2004; Fellin et al., 2004). It is possible that those neurons were actually having a 'readout' signal which coincides with the astrocytic release. Therefore, the astrocytic glutamate release might have a stronger impact on those neurons which are electrically active.

7.10.2. The downstream signalling of extrasynaptic NMDAR

The results in this thesis only demonstrate that activation of ambient glutamate-bound extrasynaptic NMDARs downregulated G_h, which is opposite to synaptic NMDARs. The possible downstream signalling pathways, i.e. ERK1/2 –dependent downregulation of HCN protein synthesis and changing channel gating properties by p38 MAPK, which were discussed in chapter 6, can be tested by using pharmacological tools that target ERK1/2 and p38 MAPK.

7.10.3. The *in vivo* impact of the glutamatergic extrasynaptic signalling

As the current study was performed in brain slices, it is important to test whether such compartmentalized synaptic and extrasynaptic signalling is also present *in vivo*. My results have shown that a large proportion of extrasynaptic glutamate is sensed by GluN2D-containing NMDARs. It is possible to manipulate the

glutamatergic extrasynaptic signalling by local injection of either GluN2D selective blockers, PPDA and UBP141, or potentiator, CIQ, into hippocampus (Mosley et al., 2010; Mullasseril et al., 2010). Thus, we can investigate whether there is any impact of glutamatergic extrasynaptic signalling on learning and memory of the animal.

7.10.4. Glutamatergic extrasynaptic signalling in epilepsy

There is growing evidence suggesting the loss of HCN channels is involved in the development of the epileptic state (Huang et al., 2009; Shah et al., 2004; Shin et al., 2008b), which makes HCN channels a new target for drug development (Postea and Biel, 2011). The detailed mechanisms for such loss in HCN1 channels after status epilepticus (SE) are still unclear. A recent study demonstrated that the loss of functional HCN1 involved sequential processes of channel internalization, loss of protein expression, and downregulation of mRNA expression following SE in hippocampal pyramidal neurons (Jung et al., 2011). However, this contradicts the finding that activation of synaptic NMDARs during burst firing upregulates HCN channels, downregulating the cell excitability and preventing excitotoxicity (Campanac et al., 2008; Fan et al., 2005). It is reasonable to hypothesize that during SE the extrasynaptic glutamatergic signal overrides the synaptic one, resulting in the downregulation of G_h. My preliminary data suggest an increased tonic NMDAR-mediated current in hippocampal CA1 pyramidal neurons after status epilepticus in an *in vivo* animal model of epilepsy (data not shown) (Walker et al., 1999). Instead of

targeting the HCN channel itself, the extrasynaptic NMDARs, especially GluN2D-containing receptors can be another candidate for preventing loss of HCN function. Therefore, it is worth trying the selective blockers for GluN2D-containing NMDAR to see whether they have any antiepileptogenic effect in animal models of epilepsy.

Reference list

Angulo, M.C., A.S. Kozlov, S. Charpak, and E. Audinat. 2004. Glutamate released from glial cells synchronizes neuronal activity in the hippocampus. *J Neurosci*. 24:6920-6927.

Aoki, C., C. Venkatesan, C.G. Go, J.A. Mong, and T.M. Dawson. 1994. Cellular and subcellular localization of NMDA-R1 subunit immunoreactivity in the visual cortex of adult and neonatal rats. *J Neurosci*. 14:5202-5222.

Araque, A., N. Li, R.T. Doyle, and P.G. Haydon. 2000. SNARE protein-dependent glutamate release from astrocytes. *J Neurosci*. 20:666-673.

Arnth-Jensen, N., D. Jabaudon, and M. Scanziani. 2002. Cooperation between independent hippocampal synapses is controlled by glutamate uptake. *Nat Neurosci*. 5:325-331.

Asztely, F., G. Erdemli, and D.M. Kullmann. 1997. Extrasynaptic glutamate spillover in the hippocampus: dependence on temperature and the role of active glutamate uptake. *Neuron*. 18:281-293.

Baker, D.A., Z.X. Xi, H. Shen, C.J. Swanson, and P.W. Kalivas. 2002. The origin and neuronal function of in vivo nonsynaptic glutamate. *J Neurosci*. 22:9134-9141.

Bannai, S. 1986. Exchange of cystine and glutamate across plasma membrane of human fibroblasts. *J Biol Chem*. 261:2256-2263.

Beique, J.C., D.T. Lin, M.G. Kang, H. Aizawa, K. Takamiya, and R.L. Huganir. 2006. Synapse-specific regulation of AMPA receptor function by PSD-95. *Proc Natl Acad Sci U S A*. 103:19535-19540.

Ben-Ari, Y. 2001. Developing networks play a similar melody. *Trends Neurosci*. 24:353-360.

Bergles, D.E., J.S. Diamond, and C.E. Jahr. 1999. Clearance of glutamate inside the synapse and beyond. *Curr Opin Neurobiol*. 9:293-298.

Bezzi, P., V. Gundersen, J.L. Galbete, G. Seifert, C. Steinhauser, E. Pilati, and A. Volterra. 2004. Astrocytes contain a vesicular compartment that is competent for regulated exocytosis of glutamate. *Nat Neurosci*. 7:613-620.

Biel, M., C. Wahl-Schott, S. Michalakis, and X. Zong. 2009. Hyperpolarization-activated cation channels: from genes to function. *Physiol Rev*. 89:847-885.

Bland, B.H. 1986. The physiology and pharmacology of hippocampal formation theta rhythms. *Prog Neurobiol*. 26:1-54.

Bloodgood, B.L., A.J. Giessel, and B.L. Sabatini. 2009. Biphasic synaptic Ca influx arising from compartmentalized electrical signals in dendritic spines. *PLoS Biol*. 7:e1000190.

Bloodgood, B.L., and B.L. Sabatini. 2007a. Ca(2+) signaling in dendritic spines. *Curr Opin Neurobiol*. 17:345-351.

Bloodgood, B.L., and B.L. Sabatini. 2007b. Nonlinear regulation of unitary synaptic signals by CaV(2.3) voltage-sensitive calcium channels located in dendritic spines. *Neuron*. 53:249-260.

Bloodgood, B.L., and B.L. Sabatini. 2008. Regulation of synaptic signalling by postsynaptic, non-glutamate receptor ion channels. *J Physiol*. 586:1475-1480.

Bordji, K., J. Becerril-Ortega, O. Nicole, and A. Buisson. 2010. Activation of extrasynaptic, but not synaptic, NMDA receptors modifies amyloid precursor protein expression pattern and increases amyloid-ss production. *J Neurosci*. 30:15927-15942.

Bourne, J.N., and K.M. Harris. 2011. Coordination of size and number of excitatory and inhibitory synapses results in a balanced structural plasticity along mature hippocampal CA1 dendrites during LTP. *Hippocampus*. 21:354-373.

Bowser, D.N., and B.S. Khakh. 2007. Two forms of single-vesicle astrocyte exocytosis imaged with total internal reflection fluorescence microscopy. *Proc Natl Acad Sci U S A*. 104:4212-4217.

Brickley, S.G., C. Misra, M.H. Mok, M. Mishina, and S.G. Cull-Candy. 2003. NR2B and NR2D subunits coassemble in cerebellar Golgi cells to form a distinct NMDA receptor subtype restricted to extrasynaptic sites. *J Neurosci*. 23:4958-4966.

Bucurenciu, I., A. Kulik, B. Schwaller, M. Frotscher, and P. Jonas. 2008. Nanodomain coupling between Ca2+ channels and Ca2+ sensors promotes fast and efficient transmitter release at a cortical GABAergic synapse. *Neuron*. 57:536-545.

Burnstock, G. 2008. Purinergic signalling and disorders of the central nervous system. *Nat Rev Drug Discov*. 7:575-590.

Busetto, G., M.J. Higley, and B.L. Sabatini. 2008. Developmental presence and disappearance of postsynaptically silent synapses on dendritic spines of rat layer 2/3 pyramidal neurons. *J Physiol*. 586:1519-1527.

Campanac, E., G. Daoudal, N. Ankri, and D. Debanne. 2008. Downregulation of dendritic I(h) in CA1 pyramidal neurons after LTP. *J Neurosci*. 28:8635-8643.

Castro, J.B., and N.N. Urban. 2009. Subthreshold glutamate release from mitral cell dendrites. *J Neurosci*. 29:7023-7030.

Cavelier, P., and D. Attwell. 2005. Tonic release of glutamate by a DIDS-sensitive mechanism in rat hippocampal slices. *J Physiol*. 564:397-410.

Cavelier, P., M. Hamann, D. Rossi, P. Mobbs, and D. Attwell. 2005. Tonic excitation and inhibition of neurons: ambient transmitter sources and computational consequences. *Prog Biophys Mol Biol*. 87:3-16.

Chalifoux, J.R., and A.G. Carter. 2011. Glutamate Spillover Promotes the Generation of NMDA Spikes. *J Neurosci*. 31:16435-16446.

Christie, J.M., and G.L. Westbrook. 2006. Lateral excitation within the olfactory bulb. *J Neurosci*. 26:2269-2277.

Clarke, R.J., and J.W. Johnson. 2006. NMDA receptor NR2 subunit dependence of the slow component of magnesium unblock. *J Neurosci*. 26:5825-5834.

Clarke, R.J., and J.W. Johnson. 2008. Voltage-dependent gating of NR1/2B NMDA receptors. *J Physiol*. 586:5727-5741.

Costa, B.M., B. Feng, T.S. Tsintsadze, R.M. Morley, M.W. Irvine, V. Tsintsadze, N.A. Lozovaya, D.E. Jane, and D.T. Monaghan. 2009. N-methyl-D-aspartate (NMDA) receptor NR2 subunit selectivity of a series of novel piperazine-2,3-dicarboxylate derivatives: preferential blockade of extrasynaptic NMDA receptors in the rat hippocampal CA3-CA1 synapse. *J Pharmacol Exp Ther*. 331:618-626.

Cull-Candy, S., S. Brickley, and M. Farrant. 2001. NMDA receptor subunits: diversity, development and disease. *Curr Opin Neurobiol*. 11:327-335.

Cull-Candy, S.G., and D.N. Leszkiewicz. 2004. Role of distinct NMDA receptor subtypes at central synapses. *Sci STKE*. 2004:re16.

D'Ascenzo, M., T. Fellin, M. Terunuma, R. Revilla-Sanchez, D.F. Meaney, Y.P. Auberson, S.J. Moss, and P.G. Haydon. 2007. mGluR5 stimulates gliotransmission in the nucleus accumbens. *Proc Natl Acad Sci U S A*. 104:1995-2000.

Dalby, N.O., and I. Mody. 2003. Activation of NMDA receptors in rat dentate gyrus granule cells by spontaneous and evoked transmitter release. *J Neurophysiol*. 90:786-797.

Dan, Y., and M.M. Poo. 2006. Spike timing-dependent plasticity: from synapse to perception. *Physiol Rev*. 86:1033-1048.

Danbolt, N.C. 2001. Glutamate uptake. *Prog Neurobiol*. 65:1-105.

Danbolt, N.C., F.A. Chaudhry, Y. Dehnes, K.P. Lehre, L.M. Levy, K. Ullensvang, and J. Storm-Mathisen. 1998. Properties and localization of glutamate transporters. *Prog Brain Res*. 116:23-43.

Dash, M.B., C.L. Douglas, V.V. Vyazovskiy, C. Cirelli, and G. Tononi. 2009. Long-term homeostasis of extracellular glutamate in the rat cerebral cortex across sleep and waking states. *J Neurosci*. 29:620-629.

De Bundel, D., A. Schallier, E. Loyens, R. Fernando, H. Miyashita, J. Van Liefferinge, K. Vermoesen, S. Bannai, H. Sato, Y. Michotte, I. Smolders, and A. Massie. 2011. Loss of system x(c)- does not induce oxidative stress but decreases extracellular glutamate in hippocampus and influences spatial working memory and limbic seizure susceptibility. *J Neurosci*. 31:5792-5803.

Del Arco, A., G. Segovia, K. Fuxe, and F. Mora. 2003. Changes in dialysate concentrations of glutamate and GABA in the brain: an index of volume transmission mediated actions? *J Neurochem*. 85:23-33.

Diamond, J.S. 2001. Neuronal glutamate transporters limit activation of NMDA receptors by neurotransmitter spillover on CA1 pyramidal cells. *J Neurosci*. 21:8328-8338.

Diamond, J.S., and C.E. Jahr. 1997. Transporters buffer synaptically released glutamate on a submillisecond time scale. *J Neurosci*. 17:4672-4687.

Diamond, J.S., and C.E. Jahr. 2000. Synaptically released glutamate does not overwhelm transporters on hippocampal astrocytes during high-frequency stimulation. *J Neurophysiol*. 83:2835-2843.

Dingledine, R., K. Borges, D. Bowie, and S.F. Traynelis. 1999. The glutamate receptor ion channels. *Pharmacol Rev*. 51:7-61.

Drose, S., and K. Altendorf. 1997. Bafilomycins and concanamycins as inhibitors of V-ATPases and P-ATPases. *J Exp Biol*. 200:1-8.

Duan, S., C.M. Anderson, E.C. Keung, Y. Chen, and R.A. Swanson. 2003. P2X7 receptor-mediated release of excitatory amino acids from astrocytes. *J Neurosci*. 23:1320-1328.

Duguid, I.C., Y. Pankratov, G.W. Moss, and T.G. Smart. 2007. Somatodendritic release of glutamate regulates synaptic inhibition in cerebellar Purkinje cells via autocrine mGluR1 activation. *J Neurosci*. 27:12464-12474.

Dunah, A.W., R.P. Yasuda, Y.H. Wang, J. Luo, M. Davila-Garcia, M. Gbadegesin, S. Vicini, and B.B. Wolfe. 1996. Regional and ontogenic expression of the NMDA receptor subunit NR2D protein in rat brain using a subunit-specific antibody. *J Neurochem*. 67:2335-2345.

Eskandari, S., G.A. Zampighi, D.W. Leung, E.M. Wright, and D.D. Loo. 2002. Inhibition of gap junction hemichannels by chloride channel blockers. *J Membr Biol*. 185:93-102.

Fan, Y., D. Fricker, D.H. Brager, X. Chen, H.C. Lu, R.A. Chitwood, and D. Johnston. 2005. Activity-dependent decrease of excitability in rat hippocampal neurons through increases in I(h). *Nat Neurosci*. 8:1542-1551.

Farrant, M., D. Feldmeyer, T. Takahashi, and S.G. Cull-Candy. 1994. NMDA-receptor channel diversity in the developing cerebellum. *Nature*. 368:335-339.

Featherstone, D.E., and S.A. Shippy. 2008. Regulation of synaptic transmission by ambient extracellular glutamate. *Neuroscientist*. 14:171-181.

Fellin, T., O. Pascual, S. Gobbo, T. Pozzan, P.G. Haydon, and G. Carmignoto. 2004. Neuronal synchrony mediated by astrocytic glutamate through activation of extrasynaptic NMDA receptors. *Neuron*. 43:729-743.

Fellin, T., T. Pozzan, and G. Carmignoto. 2006. Purinergic receptors mediate two distinct glutamate release pathways in hippocampal astrocytes. *J Biol Chem*. 281:4274-4284.

Feng, B., H.W. Tse, D.A. Skifter, R. Morley, D.E. Jane, and D.T. Monaghan. 2004. Structure-activity analysis of a novel NR2C/NR2D-preferring NMDA receptor antagonist: 1-(phenanthrene-2-carbonyl) piperazine-2,3-dicarboxylic acid. *Br J Pharmacol*. 141:508-516.

Fischer, G., V. Mutel, G. Trube, P. Malherbe, J.N. Kew, E. Mohacsi, M.P. Heitz, and J.A. Kemp. 1997. Ro 25-6981, a highly potent and selective blocker of N-methyl-D-aspartate receptors containing the NR2B subunit. Characterization in vitro. *J Pharmacol Exp Ther*. 283:1285-1292.

Fleming, T.M., V. Scott, N. Joe, K. Naskar, C.H. Brown, and J.E. Stern. 2011a. State-Dependent Changes in Astrocyte Regulation of Extrasynaptic Nmda Receptor Signaling in Neurosecretory Neurons. *J Physiol*.

Fleming, T.M., V. Scott, K. Naskar, N. Joe, C.H. Brown, and J.E. Stern. 2011b. State-dependent changes in astrocyte regulation of extrasynaptic NMDA receptor signalling in neurosecretory neurons. *J Physiol*. 589:3929-3941.

Giessel, A.J., and B.L. Sabatini. 2010. M1 muscarinic receptors boost synaptic potentials and calcium influx in dendritic spines by inhibiting postsynaptic SK channels. *Neuron*. 68:936-947.

Goebel-Goody, S.M., K.D. Davies, R.M. Alvestad Linger, R.K. Freund, and M.D. Browning. 2009. Phospho-regulation of synaptic and extrasynaptic N-methyl-d-aspartate receptors in adult hippocampal slices. *Neuroscience*. 158:1446-1459.

Govindarajan, A., I. Israely, S.Y. Huang, and S. Tonegawa. 2011. The dendritic branch is the preferred integrative unit for protein synthesis-dependent LTP. *Neuron*. 69:132-146.

Grastyan, E., K. Lissak, I. Madarasz, and H. Donhoffer. 1959. Hippocampal electrical activity during the development of conditioned reflexes. *Electroencephalogr Clin Neurophysiol*. 11:409-430.

Greer, P.L., and M.E. Greenberg. 2008. From synapse to nucleus: calcium-dependent gene transcription in the control of synapse development and function. *Neuron*. 59:846-860.

Groc, L., L. Bard, and D. Choquet. 2009. Surface trafficking of N-methyl-D-aspartate receptors: physiological and pathological perspectives. *Neuroscience*. 158:4-18.

Hamilton, N.B., and D. Attwell. 2010. Do astrocytes really exocytose neurotransmitters? *Nat Rev Neurosci*. 11:227-238.

Hammond, R.S., L. Lin, M.S. Sidorov, A.M. Wikenheiser, and D.A. Hoffman. 2008. Protein kinase a mediates activity-dependent Kv4.2 channel trafficking. *J Neurosci*. 28:7513-7519.

Hardingham, G.E., and H. Bading. 2010. Synaptic versus extrasynaptic NMDA receptor signalling: implications for neurodegenerative disorders. *Nat Rev Neurosci*. 11:682-696.

Hardingham, G.E., Y. Fukunaga, and H. Bading. 2002. Extrasynaptic NMDARs oppose synaptic NMDARs by triggering CREB shut-off and cell death pathways. *Nat Neurosci*. 5:405-414.

Harney, S.C., D.E. Jane, and R. Anwyl. 2008. Extrasynaptic NR2D-containing NMDARs are recruited to the synapse during LTP of NMDAR-EPSCs. *J Neurosci*. 28:11685-11694.

Harris, N.C., and A. Constanti. 1995. Mechanism of block by ZD 7288 of the hyperpolarization-activated inward rectifying current in guinea pig substantia nigra neurons in vitro. *J Neurophysiol*. 74:2366-2378.

Hascup, K.N., E.R. Hascup, M.L. Stephens, P.E. Glaser, T. Yoshitake, A.A. Mathe, G.A. Gerhardt, and J. Kehr. 2011. Resting glutamate levels and rapid glutamate transients in the prefrontal cortex of the Flinders Sensitive Line rat: a genetic rodent model of depression. *Neuropsychopharmacology*. 36:1769-1777.

Helmchen, F. 2002. Raising the speed limit--fast Ca(2+) handling in dendritic spines. *Trends Neurosci*. 25:438-441; discussion 441.

Henneberger, C., T. Papouin, S.H. Oliet, and D.A. Rusakov. 2010. Long-term potentiation depends on release of D-serine from astrocytes. *Nature*. 463:232-236.

Herman, M.A., and C.E. Jahr. 2007. Extracellular glutamate concentration in hippocampal slice. *J Neurosci*. 27:9736-9741.

Herman, M.A., B. Nahir, and C.E. Jahr. 2011. Distribution of extracellular glutamate in the neuropil of hippocampus. *PLoS One*. 6:e26501.

Hille, B. 2001. *Ion Channels of Excitable Membranes*, Third Edition.

Hines, M.L., and N.T. Carnevale. 1997. The NEURON simulation environment. *Neural Comput*. 9:1179-1209.

Hires, S.A., Y. Zhu, and R.Y. Tsien. 2008. Optical measurement of synaptic glutamate spillover and reuptake by linker optimized glutamate-sensitive fluorescent reporters. *Proc Natl Acad Sci U S A*. 105:4411-4416.

Hoffman, D.A., J.C. Magee, C.M. Colbert, and D. Johnston. 1997. K+ channel regulation of signal propagation in dendrites of hippocampal pyramidal neurons. *Nature*. 387:869-875.

Huang, Z., M.C. Walker, and M.M. Shah. 2009. Loss of dendritic HCN1 subunits enhances cortical excitability and epileptogenesis. *J Neurosci*. 29:10979-10988.

Hudmon, A., H. Schulman, J. Kim, J.M. Maltez, R.W. Tsien, and G.S. Pitt. 2005. CaMKII tethers to L-type Ca2+ channels, establishing a local and dedicated integrator of Ca2+ signals for facilitation. *J Cell Biol*. 171:537-547.

Husi, H., M.A. Ward, J.S. Choudhary, W.P. Blackstock, and S.G. Grant. 2000. Proteomic analysis of NMDA receptor-adhesion protein signaling complexes. *Nat Neurosci*. 3:661-669.

Iglesias, R., G. Dahl, F. Qiu, D.C. Spray, and E. Scemes. 2009. Pannexin 1: the molecular substrate of astrocyte "hemichannels". *J Neurosci*. 29:7092-7097.

Ishii, T., K. Moriyoshi, H. Sugihara, K. Sakurada, H. Kadotani, M. Yokoi, C. Akazawa, R. Shigemoto, N. Mizuno, M. Masu, and et al. 1993. Molecular characterization of the family of the N-methyl-D-aspartate receptor subunits. *J Biol Chem*. 268:2836-2843.

Ivanov, A., C. Pellegrino, S. Rama, I. Dumalska, Y. Salyha, Y. Ben-Ari, and I. Medina. 2006. Opposing role of synaptic and extrasynaptic NMDA receptors in regulation of the extracellular signal-regulated kinases (ERK) activity in cultured rat hippocampal neurons. *J Physiol*. 572:789-798.

Jabaudon, D., K. Shimamoto, Y. Yasuda-Kamatani, M. Scanziani, B.H. Gahwiler, and U. Gerber. 1999. Inhibition of uptake unmasks rapid extracellular turnover of glutamate of nonvesicular origin. *Proc Natl Acad Sci U S A*. 96:8733-8738.

Johnson, J.W., and P. Ascher. 1987. Glycine potentiates the NMDA response in cultured mouse brain neurons. *Nature*. 325:529-531.

Jones, M.W., and T.J. McHugh. 2011. Updating hippocampal representations: CA2 joins the circuit. *Trends Neurosci*. 34:526-535.

Jourdain, P., L.H. Bergersen, K. Bhaukaurally, P. Bezzi, M. Santello, M. Domercq, C. Matute, F. Tonello, V. Gundersen, and A. Volterra. 2007. Glutamate exocytosis from astrocytes controls synaptic strength. *Nat Neurosci*. 10:331-339.

Jung, S., J.B. Bullis, I.H. Lau, T.D. Jones, L.N. Warner, and N.P. Poolos. 2010. Downregulation of dendritic HCN channel gating in epilepsy is mediated by altered phosphorylation signaling. *J Neurosci*. 30:6678-6688.

Jung, S., L.N. Warner, J. Pitsch, A.J. Becker, and N.P. Poolos. 2011. Rapid loss of dendritic HCN channel expression in hippocampal pyramidal neurons following status epilepticus. *J Neurosci*. 31:14291-14295.

Kametani, H., and H. Kawamura. 1990. Alterations in acetylcholine release in the rat hippocampus during sleep-wakefulness detected by intracerebral dialysis. *Life Sci*. 47:421-426.

Kampa, B.M., J. Clements, P. Jonas, and G.J. Stuart. 2004. Kinetics of Mg2+ unblock of NMDA receptors: implications for spike-timing dependent synaptic plasticity. *J Physiol*. 556:337-345.

Kampa, B.M., J.J. Letzkus, and G.J. Stuart. 2007. Dendritic mechanisms controlling spike-timing-dependent synaptic plasticity. *Trends Neurosci*. 30:456-463.

Kandel, E.R., and W.A. Spencer. 1961. Electrophysiology of hippocampal neurons. II. After-potentials and repetitive firing. *J Neurophysiol*. 24:243-259.

Kerchner, G.A., and R.A. Nicoll. 2008. Silent synapses and the emergence of a postsynaptic mechanism for LTP. *Nat Rev Neurosci*. 9:813-825.

Kim, J., S.C. Jung, A.M. Clemens, R.S. Petralia, and D.A. Hoffman. 2007. Regulation of dendritic excitability by activity-dependent trafficking of the A-type K+ channel subunit Kv4.2 in hippocampal neurons. *Neuron*. 54:933-947.

Kim, J., M.S. Nadal, A.M. Clemens, M. Baron, S.C. Jung, Y. Misumi, B. Rudy, and D.A. Hoffman. 2008. Kv4 accessory protein DPPX (DPP6) is a critical regulator of membrane excitability in hippocampal CA1 pyramidal neurons. *J Neurophysiol*. 100:1835-1847.

Kim, M.J., A.W. Dunah, Y.T. Wang, and M. Sheng. 2005. Differential roles of NR2A- and NR2B-containing NMDA receptors in Ras-ERK signaling and AMPA receptor trafficking. *Neuron*. 46:745-760.

Kimelberg, H.K., S.K. Goderie, S. Higman, S. Pang, and R.A. Waniewski. 1990. Swelling-induced release of glutamate, aspartate, and taurine from astrocyte cultures. *J Neurosci*. 10:1583-1591.

Kleckner, N.W., and R. Dingledine. 1988. Requirement for glycine in activation of NMDA-receptors expressed in Xenopus oocytes. *Science*. 241:835-837.

Kovalchuk, Y., J. Eilers, J. Lisman, and A. Konnerth. 2000. NMDA receptor-mediated subthreshold Ca(2+) signals in spines of hippocampal neurons. *J Neurosci*. 20:1791-1799.

Kukley, M., E. Capetillo-Zarate, and D. Dietrich. 2007. Vesicular glutamate release from axons in white matter. *Nat Neurosci*. 10:311-320.

Kullmann, D.M., A. Ruiz, D.M. Rusakov, R. Scott, A. Semyanov, and M.C. Walker. 2005. Presynaptic, extrasynaptic and axonal GABAA receptors in the CNS: where and why? *Prog Biophys Mol Biol*. 87:33-46.

Larson, J., and G. Lynch. 1986. Induction of synaptic potentiation in hippocampus by patterned stimulation involves two events. *Science*. 232:985-988.

Larson, J., D. Wong, and G. Lynch. 1986. Patterned stimulation at the theta frequency is optimal for the induction of hippocampal long-term potentiation. *Brain Res*. 368:347-350.

Lau, C.G., and R.S. Zukin. 2007. NMDA receptor trafficking in synaptic plasticity and neuropsychiatric disorders. *Nat Rev Neurosci*. 8:413-426.

Le Meur, K., M. Galante, M.C. Angulo, and E. Audinat. 2007. Tonic activation of NMDA receptors by ambient glutamate of non-synaptic origin in the rat hippocampus. *J Physiol*. 580:373-383.

Lee, S.J., Y. Escobedo-Lozoya, E.M. Szatmari, and R. Yasuda. 2009. Activation of CaMKII in single dendritic spines during long-term potentiation. *Nature*. 458:299-304.

Lehre, K.P., and N.C. Danbolt. 1998. The number of glutamate transporter subtype molecules at glutamatergic synapses: chemical and stereological quantification in young adult rat brain. *J Neurosci*. 18:8751-8757.

Lehre, K.P., and D.A. Rusakov. 2002. Asymmetry of glia near central synapses favors presynaptically directed glutamate escape. *Biophys J*. 83:125-134.

Lei, Z., P. Deng, Y. Li, and Z.C. Xu. 2009. Downregulation of Kv4.2 channels mediated by NR2B-containing NMDA receptors in cultured hippocampal neurons. *Neuroscience*.

Li, D., K. Herault, E.Y. Isacoff, M. Oheim, and N. Ropert. 2012. Optogenetic activation of LiGluR-expressing astrocytes evokes anion channel-mediated glutamate release. *J Physiol*.

Li, J.H., Y.H. Wang, B.B. Wolfe, K.E. Krueger, L. Corsi, G. Stocca, and S. Vicini. 1998. Developmental changes in localization of NMDA receptor subunits in primary cultures of cortical neurons. *Eur J Neurosci*. 10:1704-1715.

Liu, H.T., T. Akita, T. Shimizu, R.Z. Sabirov, and Y. Okada. 2009. Bradykinin-induced astrocyte-neuron signalling: glutamate release is mediated by ROS-activated volume-sensitive outwardly rectifying anion channels. *J Physiol*. 587:2197-2209.

Liu, H.T., B.A. Tashmukhamedov, H. Inoue, Y. Okada, and R.Z. Sabirov. 2006. Roles of two types of anion channels in glutamate release from mouse astrocytes under ischemic or osmotic stress. *Glia*. 54:343-357.

Liu, L., T.P. Wong, M.F. Pozza, K. Lingenhoehl, Y. Wang, M. Sheng, Y.P. Auberson, and Y.T. Wang. 2004. Role of NMDA receptor subtypes in governing the direction of hippocampal synaptic plasticity. *Science*. 304:1021-1024.

Lorincz, A., T. Notomi, G. Tamas, R. Shigemoto, and Z. Nusser. 2002. Polarized and compartment-dependent distribution of HCN1 in pyramidal cell dendrites. *Nat Neurosci*. 5:1185-1193.

Losonczy, A., J.K. Makara, and J.C. Magee. 2008. Compartmentalized dendritic plasticity and input feature storage in neurons. *Nature*. 452:436-441.

Low, C.M., and K.S. Wee. 2010. New insights into the not-so-new NR3 subunits of N-methyl-D-aspartate receptor: localization, structure, and function. *Mol Pharmacol*. 78:1-11.

Lozovaya, N., S. Melnik, T. Tsintsadze, S. Grebenyuk, Y. Kirichok, and O. Krishtal. 2004a. Protective cap over CA1 synapses: extrasynaptic glutamate does not reach the postsynaptic density. *Brain Res*. 1011:195-205.

Lozovaya, N.A., S.E. Grebenyuk, T. Tsintsadze, B. Feng, D.T. Monaghan, and O.A. Krishtal. 2004b. Extrasynaptic NR2B and NR2D subunits of NMDA receptors shape 'superslow' afterburst EPSC in rat hippocampus. *J Physiol*. 558:451-463.

Magee, J.C. 1998. Dendritic hyperpolarization-activated currents modify the integrative properties of hippocampal CA1 pyramidal neurons. *J Neurosci*. 18:7613-7624.

Magee, J.C., and D. Johnston. 1995. Characterization of single voltage-gated Na+ and Ca2+ channels in apical dendrites of rat CA1 pyramidal neurons. *The Journal of physiology*. 487 (Pt 1):67-90.

Magee, J.C., and D. Johnston. 1997. A synaptically controlled, associative signal for Hebbian plasticity in hippocampal neurons. *Science*. 275:209-213.

Makara, J.K., A. Losonczy, Q. Wen, and J.C. Magee. 2009. Experience-dependent compartmentalized dendritic plasticity in rat hippocampal CA1 pyramidal neurons. *Nature neuroscience*. 12:1485-1487.

Malarkey, E.B., and V. Parpura. 2008. Mechanisms of glutamate release from astrocytes. *Neurochem Int*. 52:142-154.

Mann, E.O., and I. Mody. 2010. Control of hippocampal gamma oscillation frequency by tonic inhibition and excitation of interneurons. *Nat Neurosci*. 13:205-212.

Marchaland, J., C. Cali, S.M. Voglmaier, H. Li, R. Regazzi, R.H. Edwards, and P. Bezzi. 2008. Fast subplasma membrane Ca2+ transients control exo-endocytosis of synaptic-like microvesicles in astrocytes. *J Neurosci*. 28:9122-9132.

Marino, M.J., S.T. Rouse, A.I. Levey, L.T. Potter, and P.J. Conn. 1998. Activation of the genetically defined m1 muscarinic receptor potentiates N-methyl-D-aspartate

(NMDA) receptor currents in hippocampal pyramidal cells. *Proc Natl Acad Sci U S A*. 95:11465-11470.

Markram, H., J. Lubke, M. Frotscher, and B. Sakmann. 1997. Regulation of synaptic efficacy by coincidence of postsynaptic APs and EPSPs. *Science*. 275:213-215.

Markram, H., and M. Segal. 1990. Long-lasting facilitation of excitatory postsynaptic potentials in the rat hippocampus by acetylcholine. *J Physiol*. 427:381-393.

Marrosu, F., C. Portas, M.S. Mascia, M.A. Casu, M. Fa, M. Giagheddu, A. Imperato, and G.L. Gessa. 1995. Microdialysis measurement of cortical and hippocampal acetylcholine release during sleep-wake cycle in freely moving cats. *Brain Res*. 671:329-332.

Massie, A., A. Schallier, S.W. Kim, R. Fernando, S. Kobayashi, H. Beck, D. De Bundel, K. Vermoesen, S. Bannai, I. Smolders, M. Conrad, N. Plesnila, H. Sato, and Y. Michotte. 2011. Dopaminergic neurons of system x(c)-deficient mice are highly protected against 6-hydroxydopamine-induced toxicity. *FASEB J*. 25:1359-1369.

Matsui, K., and C.E. Jahr. 2003. Ectopic release of synaptic vesicles. *Neuron*. 40:1173-1183.

Mattinson, C.E., J.J. Burmeister, J.E. Quintero, F. Pomerleau, P. Huettl, and G.A. Gerhardt. 2011. Tonic and phasic release of glutamate and acetylcholine neurotransmission in sub-regions of the rat prefrontal cortex using enzyme-based microelectrode arrays. *J Neurosci Methods*. 202:199-208.

Mayer, M.L., and G.L. Westbrook. 1987. Permeation and block of N-methyl-D-aspartic acid receptor channels by divalent cations in mouse cultured central neurones. *J Physiol*. 394:501-527.

McBean, G.J. 2002. Cerebral cystine uptake: a tale of two transporters. *Trends Pharmacol Sci*. 23:299-302.

Megias, M., Z. Emri, T.F. Freund, and A.I. Gulyas. 2001. Total number and distribution of inhibitory and excitatory synapses on hippocampal CA1 pyramidal cells. *Neuroscience*. 102:527-540.

Milnerwood, A.J., C.M. Gladding, M.A. Pouladi, A.M. Kaufman, R.M. Hines, J.D. Boyd, R.W. Ko, O.C. Vasuta, R.K. Graham, M.R. Hayden, T.H. Murphy, and L.A. Raymond. 2010. Early increase in extrasynaptic NMDA receptor signaling and expression contributes to phenotype onset in Huntington's disease mice. *Neuron*. 65:178-190.

Milnerwood, A.J., and L.A. Raymond. 2010. Early synaptic pathophysiology in neurodegeneration: insights from Huntington's disease. *Trends Neurosci*. 33:513-523.

Min, M.Y., Z. Melyan, and D.M. Kullmann. 1999. Synaptically released glutamate reduces gamma-aminobutyric acid (GABA)ergic inhibition in the hippocampus via kainate receptors. *Proc Natl Acad Sci U S A*. 96:9932-9937.

Min, M.Y., D.A. Rusakov, and D.M. Kullmann. 1998. Activation of AMPA, kainate, and metabotropic receptors at hippocampal mossy fiber synapses: role of glutamate diffusion. *Neuron*. 21:561-570.

Mitchell, S.J., and R.A. Silver. 2000. Glutamate spillover suppresses inhibition by activating presynaptic mGluRs. *Nature*. 404:498-502.

Momiyama, A., D. Feldmeyer, and S.G. Cull-Candy. 1996. Identification of a native low-conductance NMDA channel with reduced sensitivity to Mg2+ in rat central neurones. *J Physiol*. 494 (Pt 2):479-492.

Moran, M.M., K. McFarland, R.I. Melendez, P.W. Kalivas, and J.K. Seamans. 2005. Cystine/glutamate exchange regulates metabotropic glutamate receptor presynaptic inhibition of excitatory transmission and vulnerability to cocaine seeking. *J Neurosci*. 25:6389-6393.

Mosley, C.A., T.M. Acker, K.B. Hansen, P. Mullasseril, K.T. Andersen, P. Le, K.M. Vellano, H. Brauner-Osborne, D.C. Liotta, and S.F. Traynelis. 2010. Quinazolin-4-one derivatives: A novel class of noncompetitive NR2C/D subunit-selective N-methyl-D-aspartate receptor antagonists. *J Med Chem*. 53:5476-5490.

Mothet, J.P., A.T. Parent, H. Wolosker, R.O. Brady, Jr., D.J. Linden, C.D. Ferris, M.A. Rogawski, and S.H. Snyder. 2000. D-serine is an endogenous ligand for the glycine site of the N-methyl-D-aspartate receptor. *Proc Natl Acad Sci U S A*. 97:4926-4931.

Mulholland, P.J., E.P. Carpenter-Hyland, M.C. Hearing, H.C. Becker, J.J. Woodward, and L.J. Chandler. 2008. Glutamate transporters regulate extrasynaptic NMDA receptor modulation of Kv2.1 potassium channels. *J Neurosci*. 28:8801-8809.

Mulholland, P.J., E.P. Carpenter-Hyland, J.J. Woodward, and L.J. Chandler. 2009. Ethanol disrupts NMDA receptor and astroglial EAAT2 modulation of Kv2.1 potassium channels in hippocampus. *Alcohol*. 43:45-50.

Mulholland, P.J., and L.J. Chandler. 2009. Inhibition of glutamate transporters couples to Kv4.2 dephosphorylation through activation of extrasynaptic NMDA receptors. *Neuroscience*.

Mulholland, P.J., and L.J. Chandler. 2010. Inhibition of glutamate transporters couples to Kv4.2 dephosphorylation through activation of extrasynaptic NMDA receptors. *Neuroscience*. 165:130-137.

Mullasseril, P., K.B. Hansen, K.M. Vance, K.K. Ogden, H. Yuan, N.L. Kurtkaya, R. Santangelo, A.G. Orr, P. Le, K.M. Vellano, D.C. Liotta, and S.F. Traynelis. 2010. A subunit-selective potentiator of NR2C- and NR2D-containing NMDA receptors. *Nat Commun*. 1:90.

Nakashiba, T., J.Z. Young, T.J. McHugh, D.L. Buhl, and S. Tonegawa. 2008. Transgenic inhibition of synaptic transmission reveals role of CA3 output in hippocampal learning. *Science*. 319:1260-1264.

Namiki, S., H. Sakamoto, S. Iinuma, M. Iino, and K. Hirose. 2007. Optical glutamate sensor for spatiotemporal analysis of synaptic transmission. *Eur J Neurosci*. 25:2249-2259.

Nedergaard, M. 1994. Direct signaling from astrocytes to neurons in cultures of mammalian brain cells. *Science*. 263:1768-1771.

Nevian, T., and B. Sakmann. 2004. Single spine Ca2+ signals evoked by coincident EPSPs and backpropagating action potentials in spiny stellate cells of layer 4 in the juvenile rat somatosensory barrel cortex. *J Neurosci*. 24:1689-1699.

Nevian, T., and B. Sakmann. 2006. Spine Ca2+ signaling in spike-timing-dependent plasticity. *J Neurosci*. 26:11001-11013.

Newpher, T.M., and M.D. Ehlers. 2008. Glutamate receptor dynamics in dendritic microdomains. *Neuron*. 58:472-497.

Newpher, T.M., and M.D. Ehlers. 2009. Spine microdomains for postsynaptic signaling and plasticity. *Trends Cell Biol*. 19:218-227.

Ngo-Anh, T.J., B.L. Bloodgood, M. Lin, B.L. Sabatini, J. Maylie, and J.P. Adelman. 2005. SK channels and NMDA receptors form a Ca2+-mediated feedback loop in dendritic spines. *Nat Neurosci*. 8:642-649.

Nicholls, D., and D. Attwell. 1990. The release and uptake of excitatory amino acids. *Trends Pharmacol Sci*. 11:462-468.

Nolan, M.F., G. Malleret, J.T. Dudman, D.L. Buhl, B. Santoro, E. Gibbs, S. Vronskaya, G. Buzsaki, S.A. Siegelbaum, E.R. Kandel, and A. Morozov. 2004. A behavioral role for dendritic integration: HCN1 channels constrain spatial memory and plasticity at inputs to distal dendrites of CA1 pyramidal neurons. *Cell*. 119:719-732.

Nowak, L., P. Bregestovski, P. Ascher, A. Herbet, and A. Prochiantz. 1984. Magnesium gates glutamate-activated channels in mouse central neurones. *Nature*. 307:462-465.

O'Connor, E.R., and H.K. Kimelberg. 1993. Role of calcium in astrocyte volume regulation and in the release of ions and amino acids. *J Neurosci*. 13:2638-2650.

Okamoto, S., M.A. Pouladi, M. Talantova, D. Yao, P. Xia, D.E. Ehrnhoefer, R. Zaidi, A. Clemente, M. Kaul, R.K. Graham, D. Zhang, H.S. Vincent Chen, G. Tong, M.R. Hayden, and S.A. Lipton. 2009. Balance between synaptic versus extrasynaptic NMDA receptor activity influences inclusions and neurotoxicity of mutant huntingtin. *Nat Med*. 15:1407-1413.

Okubo, Y., and M. Iino. 2011. Visualization of glutamate as a volume transmitter. *J Physiol*. 589:481-488.

Okubo, Y., H. Sekiya, S. Namiki, H. Sakamoto, S. Iinuma, M. Yamasaki, M. Watanabe, K. Hirose, and M. Iino. 2010. Imaging extrasynaptic glutamate dynamics in the brain. *Proc Natl Acad Sci U S A*. 107:6526-6531.

Okumoto, S., L.L. Looger, K.D. Micheva, R.J. Reimer, S.J. Smith, and W.B. Frommer. 2005. Detection of glutamate release from neurons by genetically encoded surface-displayed FRET nanosensors. *Proc Natl Acad Sci U S A*. 102:8740-8745.

Orellana, J.A., K.F. Shoji, V. Abudara, P. Ezan, E. Amigou, P.J. Saez, J.X. Jiang, C.C. Naus, J.C. Saez, and C. Giaume. 2011. Amyloid beta-induced death in neurons involves glial and neuronal hemichannels. *J Neurosci*. 31:4962-4977.

Pakkenberg, B., D. Pelvig, L. Marner, M.J. Bundgaard, H.J. Gundersen, J.R. Nyengaard, and L. Regeur. 2003. Aging and the human neocortex. *Exp Gerontol*. 38:95-99.

Paoletti, P., and J. Neyton. 2007. NMDA receptor subunits: function and pharmacology. *Curr Opin Pharmacol*. 7:39-47.

Park, H., S.J. Oh, K.S. Han, D.H. Woo, G. Mannaioni, S.F. Traynelis, and C.J. Lee. 2009. Bestrophin-1 encodes for the Ca2+-activated anion channel in hippocampal astrocytes. *J Neurosci*. 29:13063-13073.

Parpura, V., T.A. Basarsky, F. Liu, K. Jeftinija, S. Jeftinija, and P.G. Haydon. 1994. Glutamate-mediated astrocyte-neuron signalling. *Nature*. 369:744-747.

Parri, H.R., T.M. Gould, and V. Crunelli. 2001. Spontaneous astrocytic Ca2+ oscillations in situ drive NMDAR-mediated neuronal excitation. *Nat Neurosci*. 4:803-812.

Perea, G., and A. Araque. 2007. Astrocytes potentiate transmitter release at single hippocampal synapses. *Science*. 317:1083-1086.

Petralia, R.S., Y.X. Wang, F. Hua, Z. Yi, A. Zhou, L. Ge, F.A. Stephenson, and R.J. Wenthold. 2010. Organization of NMDA receptors at extrasynaptic locations. *Neuroscience*. 167:68-87.

Pirttimaki, T.M., S.D. Hall, and H.R. Parri. 2011. Sustained neuronal activity generated by glial plasticity. *J Neurosci*. 31:7637-7647.

Poirazi, P., T. Brannon, and B.W. Mel. 2003. Arithmetic of subthreshold synaptic summation in a model CA1 pyramidal cell. *Neuron*. 37:977-987.

Poolos, N.P., J.B. Bullis, and M.K. Roth. 2006. Modulation of h-channels in hippocampal pyramidal neurons by p38 mitogen-activated protein kinase. *J Neurosci*. 26:7995-8003.

Poolos, N.P., M. Migliore, and D. Johnston. 2002. Pharmacological upregulation of h-channels reduces the excitability of pyramidal neuron dendrites. *Nat Neurosci*. 5:767-774.

Postea, O., and M. Biel. 2011. Exploring HCN channels as novel drug targets. *Nat Rev Drug Discov*. 10:903-914.

Pow, D.V. 2001. Visualising the activity of the cystine-glutamate antiporter in glial cells using antibodies to aminoadipic acid, a selectively transported substrate. *Glia*. 34:27-38.

Racca, C., F.A. Stephenson, P. Streit, J.D. Roberts, and P. Somogyi. 2000. NMDA receptor content of synapses in stratum radiatum of the hippocampal CA1 area. *J Neurosci*. 20:2512-2522.

Ranck, J.B., Jr. 1973. Studies on single neurons in dorsal hippocampal formation and septum in unrestrained rats. I. Behavioral correlates and firing repertoires. *Exp Neurol*. 41:461-531.

Rebola, N., B.N. Srikumar, and C. Mulle. 2010. Activity-dependent synaptic plasticity of NMDA receptors. *J Physiol*. 588:93-99.

Rose, G. 1983. Physiological and behavioral characteristics of dentate granule cells. *In Neurobiology of the Hippocampus, W. Seifert, ed. pp. 449-412, Academic, London.*

Rose, G.M., and T.V. Dunwiddie. 1986. Induction of hippocampal long-term potentiation using physiologically patterned stimulation. *Neurosci Lett*. 69:244-248.

Rossi, D.J., T. Oshima, and D. Attwell. 2000. Glutamate release in severe brain ischaemia is mainly by reversed uptake. *Nature*. 403:316-321.

Rusakov, D.A. 2012. Depletion of extracellular Ca2+ prompts astroglia to moderate synaptic network activity. *Sci Signal*. 5:pe4.

Rusakov, D.A., and D.M. Kullmann. 1998. Extrasynaptic glutamate diffusion in the hippocampus: ultrastructural constraints, uptake, and receptor activation. *J Neurosci*. 18:3158-3170.

Rusakov, D.A., L.P. Savtchenko, K. Zheng, and J.M. Henley. 2011. Shaping the synaptic signal: molecular mobility inside and outside the cleft. *Trends Neurosci*.

Rutherford, E.C., F. Pomerleau, P. Huettl, I. Stromberg, and G.A. Gerhardt. 2007. Chronic second-by-second measures of L-glutamate in the central nervous system of freely moving rats. *J Neurochem*. 102:712-722.

Sabatini, B.L., T.G. Oertner, and K. Svoboda. 2002. The life cycle of Ca(2+) ions in dendritic spines. *Neuron*. 33:439-452.

Sabatini, B.L., and K. Svoboda. 2000. Analysis of calcium channels in single spines using optical fluctuation analysis. *Nature*. 408:589-593.

Sah, P., S. Hestrin, and R.A. Nicoll. 1989. Tonic activation of NMDA receptors by ambient glutamate enhances excitability of neurons. *Science*. 246:815-818.

Sans, N., R.S. Petralia, Y.X. Wang, J. Blahos, 2nd, J.W. Hell, and R.J. Wenthold. 2000. A developmental change in NMDA receptor-associated proteins at hippocampal synapses. *J Neurosci*. 20:1260-1271.

Scanziani, M., P.A. Salin, K.E. Vogt, R.C. Malenka, and R.A. Nicoll. 1997. Use-dependent increases in glutamate concentration activate presynaptic metabotropic glutamate receptors. *Nature*. 385:630-634.

Schell, M.J., M.E. Molliver, and S.H. Snyder. 1995. D-serine, an endogenous synaptic modulator: localization to astrocytes and glutamate-stimulated release. *Proc Natl Acad Sci U S A*. 92:3948-3952.

Schiller, J., G. Major, H.J. Koester, and Y. Schiller. 2000. NMDA spikes in basal dendrites of cortical pyramidal neurons. *Nature*. 404:285-289.

Schiller, J., Y. Schiller, and D.E. Clapham. 1998. NMDA receptors amplify calcium influx into dendritic spines during associative pre- and postsynaptic activation. *Nat Neurosci*. 1:114-118.

Scimemi, A., A. Fine, D.M. Kullmann, and D.A. Rusakov. 2004. NR2B-containing receptors mediate cross talk among hippocampal synapses. *J Neurosci*. 24:4767-4777.

Semyanov, A. 2008. Can diffuse extrasynaptic signaling form a guiding template? *Neurochem Int*. 52:31-33.

Semyanov, A., and D.M. Kullmann. 2000. Modulation of GABAergic signaling among interneurons by metabotropic glutamate receptors. *Neuron*. 25:663-672.

Semyanov, A., and D.M. Kullmann. 2001. Kainate receptor-dependent axonal depolarization and action potential initiation in interneurons. *Nat Neurosci*. 4:718-723.

Shah, M.M., A.E. Anderson, V. Leung, X. Lin, and D. Johnston. 2004. Seizure-induced plasticity of h channels in entorhinal cortical layer III pyramidal neurons. *Neuron*. 44:495-508.

Sheng, M., and C.C. Hoogenraad. 2007. The postsynaptic architecture of excitatory synapses: a more quantitative view. *Annu Rev Biochem*. 76:823-847.

Shin, J.H., Y.S. Kim, and D.J. Linden. 2008a. Dendritic glutamate release produces autocrine activation of mGluR1 in cerebellar Purkinje cells. *Proc Natl Acad Sci U S A*. 105:746-750.

Shin, M., D. Brager, T.C. Jaramillo, D. Johnston, and D.M. Chetkovich. 2008b. Mislocalization of h channel subunits underlies h channelopathy in temporal lobe epilepsy. *Neurobiol Dis*. 32:26-36.

Shinoe, T., M. Matsui, M.M. Taketo, and T. Manabe. 2005. Modulation of synaptic plasticity by physiological activation of M1 muscarinic acetylcholine receptors in the mouse hippocampus. *J Neurosci*. 25:11194-11200.

Shleper, M., E. Kartvelishvily, and H. Wolosker. 2005. D-serine is the dominant endogenous coagonist for NMDA receptor neurotoxicity in organotypic hippocampal slices. *J Neurosci*. 25:9413-9417.

Spray, D.C., Z.C. Ye, and B.R. Ransom. 2006. Functional connexin "hemichannels": a critical appraisal. *Glia*. 54:758-773.

Stuart, G., J. Schiller, and B. Sakmann. 1997. Action potential initiation and propagation in rat neocortical pyramidal neurons. *J Physiol*. 505 (Pt 3):617-632.

Stuart, G.J., and M. Hausser. 2001a. Dendritic coincidence detection of EPSPs and action potentials. *Nature neuroscience*. 4:63-71.

Stuart, G.J., and M. Hausser. 2001b. Dendritic coincidence detection of EPSPs and action potentials. *Nat Neurosci*. 4:63-71.

Suzuki, S.S., and G.K. Smith. 1985. Burst characteristics of hippocampal complex spike cells in the awake rat. *Exp Neurol*. 89:90-95.

Szatkowski, M., B. Barbour, and D. Attwell. 1990. Non-vesicular release of glutamate from glial cells by reversed electrogenic glutamate uptake. *Nature*. 348:443-446.

Takano, T., J. Kang, J.K. Jaiswal, S.M. Simon, J.H. Lin, Y. Yu, Y. Li, J. Yang, G. Dienel, H.R. Zielke, and M. Nedergaard. 2005. Receptor-mediated glutamate release from volume sensitive channels in astrocytes. *Proc Natl Acad Sci U S A*. 102:16466-16471.

Thalhammer, A., Y. Rudhard, C.M. Tigaret, K.E. Volynski, D.A. Rusakov, and R. Schoepfer. 2006. CaMKII translocation requires local NMDA receptor-mediated Ca2+ signaling. *EMBO J*. 25:5873-5883.

Thimm, J., A. Mechler, H. Lin, S. Rhee, and R. Lal. 2005. Calcium-dependent open/closed conformations and interfacial energy maps of reconstituted hemichannels. *J Biol Chem*. 280:10646-10654.

Thompson, R.J., and B.A. Macvicar. 2008. Connexin and pannexin hemichannels of neurons and astrocytes. *Channels (Austin)*. 2:81-86.

Thyssen, A., D. Hirnet, H. Wolburg, G. Schmalzing, J.W. Deitmer, and C. Lohr. 2010. Ectopic vesicular neurotransmitter release along sensory axons mediates neurovascular coupling via glial calcium signaling. *Proc Natl Acad Sci U S A*. 107:15258-15263.

Tong, G., and C.E. Jahr. 1994. Block of glutamate transporters potentiates postsynaptic excitation. *Neuron*. 13:1195-1203.

Torres, A., F. Wang, Q. Xu, T. Fujita, R. Dobrowolski, K. Willecke, T. Takano, and M. Nedergaard. 2012. Extracellular Ca2+ acts as a mediator of communication from neurons to glia. *Sci Signal*. 5:ra8.

Tovar, K.R., and G.L. Westbrook. 1999. The incorporation of NMDA receptors with a distinct subunit composition at nascent hippocampal synapses in vitro. *J Neurosci*. 19:4180-4188.

Trussell, L.O., and G.D. Fischbach. 1989. Glutamate receptor desensitization and its role in synaptic transmission. *Neuron*. 3:209-218.

Tsien, J.Z., P.T. Huerta, and S. Tonegawa. 1996. The essential role of hippocampal CA1 NMDA receptor-dependent synaptic plasticity in spatial memory. *Cell*. 87:1327-1338.

Tzingounis, A.V., and J.I. Wadiche. 2007. Glutamate transporters: confining runaway excitation by shaping synaptic transmission. *Nat Rev Neurosci*. 8:935-947.

Vanderwolf, C.H. 1969. Hippocampal electrical activity and voluntary movement in the rat. *Electroencephalogr Clin Neurophysiol*. 26:407-418.

Vargas-Caballero, M., and H.P. Robinson. 2003. A slow fraction of Mg2+ unblock of NMDA receptors limits their contribution to spike generation in cortical pyramidal neurons. *J Neurophysiol*. 89:2778-2783.

Vizi, E.S. 2000. Role of high-affinity receptors and membrane transporters in nonsynaptic communication and drug action in the central nervous system. *Pharmacol Rev*. 52:63-89.

Vizi, E.S., J.P. Kiss, and B. Lendvai. 2004. Nonsynaptic communication in the central nervous system. *Neurochem Int*. 45:443-451.

Walker, M.C., H. Perry, F. Scaravilli, P.N. Patsalos, S.D. Shorvon, and J.G. Jefferys. 1999. Halothane as a neuroprotectant during constant stimulation of the perforant path. *Epilepsia*. 40:359-364.

Warr, O., M. Takahashi, and D. Attwell. 1999. Modulation of extracellular glutamate concentration in rat brain slices by cystine-glutamate exchange. *J Physiol*. 514 (Pt 3):783-793.

Waxman, E.A., and D.R. Lynch. 2005. N-methyl-D-aspartate receptor subtype mediated bidirectional control of p38 mitogen-activated protein kinase. *J Biol Chem*. 280:29322-29333.

Weber, A.M., F.K. Wong, A.R. Tufford, L.C. Schlichter, V. Matveev, and E.F. Stanley. 2010. N-type Ca2+ channels carry the largest current: implications for nanodomains and transmitter release. *Nat Neurosci*. 13:1348-1350.

Wenzel, A., J.M. Fritschy, H. Mohler, and D. Benke. 1997. NMDA receptor heterogeneity during postnatal development of the rat brain: differential expression of the NR2A, NR2B, and NR2C subunit proteins. *J Neurochem*. 68:469-478.

Wheeler, D.G., R.D. Groth, H. Ma, C.F. Barrett, S.F. Owen, P. Safa, and R.W. Tsien. 2012. Ca(V)1 and Ca(V)2 channels engage distinct modes of Ca(2+) signaling to control CREB-dependent gene expression. *Cell*. 149:1112-1124.

Williams, K. 1993. Ifenprodil discriminates subtypes of the N-methyl-D-aspartate receptor: selectivity and mechanisms at recombinant heteromeric receptors. *Mol Pharmacol*. 44:851-859.

Wyllie, D.J., P. Behe, and D. Colquhoun. 1998. Single-channel activations and concentration jumps: comparison of recombinant NR1a/NR2A and NR1a/NR2D NMDA receptors. *J Physiol*. 510 (Pt 1):1-18.

Xu, T.L., and N. Gong. 2010. Glycine and glycine receptor signaling in hippocampal neurons: diversity, function and regulation. *Prog Neurobiol*. 91:349-361.

Yamashita, T., K. Eguchi, N. Saitoh, H. von Gersdorff, and T. Takahashi. 2010. Developmental shift to a mechanism of synaptic vesicle endocytosis requiring nanodomain Ca2+. *Nat Neurosci*. 13:838-844.

Yang, Y., W. Ge, Y. Chen, Z. Zhang, W. Shen, C. Wu, M. Poo, and S. Duan. 2003. Contribution of astrocytes to hippocampal long-term potentiation through release of D-serine. *Proc Natl Acad Sci U S A*. 100:15194-15199.

Yasuda, R., E.A. Nimchinsky, V. Scheuss, T.A. Pologruto, T.G. Oertner, B.L. Sabatini, and K. Svoboda. 2004. Imaging calcium concentration dynamics in small neuronal compartments. *Sci STKE*. 2004:pl5.

Ye, Z.C., N. Oberheim, H. Kettenmann, and B.R. Ransom. 2009. Pharmacological "cross-inhibition" of connexin hemichannels and swelling activated anion channels. *Glia*. 57:258-269.

Ye, Z.C., M.S. Wyeth, S. Baltan-Tekkok, and B.R. Ransom. 2003. Functional hemichannels in astrocytes: a novel mechanism of glutamate release. *J Neurosci*. 23:3588-3596.

Yi, Z., R.S. Petralia, Z. Fu, C.C. Swanwick, Y.X. Wang, K. Prybylowski, N. Sans, S. Vicini, and R.J. Wenthold. 2007. The role of the PDZ protein GIPC in regulating NMDA receptor trafficking. *J Neurosci*. 27:11663-11675.

Yuste, R., and W. Denk. 1995. Dendritic spines as basic functional units of neuronal integration. *Nature*. 375:682-684.

Zheng, C.Y., R.S. Petralia, Y.X. Wang, B. Kachar, and R.J. Wenthold. 2010. SAP102 is a highly mobile MAGUK in spines. *J Neurosci*. 30:4757-4766.

Zheng, K., A. Scimemi, and D.A. Rusakov. 2008. Receptor actions of synaptically released glutamate: the role of transporters on the scale from nanometers to microns. *Biophys J*. 95:4584-4596.

Zilberter, Y. 2000. Dendritic release of glutamate suppresses synaptic inhibition of pyramidal neurons in rat neocortex. *J Physiol*. 528:489-496.

Ziskin, J.L., A. Nishiyama, M. Rubio, M. Fukaya, and D.E. Bergles. 2007. Vesicular release of glutamate from unmyelinated axons in white matter. *Nat Neurosci*. 10:321-330.

Zucker, R.S. 1999. Calcium- and activity-dependent synaptic plasticity. *Curr Opin Neurobiol*. 9:305-313.